ONTARIO GEOLOGICAL SURVEY

Geophysical Data Sets 1086a and 1086b

Ontario Airborne Geophysical Surveys Airborne Magnetic Gradiometer and Gamma-Ray Spectrometer Geophysical Survey, Ramsey–Algoma Area, Northeastern Ontario, 2018

by

Ontario Geological Survey

2019

Users of OGS products should be aware that Indigenous communities may have Aboriginal or treaty rights or other interests that overlap with areas of mineral potential and exploration.

Contents

FIGURES

TABLES

CREDITS

List of accountabilities and responsibilities.

- Renée-Luce Simard, Senior Manager, Earth Resources and Geoscience Mapping Section, Ontario Geological Survey (OGS), Ministry of Energy, Northern Development and Mines (ENDM) – accountable for the geophysical survey projects, including contract management
- Edna Mueller-Markham, Senior Consulting Geophysicist, Paterson, Grant & Watson Limited (PGW), Toronto, Ontario, Geophysicist under contract to ENDM – responsible for the airborne geophysical survey project management, quality assurance (QA) and quality control (QC)
- Tom Watkins, Manager, Publication Services Unit, GeoServices Section, Ontario Geological Survey, ENDM – managed the project-related hard-copy products
- Desmond Rainsford, Geophysicist, Earth Resources and Geoscience Mapping Section, Ontario Geological Survey – responsible for initial quality assurance (QA), quality control (QC) and project-related digital products
- Sander Geophysics Limited (SGL), Ottawa, Ontario – data acquisition and data compilation

DISCLAIMER

Every possible effort has been made to ensure the accuracy of the information presented in this report and the accompanying data; however, the Ministry of Energy, Northern Development and Mines does not assume liability for errors that may occur. Users should verify critical information.

CITATION

Parts of this publication may be quoted if credit is given. It is recommended that reference to this **report** be made in the following form:

Ontario Geological Survey 2019. Survey report on Ramsey–Algoma area, 112p. [PDF document]; report *in* Ontario airborne geophysical surveys, magnetic gradiometer and gamma-ray spectrometric data, grid and profile data (ASCII format) and vector data, Ramsey–Algoma area; Ontario Geological Survey, Geophysical Data Set 1086a.

or

Ontario Geological Survey 2019. Survey report on Ramsey–Algoma area, 112p. [PDF document]; report *in* Ontario airborne geophysical surveys, magnetic gradiometer and gamma-ray spectrometric data, grid and profile data (Geosoft® format) and vector data, Ramsey–Algoma area; Ontario Geological Survey, Geophysical Data Set 1086b.

It is recommended that reference to the **data** be made in the following form:

Ontario Geological Survey 2019. *in* Ontario airborne geophysical surveys, magnetic gradiometer and gamma-ray spectrometric data, grid and profile data (ASCII format) and vector data, Ramsey–Algoma area; Ontario Geological Survey, Geophysical Data Set 1086a.

or

Ontario Geological Survey 2019. Ontario airborne geophysical surveys, magnetic gradiometer and gamma-ray spectrometric data, grid and profile data (Geosoft® format) and vector data, Ramsey–Algoma area; Ontario Geological Survey, Geophysical Data Set 1086b.

NOTE

1. Introduction

The airborne survey contract was awarded through a Request for Proposal and Contractor Selection process. The system and contractor selected for the survey area were judged on many criteria, including the following

- applicability of the proposed system to the local geology and potential deposit types
- aircraft capabilities and safety plan
- experience with similar surveys
- QA/QC plan
- capacity to acquire the data and prepare final products in the allotted time
- price-performance

2. Survey Location and Specifications

2.1. SURVEY GENERAL GEOLOGY AND LOCATION

The proposed survey area is mostly located in the western Abitibi Subprovince, a division of the Archean Superior Province. The northwestern corner of the survey area is occupied by part of the Wawa Subprovince. The Wawa Subprovince is thought to have been thrust over the western Abitibi Subprovince.

The dominant rock types are gneisses and granitoid intrusions belonging to the Ramsey–Algoma granitoid complex and represented on Figure 1 by pink and bisque colours. Located within the granitoid complex are 3 principle greenstone belts. These are the Batchawana, Swayze and Benny greenstone belts located near the western, northern and eastern edges of the survey area, respectively (*see* Figure 1, greenish areas). Other, smaller greenstone slivers are present elsewhere in the area (e.g., Whiskey Lake greenstone belt, east of Elliot Lake). The greenstone belts may generally be characterized as a sequence of steeply dipping mafic metavolcanic rocks with lesser amounts of felsic to intermediate metavolcanic rocks and metasedimentary rocks.

Rocks of the Proterozoic Huronian Supergroup overlie rocks of the Archean western Abitibi Subprovince, and are extensive in the southern part of the survey area, extending eastward from Sault Ste. Marie to beyond the eastern survey boundary (*see* Figure 1, tan areas). The Huronian Supergroup rocks consist primarily of shallow to moderately dipping conglomerates, sandstones, siltstones and argillites with minor volcanic rocks. The southwestern part of the Proterozoic Sudbury Structure is also included within the eastern margin of the survey area.

With respect to economic mineralization, the most prolific areas have been the Sudbury Basin for nickel production and the Elliot Lake area for its past-producing uranium mines. Although there was some historical gold production from the Huronian Supergroup rocks in the southeast of the survey area, most gold occurrences were recorded in the 3 greenstone belts noted above. Several old copper mines had historic production either mostly in the Batchawana greenstone belt or across the breadth of the Huronian Supergroup. Numerous copper occurrences have been noted in both of these areas.

Further details about the regional geology can be found in Ontario Geological Survey Special Volume 4 Part 1 *Geology of Ontario* (specifically, Bennett, Dressler and Robertson 1991; Jackson and Fyon 1991; Williams et al. 1991).

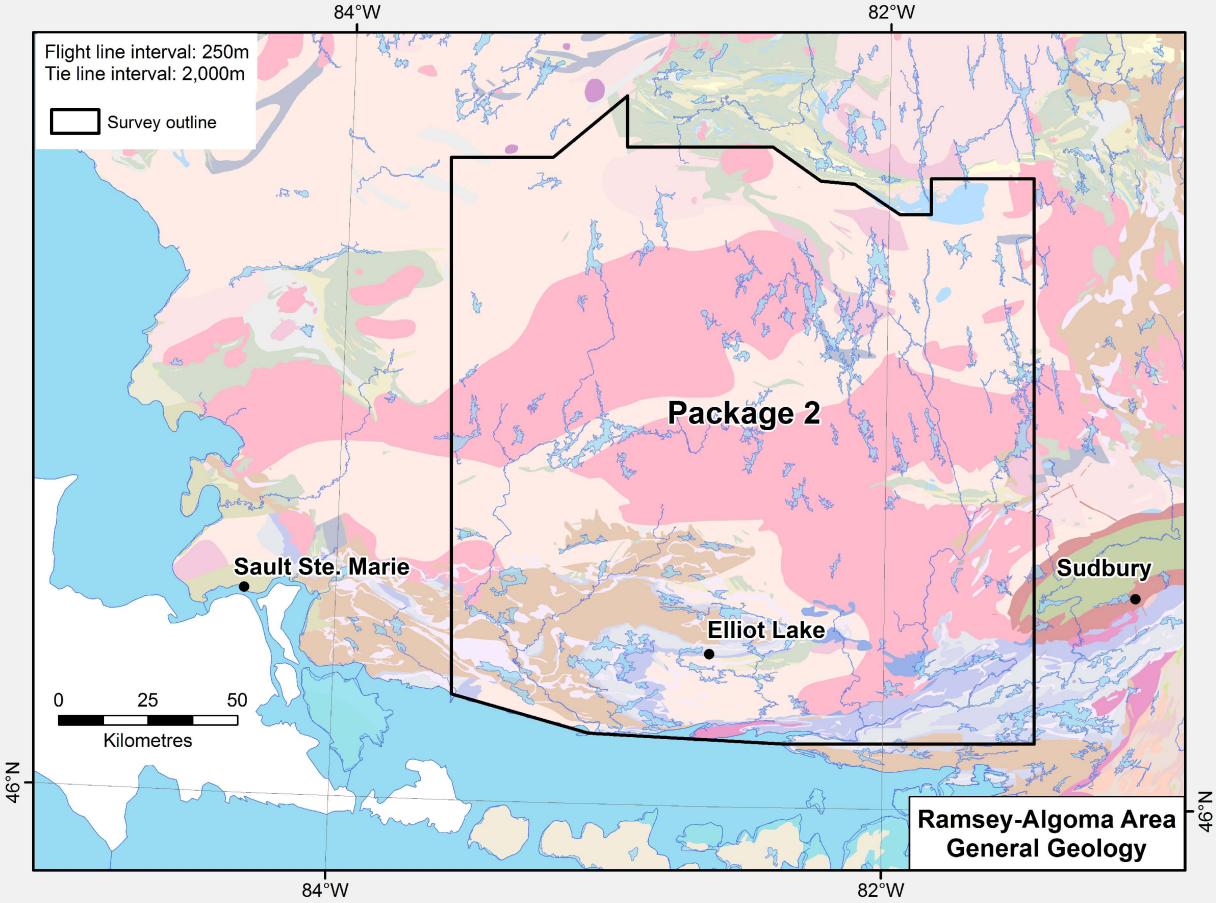

Figure 1. The bedrock geology of the Ramsey–Algoma survey area (*from* Ontario Geological Survey 2011); survey boundary shown in black.

2.2. SURVEY SPECIFICATIONS

The Ramsey–Algoma survey area specifications and tolerances are as follows:

1. Line spacing and direction for the magnetic gradiometer survey
   - the nominal flight-line spacing is 250 m
   - flight-line direction 0°
   - maximum deviation from the nominal flight-line location could not exceed 50 m over a distance greater than 2000 m
   - minimum separation between 2 adjacent lines could be no smaller than 200 m or larger than 300 m
   - for each survey flight, adjacent lines must be flown separately and in opposite directions. A racetrack-flying pattern is not permitted
2. Control-line spacing and direction
   - the nominal control-line spacing is 2000 m, perpendicular to the traverse-line direction
   - control-line direction 90°
   - along each survey boundary (if not parallel with the flight-line direction)
   - maximum deviation from the nominal control-line location could not exceed 50 m over a distance greater than 2000 m

3. Terrain clearance of the magnetometers
   - nominal terrain clearance is 100 m and will be consistent with safety of aircraft and crew
   - altitude tolerance limited to ±15 m, except in areas of severe topography
   - altitude tolerance limited to ±10 m at flight-line–control-line intersections, except in areas of severe topography
4. Aircraft speed
   - nominal aircraft speed is 54 to 74 m/sec
   - aircraft speed tolerance limited to ±10.0 m/sec, except in areas of severe topography
5. Magnetic diurnal variation
   - could not exceed a maximum deviation of 3.0 nT peak-to-peak over a long chord equivalent to 1 minute
6. Magnetometer noise envelope
   - in-flight noise envelope, calculated using a non-normalized 4th difference, shall not exceed 0.1 nT, for straight and level flight
   - heading error not to exceed 2.0 nT
   - base station noise envelope, calculated using a non-normalized 4th difference, shall not exceed 0.1 nT
7. Reflights and turns
   - all reflights of flight-line segments intersected at least 2 control lines
   - all turns at the end of flight lines or control lines took place beyond the survey or block boundaries

3. Aircraft, Equipment and Personnel

3.1. AIRCRAFT: C-GSGW

Operator:	Sander Geophysics Limited
Registration:	C-GSGW
Type:	Cessna® 208B Grand Caravan®
Mean Survey Speed:	54 to 74 m/s

3.1.1. EQUIPMENT

3.1.1.1. MAGNETOMETER: GEOMETRICS® G-822A

The magnetometers are non-oriented (strap-down) optically pumped cesium split-beam sensors with a sensitivity of 0.005 nT, a range of 20 000 to 100 000 nT and noise of less than 0.0005 nT. The airborne sensor was mounted in a fibreglass stinger extending from the tail of the aircraft. The system included 2 additional sensors, housed in each wingtip pod. Total magnetic field measurements were recorded at 160 Hz in the aircraft, then later down sampled to 10 Hz in the processing.

3.1.1.2. SPECTROMETER: EXPLORANIUM™ GR-820

The spectrometer consists of 33.6 L (2048 cubic inches) of main (downward) sodium iodide (NaI) crystal detectors and 8.4 L (512 cubic inches) of upward-looking detectors. The entire 256 channel spectra were recorded with a sample rate of 1 second.

3.1.1.3. DIGITAL ACQUISITION: SANDER GEOPHYSICS DATA ACQUISITION SYSTEM (SGDAS)

The SGDAS is the latest version of airborne navigation and data acquisition computers developed by SGL. It is the data gathering core for all the different types of survey data. The computer incorporates a magnetometer coupler, an altimeter analog to digital converter and a NovAtel® GPS multi-frequency receiver (*see* "GPS Receivers" for details), which automatically provides the UTC time base for the recorded data. The system acquires the different data streams from the sensors and receives and processes GPS signals from the GPS antenna. Navigation information from the navigation side of the computer guides the pilots along the pre-planned flight path in all 3 dimensions. Profiles of the incoming data are displayed in real-time to the pilots for continuous monitoring. The data are recorded in database format on redundant solid-state data storage modules.

3.1.1.4. BAROMETRIC ALTIMETER: HONEYWELL MODEL TJE DIGITAL BAROMETRIC PRESSURE SENSOR

The barometric pressure sensor measures static pressure to an accuracy of ±4 m and resolution of 2 m over a range up to 9144 m above sea level. The barometric altimeter data is sampled at 10 Hz.

3.1.1.5. RADAR ALTIMETER: BENDIX/KING® KRA-10A

The Bendix/King® KRA-10A altimeter has a resolution of 0.5 m, an accuracy of 5%, a range of 6 to 760 m, and a 10 Hz data rate. This system is employed as a backup system and not actively employed for survey guidance or data processing.

3.1.1.6. DIGITAL RADAR ALTIMETER: THOMSON-CSF ERT 530A

The Thomson-CSF ERT 530A uses radio wave echoing to determine the height above ground. It will generally "see through" foliage. The Thomson-CSF ERT 530A radar altimeter has a resolution of 0.5 m, an accuracy of 1%, a range of 1 to 2440 m and a 10 Hz data rate.

3.1.1.7. LASER ALTIMETER: SGLAS-P–RIEGL® LD90-31K-HIP LASER RANGEFINDER

The Riegl® laser altimeter uses a single optical laser beam to measure distance to the ground. It is effective over water and is eye safe. This profilometer has a range of 1500 m, a resolution of 0.01 m with an accuracy of 5 cm and a 3.3 Hz data rate.

3.1.1.8. DIGITAL IMAGING SYSTEM: SGDIS–DATATOYS™ E580 BULLET CAMERA

The Digital Imaging System is mounted in the floor of the aircraft and oriented to look vertically below while in flight. The system automatically records the position, time (fiducials), line and flight number on the video. The data are stored by flight line in *.avi* format, viewable by any commercial media player.

3.1.1.9. GPS RECEIVER: NOVATEL® OEMV®-3 RECEIVER BOARD

The NovAtel® OEMV®-3, multi-frequency GNSS (Global Navigation Satellite System) receiver is configurable up to 72 channels with the tracking of GPS (L1, L2, L5), GLONASS (L1, L2), SBAS, and L-band satellites and signals. It provides averaged position and raw range information of all satellites in view. The GNSS positional data are recorded at 10 Hz.

3.2. AIRCRAFT: C-GSGL

Operator:	Sander Geophysics Limited
Registration:	C-GSGL
Type:	Cessna® 208B Grand Caravan®
Mean Survey Speed:	54 to 74 m/s

3.2.1. EQUIPMENT

3.2.1.1. MAGNETOMETER: GEOMETRICS® G-822A

The magnetometers are non-oriented (strap-down) optically pumped cesium split-beam sensors with a sensitivity of 0.005 nT, a range of 20 000 to 100000 nT and noise of less than 0.0005 nT. The airborne sensor was mounted in a fibreglass stinger extending from the tail of the aircraft. The system included 2 additional sensors, housed in each wingtip pod. Total magnetic field measurements were recorded at 160 Hz in the aircraft, then later down sampled to 10 Hz in the processing.

3.2.1.2. SPECTROMETER: EXPLORANIUM™ GR-820

The spectrometer consists of 33.6 L (2048 cubic inches) of main (downward) sodium iodide (NaI) crystal detectors and 8.4 L (512 cubic inches) of upward-looking detectors. The entire 256 channel spectra were recorded with a sample rate of 1 second.

3.2.1.3. DIGITAL ACQUISITION: SANDER GEOPHYSICS DATA ACQUISITION SYSTEM (SGDAS)

The SGDAS is the latest version of airborne navigation and data acquisition computers developed by SGL. It is the data gathering core for all the different types of survey data. The computer incorporates a magnetometer coupler, an altimeter analog to digital converter and a NovAtel® GPS multi-frequency receiver (*see* "GPS Receivers" for details), which automatically provides the UTC time base for the recorded data. The system acquires the different data streams from the sensors and receives and processes GPS signals from the GPS antenna. Navigation information from the navigation side of the computer guides the pilots along the pre-planned flight path in all 3 dimensions. Profiles of the incoming data are displayed in real-time to the pilots for continuous monitoring. The data are recorded in database format on redundant solid-state data storage modules.

3.2.1.4. BAROMETRIC ALTIMETER: HONEYWELL MODEL TJE DIGITAL BAROMETRIC PRESSURE SENSOR

The barometric pressure sensor measures static pressure to an accuracy of ±4 m and resolution of 2 m over a range up to 9144 m above sea level. The barometric altimeter data is sampled at 10 Hz.

3.2.1.5. RADAR ALTIMETER: BENDIX/KING® KRA-10A

The Bendix/King® KRA-10A altimeter has a resolution of 0.5 m, an accuracy of 5%, a range of 6 to 760 m, and a 10 Hz data rate. This system is employed as a backup system and not actively employed for survey guidance or data processing.

3.2.1.6. DIGITAL RADAR ALTIMETER: THOMSON-CSF ERT 530A

The Thomson-CSF ERT 530A uses radio wave echoing to determine the height above ground. It will generally "see through" foliage. The Thomson-CSF ERT 530A radar altimeter has a resolution of 0.5 m, an accuracy of 1%, a range of 1 to 2440 m and a 10 Hz data rate.

3.2.1.7. LASER ALTIMETER: SGLAS-P–RIEGL® LD90-31K-HIP LASER RANGEFINDER

The Riegl® laser altimeter uses a single optical laser beam to measure distance to the ground. It is effective over water and is eye safe. This profilometer has a range of 1500 m, a resolution of 0.01 m with an accuracy of 5 cm and a 3.3 Hz data rate.

3.2.1.8. DIGITAL IMAGING SYSTEM: SGDIS–DATATOYS™ E580 BULLET CAMERA

The Digital Imaging System is mounted in the floor of the aircraft and oriented to look vertically below while in flight. The system automatically records the position, time (fiducials), line and flight number on the video. The data are stored by flight line in *.avi* format, viewable by any commercial media player.

3.2.1.9. GPS RECEIVER: NOVATEL® OEMV®-3 RECEIVER BOARD

The NovAtel® OEMV®-3, multi-frequency GNSS (Global Navigation Satellite System) receiver is configurable up to 72 channels with the tracking of GPS (L1, L2, L5), GLONASS (L1, L2), SBAS, and L-band satellites and signals. It provides averaged position and raw range information of all satellites in view. The GNSS positional data are recorded at 10 Hz.

3.3. AIRCRAFT: C-GSGV

Operator:	Sander Geophysics Limited
Registration:	C-GSGV
Type:	Cessna® 208B Grand Caravan®
Mean Survey Speed:	54 to 74 m/s

3.3.1. EQUIPMENT

3.3.1.1. MAGNETOMETER: GEOMETRICS® G-822A

The magnetometers are non-oriented (strap-down) optically pumped cesium split-beam sensors with a sensitivity of 0.005 nT, a range of 20 000 to 100 000 nT and noise of less than 0.0005 nT. The airborne sensor was mounted in a fibreglass stinger extending from the tail of the aircraft. The system included 2 additional sensors, housed in each wingtip pod. Total magnetic field measurements were recorded at 160 Hz in the aircraft, and then later down sampled to 10 Hz in the processing.

3.3.1.2. SPECTROMETER: EXPLORANIUM™ GR-820

The spectrometer consists of 33.6 L (2048 cubic inches) of main (downward) sodium iodide (NaI) crystal detectors and 8.4 L (512 cubic inches) of upward-looking detectors. The entire 256 channel spectra were recorded with a sample rate of 1 second.

3.3.1.3. DIGITAL ACQUISITION: SANDER GEOPHYSICS DATA ACQUISITION SYSTEM (SGDAS)

The SGDAS is the latest version of airborne navigation and data acquisition computers developed by SGL. It is the data gathering core for all the different types of survey data. The computer incorporates a magnetometer coupler, an altimeter analog to digital converter and a NovAtel® GPS multi-frequency receiver (*see* "GPS Receivers" for details), which automatically provides the UTC time base for the recorded data. The system acquires the different data streams from the sensors and receives and processes GPS signals from the GPS antenna. Navigation information from the navigation side of the computer guides the pilots along the pre-planned flight path in all 3 dimensions. Profiles of the incoming data are displayed in real-time to the pilots for continuous monitoring. The data are recorded in database format on redundant solid-state data storage modules.

3.3.1.4. BAROMETRIC ALTIMETER: HONEYWELL MODEL TJE DIGITAL BAROMETRIC PRESSURE SENSOR

The barometric pressure sensor measures static pressure to an accuracy of ±4 m and resolution of 2 m over a range up to 9144 m above sea level. The barometric altimeter data is sampled at 10 Hz.

3.3.1.5. RADAR ALTIMETER: BENDIX/KING® KRA-10A

The Bendix/King® KRA-10A altimeter has a resolution of 0.5 m, an accuracy of 5%, a range of 6 to 760 m, and a 10 Hz data rate. This system is employed as a backup system and not actively employed for survey guidance or data processing.

3.3.1.6. DIGITAL RADAR ALTIMETER: THOMSON-CSF ERT 530A

The Thomson-CSF ERT 530A uses radio wave echoing to determine the height above ground. It will generally "see through" foliage. The Thomson-CSF ERT 530A radar altimeter has a resolution of 0.5 m, an accuracy of 1%, a range of 1 to 2440 m and a 10 Hz data rate.

3.3.1.7. LASER ALTIMETER: SGLAS-P–RIEGL® LD90-31K-HIP LASER RANGEFINDER

The Riegl® laser altimeter uses a single optical laser beam to measure distance to the ground. It is effective over water and is eye safe. This profilometer has a range of 1500 m, a resolution of 0.01 m with an accuracy of 5 cm and a 3.3 Hz data rate.

3.3.1.8. DIGITAL IMAGING SYSTEM: SGDIS–DATATOYS™ E580 BULLET CAMERA

The Digital Imaging System is mounted in the floor of the aircraft and oriented to look vertically below while in flight. The system automatically records the position, time (fiducials), line and flight number on the video. The data are stored by flight line in *.avi* format, viewable by any commercial media player.

3.3.1.9. GPS RECEIVER: NOVATEL® OEMV®-3 RECEIVER BOARD

The NovAtel® OEMV®-3, multi-frequency GNSS (Global Navigation Satellite System) receiver is configurable up to 72 channels with the tracking of GPS (L1, L2, L5), GLONASS (L1, L2), SBAS, and L-band satellites and signals. It provides averaged position and raw range information of all satellites in view. The GNSS positional data are recorded at 10 Hz.

3.4. BASE STATION EQUIPMENT

3.4.1. MAGNETOMETER: GEOMETRICS® G-822A

The magnetometer is a non-oriented (strap-down) optically pumped cesium split-beam sensor with a sensitivity of 0.005 nT, a range of 20 000 to 100 000 nT and noise of less than 0.0005 nT. Total magnetic field measurements were recorded at 11 Hz, then later down sampled to 10 Hz in the processing.

3.4.2. GPS RECEIVER: NOVATEL® OEM®-4 RECEIVER BOARD

The NovAtel® dual frequency NovAtel® OEM®-4 measures all GPS channels, for up to 12 satellites. The GNSS positional data are recorded at 10 Hz.

3.5. PERSONNEL

Pilots:	Randall Forwell Alex Faulkner George Sakgaev Martin Stirajs Andrew Fleider Marco Ottaviano Charles Dicks Steven Hyde Katherine Svarckopf Allison Gougeon
Field Crew Chief:	Kevin Charles Lindsay Upiter Mike McManus Keith Wells
Field Data Analysts:	Derek Kouhi Kerri Campbell Nick Lynch
Field Technician:	Zachary Seguin-Forest
Aircraft Maintenance Engineer:	Roger Knott Mike Devenny Ed Deluca
Project Manager:	Kevin Charles

4. Data Acquisition

4.1. ACQUISITION SUMMARY

Sander Geophysics Limited (SGL) was selected by the Ministry of Energy, Northern Development and Mines (ENDM) to perform the Ramsey–Algoma area horizontal magnetic gradient and gamma-ray survey.

The principal geophysical sensors were 3 high-sensitivity, optically pumped cesium split-beam magnetometers and a gamma-ray spectrometer linked to 42 L (33.6 L downward-looking and 8.4 L upward-looking) of sodium iodide (NaI) detectors. Ancillary equipment included a GPS navigation system with GPS base station, a digital imaging system, temperature and pressure sensors, radar altimeters and 2 base station magnetometers.

A pre-planned drape surface was prepared for the survey to guide the aircraft over the topography in a consistent manner, as close to the minimum clearance as possible. The drape surface was prepared with digital elevation model (DEM) data obtained from the Shuttle Radar Topography Mission (http://srtm.usgs.gov/) for the area in question. The DEM included an extension beyond the survey boundary to allow the aircraft to achieve the drape clearance before coming on line.

The drape surface created used a climb and descent rate of 345 ft/nm at 130.8 m above mean sea level (msl) and 338 ft/nm at an altitude of 600 m msl. Interpolation or extrapolation was used to calculate climb and descent rates for the smooth surface for all locations. The temperature component used for the

calculation was based on published weather history. The gentle drape surface created was below the maximum climbing and descending capabilities of the survey aircraft and guided the aircraft to a target height of 100 m above the terrain.

Sander Geophysics Limited utilized 3 of its aircraft—registrations C-GSGW, C-GSGL and C-GSGV—for this survey and based its operations out of Elliot Lake, Ontario.

The survey was flown as a single block with the traverse lines oriented north–south and the control lines situated perpendicular to the traverse lines. The traverse-line spacing was 250 m, whereas the control-line spacing was 2000 m. Additional control lines were flown along the off-angle survey borders. Total survey coverage was 117 772 line-kilometres.

The aircraft, C-GSGV and C-GSGL, first mobilized to Elliot Lake, Ontario on June 17, 2018. This was followed by a few days of equipment setup and safety briefings prior to the first data acquisition on June 20, 2018. The third aircraft, C-GSGW, mobilized to Elliot Lake on July 4, 2018, and commenced survey flying the following day.

The 2 ground reference stations used were dual reference stations. One half consisted of a data acquisition computer with a cesium magnetometer interface and frequency counter to process the signal from the magnetometer sensor and from the GPS receiver. The other half contains only a GPS receiver. These 2 halves operate independently of each other. The time base (UTC) of both the ground and airborne systems is automatically provided by the GPS receiver, ensuring proper merging of both data sets. All data are displayed on an LCD flat panel monitor. The magnetic data, sampled at 11 Hz and the GPS data, sampled at 10 Hz, are recorded on solid state data storage modules. The entire reference data acquisition system was set for automatic, unattended recording. The noise level of the reference station magnetometer is less than 0.1 nT.

Both reference stations were set up in a forested location inside the secure area at the Elliot Lake Municipal Airport. The co-ordinates of REF1 were 46°21′05.0028″N, 82°33′21.7905″W with respect to WGS84 at an elevation of 289.51 m above the geoid. REF2 was located at 46°21′05.1164″ N, 82°33′21.7073″W at an elevation of 289.42 m above the geoid.

General Statistics:

Survey dates:	June 20, 2018 to September 3, 2018
Total kilometres flown:	117 772 km
Total flying hours:	677.9 hours
Number of production days:	53 days
Number of production flights:	123 flights

4.2. PRESURVEY TESTS AND CALIBRATIONS

The following tests and calibrations were performed prior to the commencement of the survey:

- magnetometer lag test
- radar and laser altimeter test
- magnetometer Figure of Merit test
- magnetometer heading test and GPS navigation test
- spectrometer stripping calibration
- spectrometer dynamic calibration range

The compensation flight was performed at high altitude (roughly 10 000 feet) in the Ottawa area. The heading test and GPS test were flown over the Morewood site near Ottawa. The lag test was flown over a railway bridge that crosses the Ottawa River near the township of Pontiac. The altimeter calibration was carried out over the Gatineau Airport runway and Lac Deschenes. The gamma-ray spectrometer pad calibration was completed in the SGL hangar located at the Ottawa Airport using the Geological Survey of Canada (GSC) calibration pads. The altitude attenuation and sensitivity calibrations were flown over the GSC–approved Breckenridge dynamic calibration range. Details of these tests and their results are provided in Appendix A.

4.3. SURVEY TESTS AND CALIBRATIONS

The following tests and calibrations were performed during the survey:

- cosmic and aircraft background calibration
- radon background calibration

All tests were performed in the Elliot Lake area. Details of these tests and their results are provided in Appendix A.

4.4. POSTSURVEY TESTS AND CALIBRATIONS

The following tests and calibrations were performed following survey completion:

- magnetometer Figure of Merit test
- magnetometer lag test

The compensation flight was performed at high altitude (roughly 10 000 feet) in the Ottawa area. The lag test was flown over a railway bridge that crosses the Ottawa River near the township of Pontiac. Details of these tests and their results are provided in Appendix A.

4.5. FIELD PROCESSING PROCEDURES

All digital data were verified for validity and continuity. The data from the aircraft and base station were transferred to the personal computer's hard disk. Two additional data copies were written to external hard disks. Basic statistics were generated for each parameter recorded. These included the minimum, maximum and mean values, the standard deviation and any null values located. Editing of all recorded parameters for spikes or datum shifts was done, followed by final data verification via an interactive graphics screen with on-screen editing and interpolation routines.

A NovAtel® OEMV®-3, multi-frequency GNSS (Global Navigation Satellite System) receiver was used to ferry to the survey site and to survey along each line. Co-ordinates for the survey blocks were supplied by ENDM and were used to establish the survey boundaries and the flight lines. Any other aircraft operating in the area were notified about the location of the survey blocks and flying height for safety reasons.

A video camera recorded the ground image in *.avi* format along the flight path. The field data processor reviewed the flight path after each survey flight for continuity and quality. Issues regarding the video are listed in Appendix D.

Checking all data for adherence to specifications was carried out in the office by an experienced SGL data processor.

5. Data Compilation and Processing

5.1. PERSONNEL

The following personnel were involved in the compilation of data and creation of the final products:

Project Manager:	Kevin Charles
Processing Manager:	Martin Bates
Data Analysts:	Sol Meyer Nick Lynch Aamna Sirohey Kerri Campbell Martin Mushayandebvu

5.2. BASE MAPS

Base maps of the survey area were supplied by the Ontario Ministry of Energy, Northern Development and Mines.

5.2.1. PROJECT DESCRIPTION

Datum:	North American Datum 1983 (NAD83) Canadian Spatial Reference System (CSRS)
Ellipsoid:	Geodetic Reference System 1980 (GRS 80)
Projection:	UTM 17N
Central Meridian:	81°W
False Northing:	0 m
False Easting:	500 000 m
Scale Factor:	0.9996

5.3. PROCESSING OF THE POSITIONAL AND ALTITUDE DATA

5.3.1. PREPROCESSING OF THE POSITIONAL DATA (GPS)

Positional data flow chart is presented in Figure 2.

Accurate locations of the GPS antenna were determined through Precise Point Positioning (PPP). Positions were recalculated using the algorithm developed by Natural Resources Canada (NRCAN) (http://webapp.geod.nrcan.gc.ca/geod/tools-outils/ppp.php) adapted to run under SGL's suite of software. Precise satellite orbit and clock data files were obtained from the International GPS Service. This technique provides a final receiver location with an accuracy of better than 5 cm. All survey lines were processed using this method.

Positional data (x, y, z) were recorded and all data processing was performed in the WGS84 datum. The delivered data were provided in x, y locations in UTM projection zone UTM 17N, with respect to the NAD83 CSRS datum. Tables 1, 2 and 3 provide the ellipsoid and datum conversion parameters.

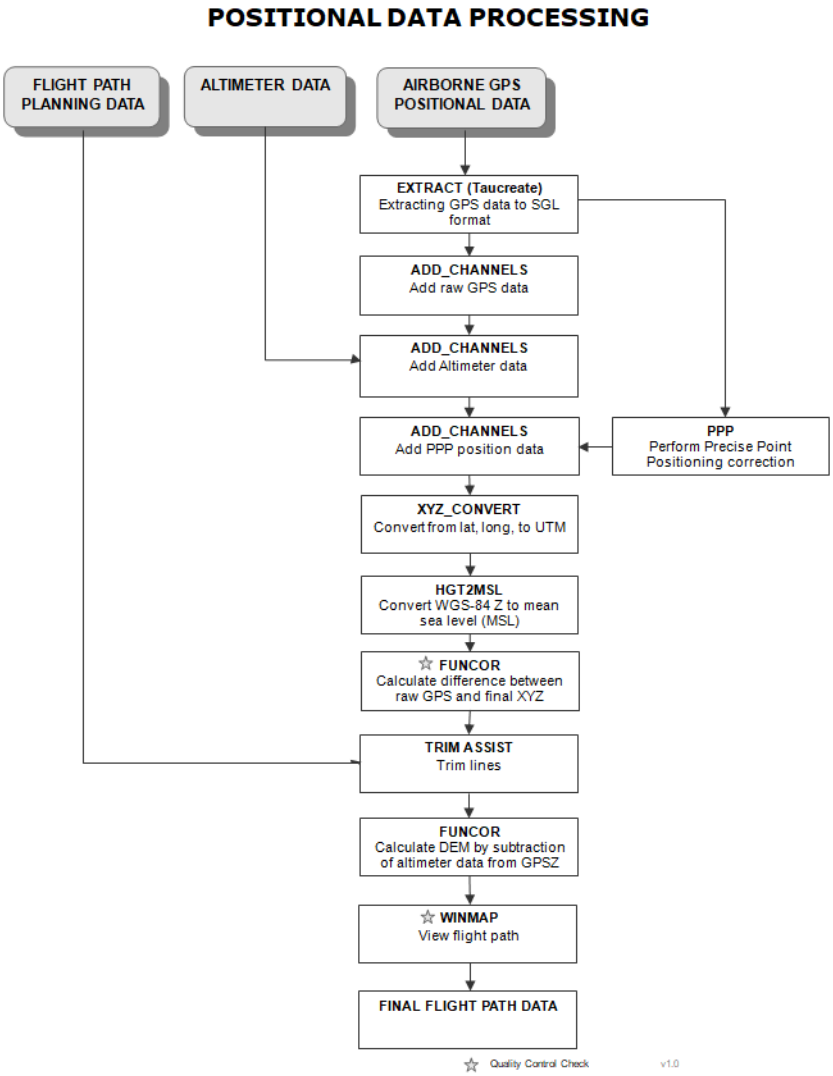

Figure 2. Positional data flow chart ("Precise Point Positioning").

Table 1. Ellipsoid parameters for World Geodetic System 1984 (WGS84).

Ellipsoid	**WGS84**
Semi-major axis	6378137.0
1/flattening	298.257223563

Table 2. Ellipsoid parameters for NAD83 Canadian Spatial Reference System.

Ellipsoid	**GRS 80**
Semi-major axis	6378137.0
1/flattening	298.257222101

Table 3. Datum conversion parameters from WGS84 to NAD83 Canadian Spatial Reference System.

x shift (m)	0.9910
y shift (m)	−1.9072
z shift (m)	−0.5129
x rotation (rad)	$1.2581 \times E^{-7}$
y rotation (rad)	$3.5990 \times E^{-7}$
z rotation (rad)	$5.6070 \times E^{-7}$

Elevation data were recorded relative to the GRS 80 ellipsoid and transformed to mean sea level (msl) using the CGVD2013 model.

5.3.2. Processing of the Positional Data

The terrain clearance measured by the radar altimeter and the barometric altitude were recorded at 10 Hz. The barometric altimeter was recorded, but was not used for locational purposes because of the availability of more accurate GPS altitudes.

The laser altimeter recorded terrain clearance at 3.3 Hz. The laser data show the effects of the dense tree cover; variable penetration of the canopy results in a high frequency variation of recorded altitude.

The Thomson-CSF radar data penetrate the canopy less as it records the first return within the footprint of its signal. The radar altimeter data were filtered to remove high-frequency noise using a 67-point low-pass filter. The final data were plotted and inspected for quality.

Two versions of digital elevation model (DEM) were derived, one by subtracting the laser altimeter data and one by subtracting the Thomson-CSF radar data from the GPS altitude with respect to mean sea level. Short sections of poor laser data, resulting from locally weak reflectivity or the effects of clouds, were replaced using Thomson-CSF radar data. Microlevelling was selectively employed to the DEM over large lakes and some low-lying areas in the south to remove some residual line-parallel artifacts.

5.4. PROCESSING OF THE MAGNETIC DATA

5.4.1. Processing of Base Station Data

Ground magnetometer data were inspected for cultural interference and edited where necessary. All reference station magnetometer data were filtered using a 121-point low-pass filter to remove any high-frequency signal, but retain the low-frequency diurnal variations. The mean residual value of the ground stations was subtracted to remove any bias from the local anomalous field. For base station REF1, the mean was 54961.3 nT and, for base station REF2, the mean was 54883.6 nT. The ground station data for

REF1 during flights 1001, 2002, 1017 and 3007 were visibly offset from the remainder of flights. Therefore, a constant shift was applied to bring the average daily value to the statistical average level calculated from data spanning the duration of the survey. A shift of 78 nT was applied to flights 1001 and 2002, and a shift of 85.6985 nT was applied to flights 1017 and 3007.

5.4.2. PROCESSING OF AIRBORNE MAGNETIC DATA

Figure 3 summarizes the steps involved in processing the magnetic data collected during the survey.

The tail boom–mounted sensor #3 was used to make the standard magnetic anomaly field grid of data. The airborne magnetometer data were recorded at 160 Hz, and down sampled to 10 Hz for processing. All magnetic data were plotted and checked for any spikes or noise. A 0.244 s static lag correction resulting from signal processing, plus a dynamic lag correction for the tail sensor and 2 wingtip sensors were applied to each data point. The actual correction, applied to each data point, depends on the instantaneous velocity of the aircraft, and varies between 0.04 s and 0.06 s. The aircraft speed dependent dynamic lag was calculated using SGL's Dynlag software.

Diurnal variations in the airborne magnetometer data were removed by subtracting the corrected reference station data. REF1 was used for all diurnal corrections except for flight 2049.

Intersections between control and traverse lines were determined by a program that extracts the magnetic, altitude, and X and Y values of the traverse and control lines at each intersection point. Each control line was then adjusted by a constant value to minimize the intersection differences that were calculated using the following equation:

$$\sum |i - a| \quad \text{summed over all traverse lines,}$$

where, i = individual intersection difference; and
a = average intersection difference for that traverse line

Adjusted control lines were further corrected locally to minimize the difference between individual corrections and the average correction for the control line that results from residual diurnal variations along the line. Traverse-line levelling was then carried out by a program that interpolates and extrapolates levelling values for each point based on the 2 closest levelling values. After traverse lines have been levelled, the control lines were matched to them. This ensures that all intersections tie perfectly and permits the use of all data in the final products. At this point, the total magnetic intensity (TMI) field has been derived.

The levelling procedure was verified through inspection of magnetic intensity contour maps, inspection of vertical derivative grids, plotting profiles of corrections along lines, and examining levelling statistics to check for steep correction gradients. Microlevelling was applied with a cut-off value of ±0.5 nT.

The International Geomagnetic Reference Field (IGRF) was then calculated from the 2015 model year extrapolated to 2018.584 (August 1, 2018) at the mean survey elevation of 484.63 m above the WGS84 ellipsoid and removed from the corrected values to generate the residual magnetic anomaly field.

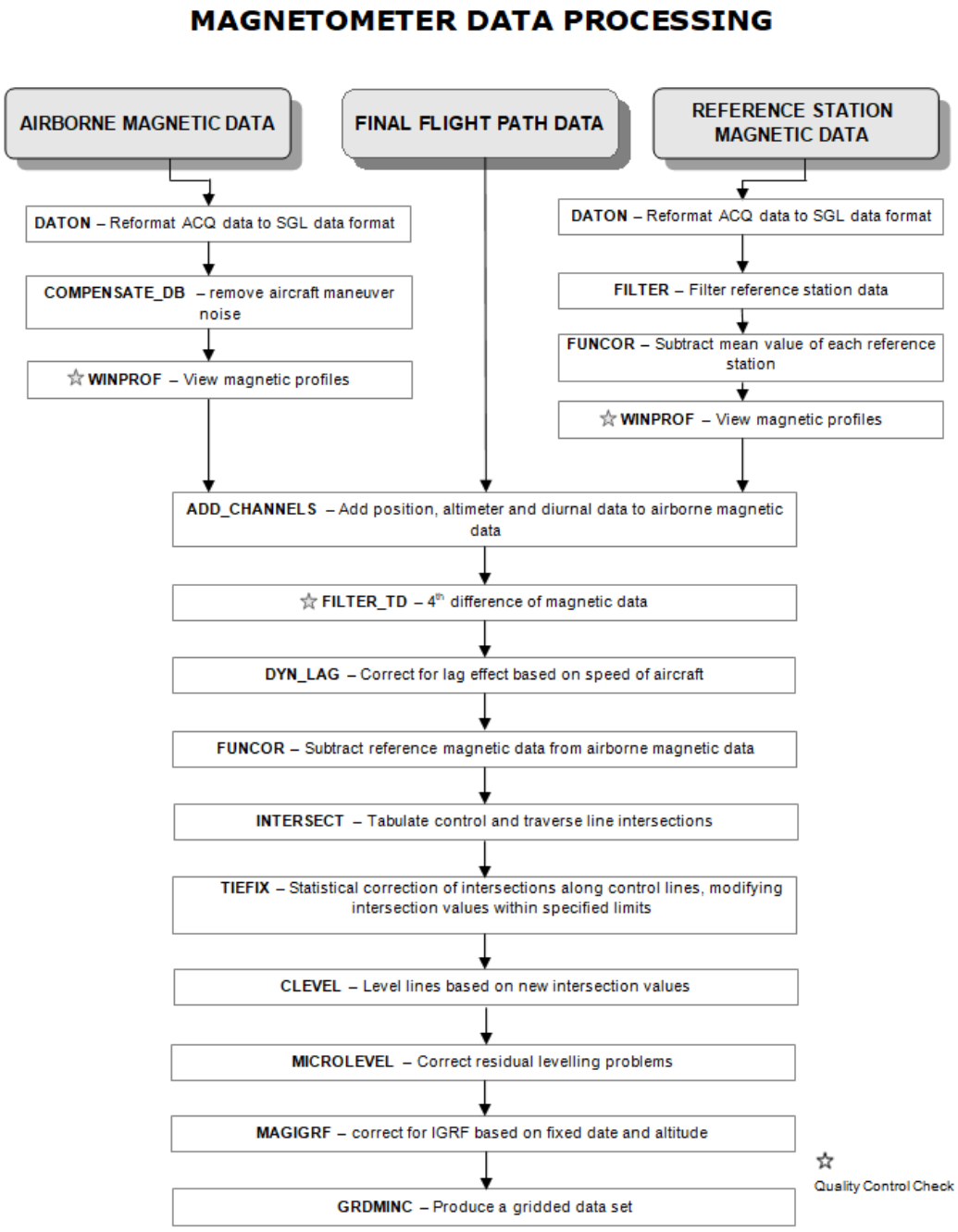

Figure 3. Magnetometer data processing flow chart.

5.4.3. PROCESSING OF MEASURED MAGNETIC GRADIENTS

The measured lateral and longitudinal gradients provide an improved rendition of the shorter wavelengths in magnetic field than the total magnetic field measured by the tail sensor #3 alone. This is because the direction and amplitude of the field's total horizontal gradient can be determined using the 2 measured gradients, providing information regarding the behaviour of the magnetic field in between traverse lines.

Initially, the magnetic gradients were derived with respect to the aircraft frame. The across-aircraft gradient data were derived from the difference in total magnetic intensity recorded at the wingtip sensors #1 and #2 divided by the separation across the wings, which is 19.2 m for C-GSGW and C-GSGV, and 19.0 m for C-GSGL. The along-aircraft gradient is derived from all sensors, being the difference in total magnetic intensity between the mean value of the wingtip sensors #1 and #2 and the tail sensor #3 divided by the longitudinal separation along the aircraft body, which is 11.0 m for C-GSGL and C-GSGV, and 10.9 m for C-GSGW.

The across and along the aircraft gradients and the azimuth of the aircraft, available from the aircraft avionics, are combined to calculate the horizontal and longitudinal gradients with respect to the survey lines, so that positive gradients are eastward and northward, respectively. After correcting for orientation, there remains an inherent directional bias in the horizontal gradients because of the different sensors employed on the aircraft. An algorithm based on comparing the average value of a line compared to the global average was used to apply a zeroth order shift to the lateral and longitudinal gradient for every traverse line.

Lateral and longitudinal gradients were then "levelled" to gradients derived from the tail sensor total magnetic intensity (TMI). This was done by taking the difference between the measured and derived gradients, applying a moving 175-point filter, and adding back the filtered difference.

The 2 horizontal gradients, lateral gradient and longitudinal gradient, can be utilized to create a first vertical derivative using the Hilbert transform relationship (Nabighian 1984). Once the Hilbert transform had been applied to the lateral and longitudinal gradients, the outputs were summed to create a first vertical derivative grid. The first vertical derivation was then integrated to create a gradient-enhanced TMI.

However, the integrated gradient-enhanced TMI does not contain the long wavelength signal that is well sampled and retained in the single-sensor TMI data. To account for this, the long wavelength magnetic anomaly must be recovered. This was achieved by analysis of the power spectrum of the integrated data. The wavelength at which the power drops off was determined to be at 3.0 km, so a low-pass second-order Butterworth filter was applied to the single-sensor TMI data using this value as the cut off to isolate the missing long wave content of the integrated data. The long wavelength data were then added to the integrated data to create the gradient-enhanced TMI grid.

The International Geomagnetic Reference Field (IGRF) was then calculated from the 2015 model year extrapolated to 2018.584 (August 1, 2018) at the mean survey elevation of 484.63 m above the WGS84 ellipsoid and removed from the corrected values to generate the enhanced residual magnetic anomaly field.

The gradient-enhanced residual magnetic anomaly was then subjected to the GSC-levelling procedure (*see* section 5.4.4. "Geological Survey of Canada Data Levelling").

All grids generated during this procedure were created using a minimum curvature algorithm and a cell size of 50 m.

5.4.4. GEOLOGICAL SURVEY OF CANADA DATA LEVELLING

In 1989, as part of the requirements for the contract with the Ontario Geological Survey to compile and level all existing Geological Survey of Canada aeromagnetic data (flown prior to 1989) in Ontario, Paterson, Grant and Watson Limited developed a robust method to level the magnetic data of various base levels to a common datum provided by the GSC as 812.8 m grids. The essential theoretical aspects of the levelling methodology were fully discussed by Gupta et al. (1989) and Reford et al. (1990). The method

was later applied to the remainder of the GSC data across Canada and the high-resolution airborne magnetic and electromagnetic surveys flown by the OGS (Ontario Geological Survey 2003a). It has since been applied to all newly acquired OGS aeromagnetic surveys.

a) Terminology

- Master grid: refers to the 200 m Ontario magnetic grid compiled and levelled to the 812.8 m magnetic datum from the GSC
- GSC levelling: the process of levelling profile data to a master grid, first applied to GSC data
- Intrasurvey levelling or microlevelling: refers to the removal of residual line noise described earlier in this chapter; the wavelengths of the noise removed are usually shorter than tie-line spacing
- Intersurvey levelling or GSC levelling: refers to the level adjustments applied to a block of data; the adjustments are the long wavelength (in the order of tens of kilometres) differences with respect to a common datum, in this case, the 200 m Ontario master grid, which was derived from all pre-1989 GSC magnetic data and adjusted, in turn, by the 812.8 m GSC Canada-wide grid

b) The GSC-Levelling Methodology

The GSC-levelling methodology is described below, using, as an example, the Ramsey–Algoma survey flown for the OGS. This procedure was applied to the gradient-enhanced residual magnetic field.

Several data processing procedures are assumed to be applied to the survey data prior to levelling, such as microlevelling, IGRF calculation and removal. The final levelled data are gridded at 1/5 of the line spacing. If a survey was flown as several distinct blocks with different flight directions, then each block is treated as an independent survey.

The steps in the GSC levelling process were as follows:

1. Create an upward continuation of the survey grid to 305 m.

   Almost all recent surveys (1990 and later) to be compiled were flown at a nominal terrain clearance of 100 m or less. The first step in the levelling method was to upward continue the survey grid to 305 m, the nominal terrain clearance of the Ontario master grid (Figure 4).

   The grid cell size for the survey grids was set at 100 m. Since the wavelengths of level corrections will be greater than 10 to 15 km, working with 100 m or even 200 m grids at this stage will not affect the integrity of the levelling method. Only at the very end, when the level corrections were imported into the databases, will the level correction grids be regridded to 1/5 of line spacing.

   The unlevelled 100 m grid was extended by at least 2 grid cells beyond the actual survey boundary, so that in the subsequent processing, all data points are covered.

2. Create a difference grid between the survey grid and the Ontario master grid.

   The difference between the upward-continued survey grid and the Ontario master grid, regridded at 100 m, was computed (Figure 5). The short wavelengths represent the higher resolution of the survey grid. The long wavelengths represent the level difference between the 2 grids.

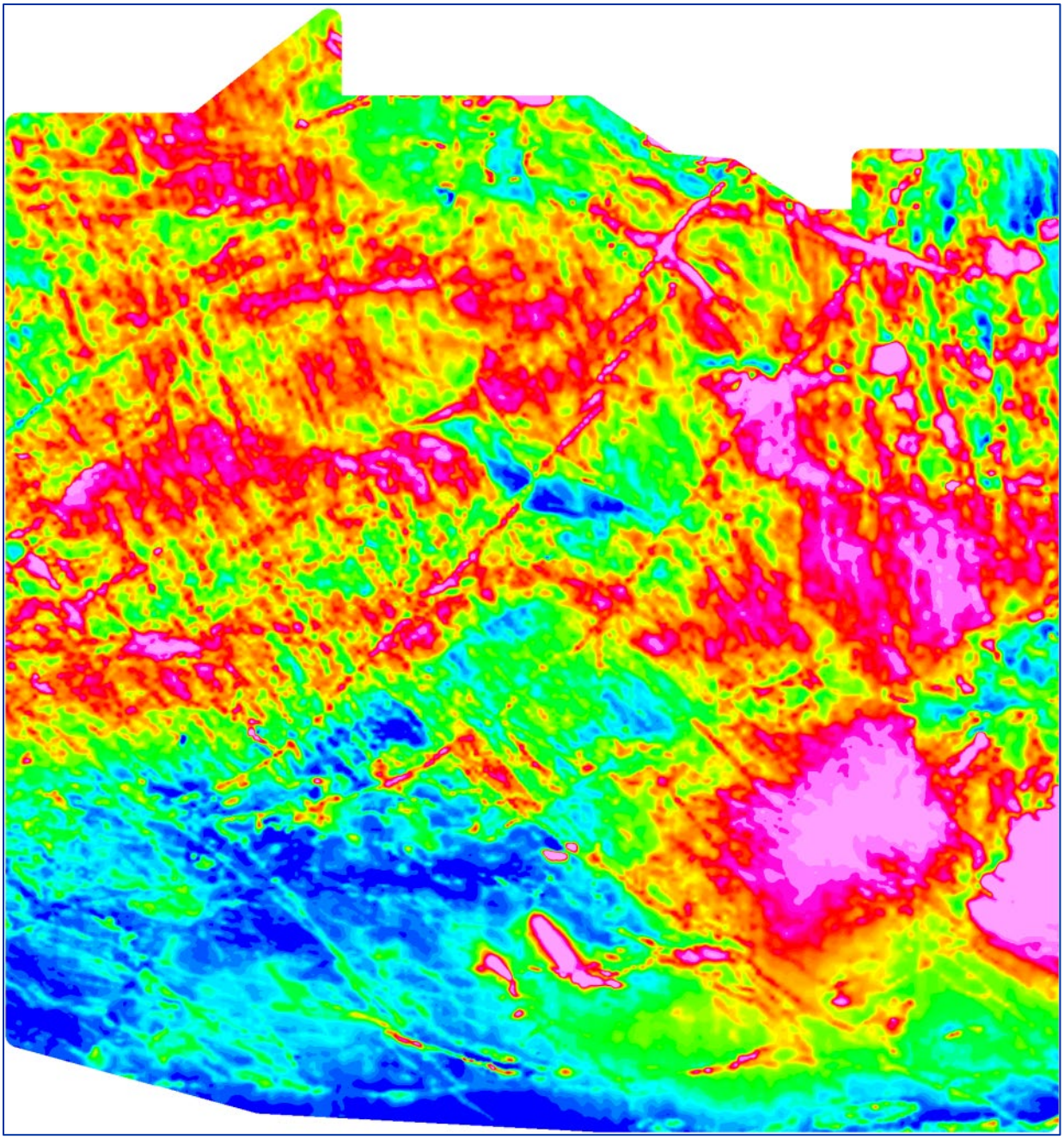

Figure 4. Ontario master aeromagnetic grid (Ontario Geological Survey 2003b). The outline for the sample data set to be levelled, using the Ramsey–Algoma survey area as the example, is shown.

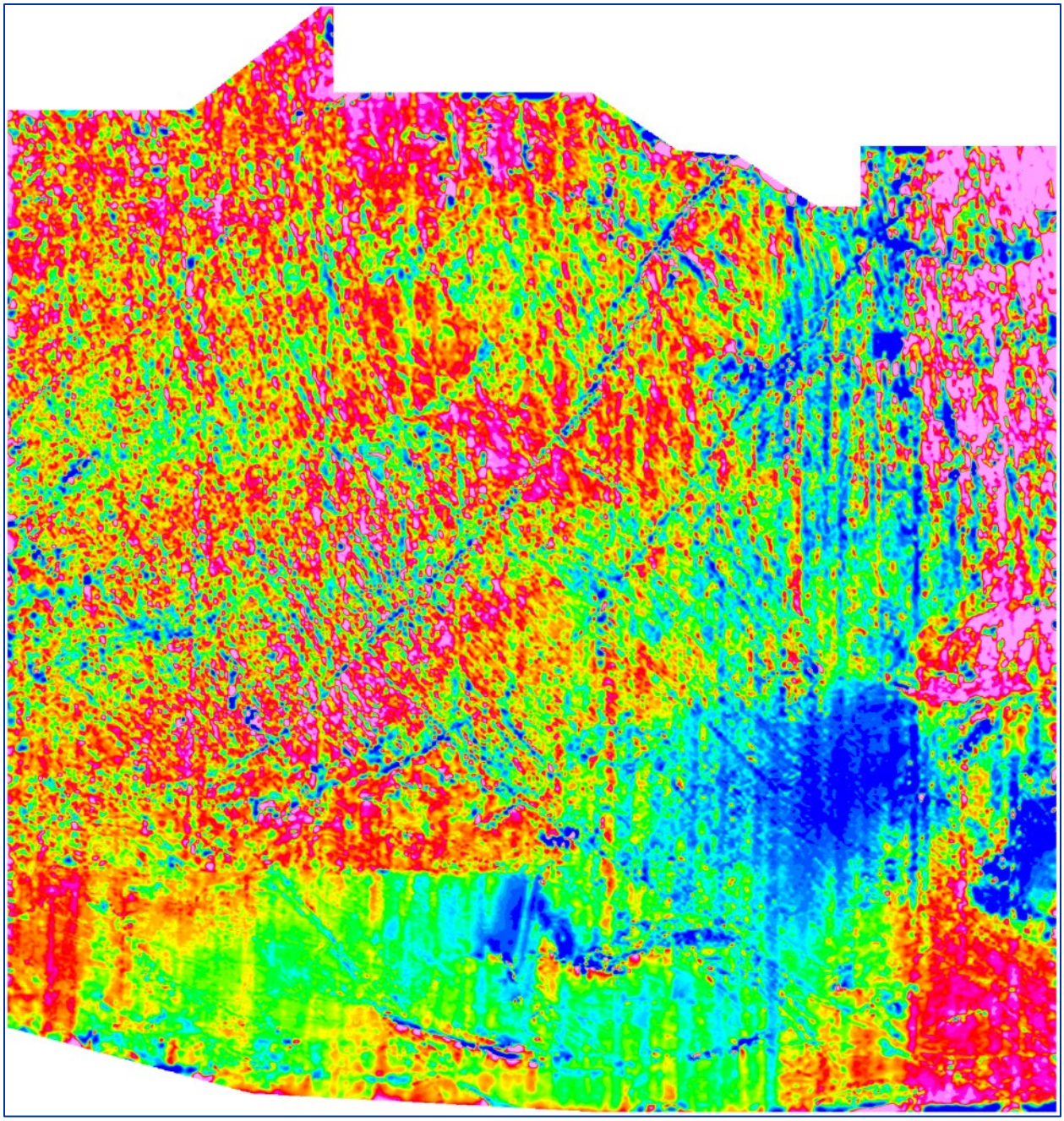

Figure 5. Difference grid (difference between survey grid and master grid), using the Ramsey–Algoma survey as the example.

3. Rotate difference grid so that flight-line direction is parallel with grid column or row, if necessary.
4. Apply the first pass of a nonlinear filter (Naudy and Dreyer 1968) of wavelength on the order of roughly half the length of the shortest dimension of the grid along the flight-line direction. Reapply the same nonlinear filter across the tie-line direction.
5. Apply the second pass of a nonlinear filter with approximately 1/2 the filter cut-off from the previous step along the flight-line direction. Reapply the same nonlinear filter across the tie-line direction.
6. Rotate the filtered grid back to its original (true) orientation (Figure 6).
7. Apply a low-pass filter to the nonlinear filtered grid.
8. Streaks may remain in the nonlinear filtered grid, mostly caused by edge effects. They must be removed by a frequency-domain, low-pass filter with a wavelength cut-off sufficient to remove these streaks (Figure 7).
9. Regrid to 1/5 line spacing and import level corrections into database.
10. Subtract the level correction channel from the unlevelled channel to obtain the level corrected channel.
11. Make final grid using the gridding algorithm of choice with grid cell size at 1/5 of line spacing.

c) Survey Specific Parameters

The following GSC-levelling parameters were used in the Ramsey–Algoma survey:

- Upward continuation distance: 205 m
- First pass nonlinear filter length: 80 000 m
- Second pass nonlinear filter length: 40 000 m
- Low-pass filter cut-off wavelength: 100 000 m

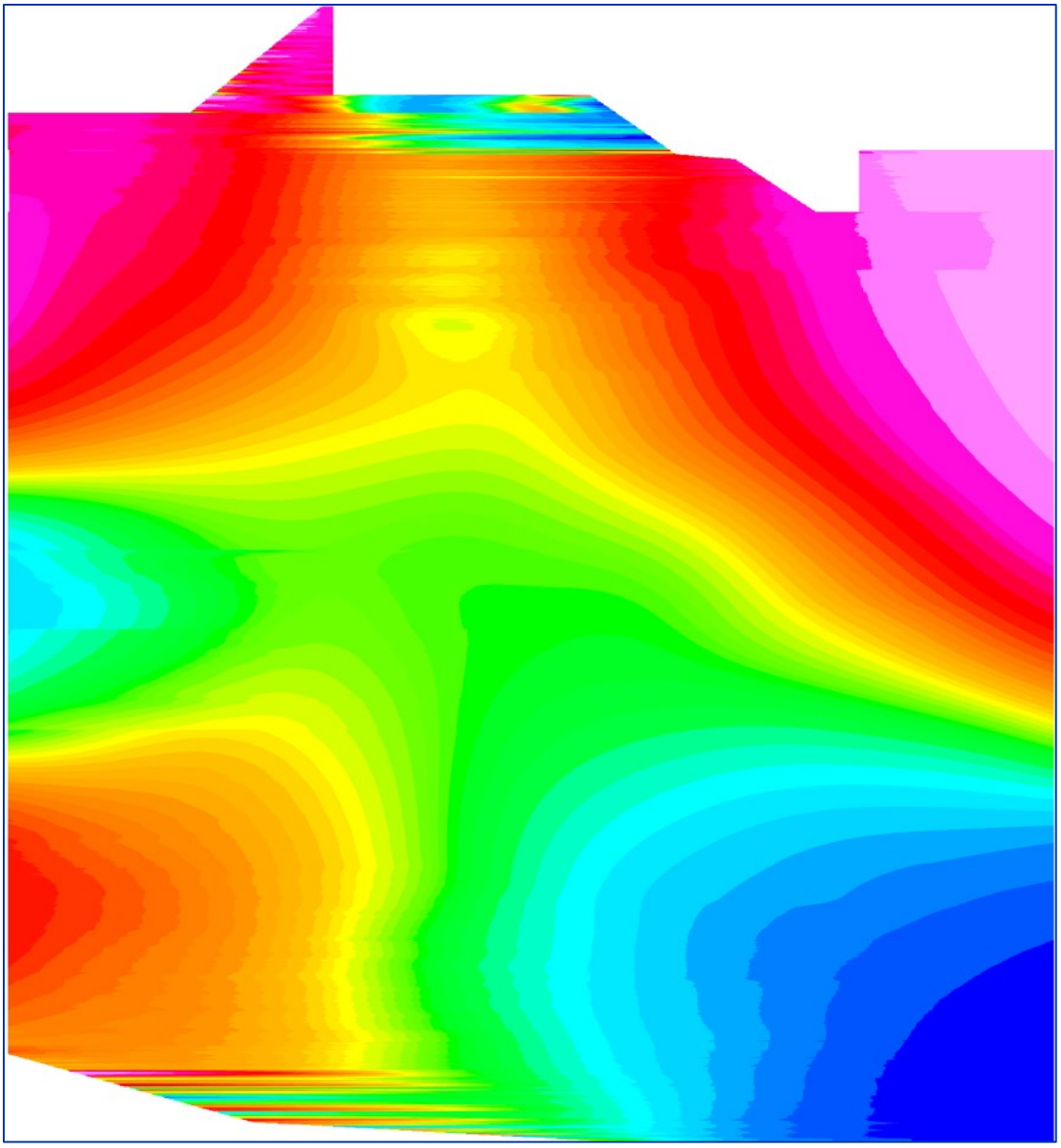

Figure 6. Difference grid after application of nonlinear filtering and rotation, using the Ramsey–Algoma survey as the example.

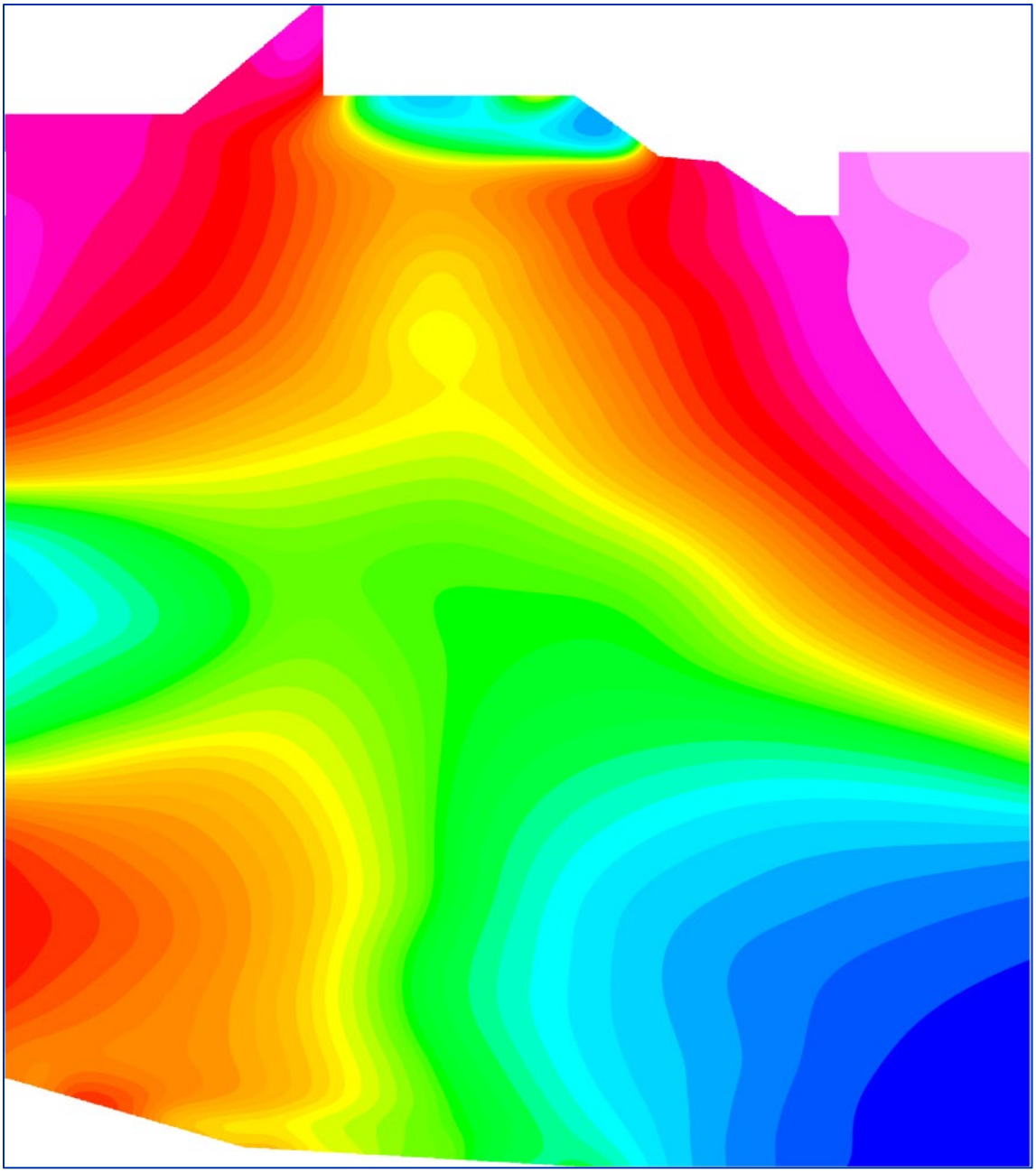

Figure 7. Level correction grid, using the Ramsey–Algoma survey as the example.

5.4.5. FINAL MAGNETIC FIELD AND SECOND VERTICAL DERIVATIVE GRIDS

After GSC levelling was applied to the gradient-enhanced residual magnetic field data, they were used to create derivative grids. The magnetic grids were calculated from the final reprocessed profiles using a bidirectional minimum curvature algorithm (Briggs 1974). The accuracy standard for gridding is that the grid values fit the profile data to within 0.001 nT for 99.99% of the profile data points, for 100 iterations (or 0.00001 nT/m for the horizontal gradient data). The average gridding error is well below 0.1 nT.

Minimum curvature gridding provides the smoothest possible grid surface that also honours the profile line data. However, sometimes this can cause narrow linear anomalies cutting across flight lines to appear as a series of isolated spots. This effect is minimized in the gradient-enhanced GSC-levelled magnetic grid, and as a result it was used for the map products.

The final GSC-levelled gradient-enhanced grid values were then used as input to create the second vertical derivative grids.

5.4.6. CALCULATION OF THE KEATING COEFFICIENTS

Possible kimberlite targets were identified from the GSC-levelled gradient enhanced residual magnetic intensity data, based on the identification of roughly circular anomalies. This procedure was automated by using a known pattern recognition technique (Keating 1995, 2001), which consists of computing, over a moving window, a first-order regression between a vertical cylinder model anomaly and the gridded magnetic data. Only the results where the absolute value of the correlation coefficient is above a threshold of 75% were retained. On the magnetic maps, the results are depicted as circular symbols, scaled to reflect the correlation value. The most favourable targets are those that exhibit a cluster of high-amplitude solutions. Correlation coefficients with a negative value correspond to reversely magnetized sources.

The cylinder model parameters are as follows:

- Cylinder Radius 100 m
- Cylinder length: infinite
- Overburden thickness: 5.9 m
- Magnetic inclination: 72.2° N
- Magnetic declination: 9.2° W
- Window size: 800 m x 800 m
- Susceptibility: 0.005

An example of the model's magnetic response is shown in Figure 8.

It is important to be aware that other magnetic sources may correlate well with the vertical cylinder model, whereas some kimberlite pipes of irregular geometry may not. The user should study the magnetic anomaly that corresponds with the Keating symbols, to determine whether it does resemble a kimberlite pipe signature, reflects some other type of source or even noise in the data, e.g., boudinage (beading) effect of the minimum curvature gridding. All available geological information should be incorporated in kimberlite pipe target selection.

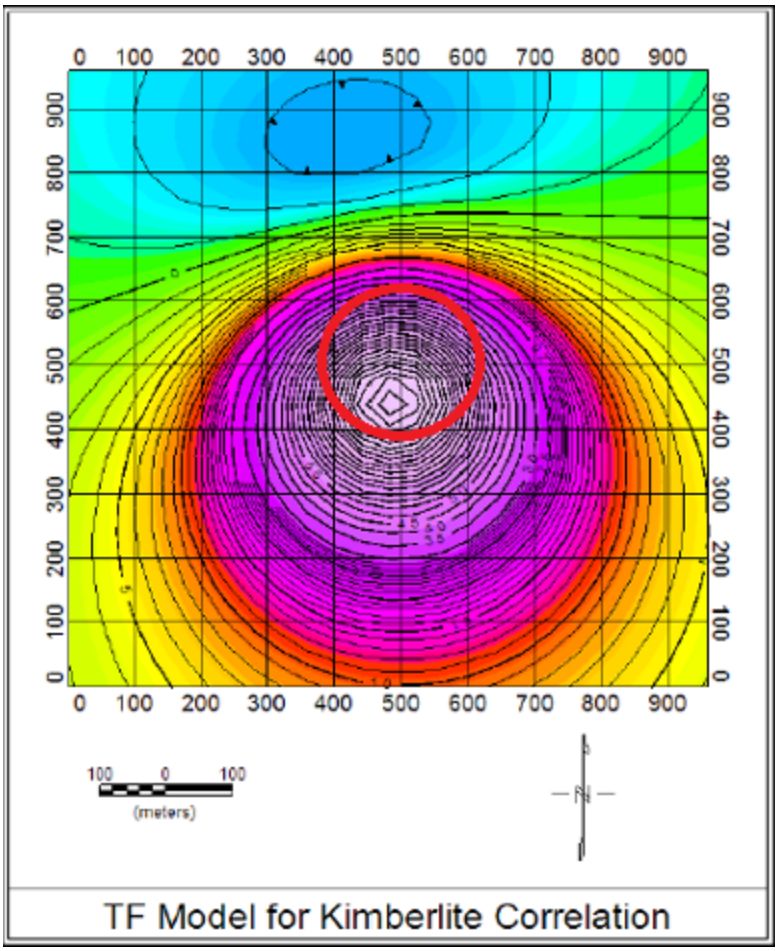

Figure 8. Vertical cylinder anomaly model used for Keating correlation.

5.5. PROCESSING OF RADIOMETRIC DATA

A spectrometer data compilation flow chart is presented in Figure 9.

A 0.5 second lag correction was applied to all data to correct for the time delay between detection and recording of the airborne data. The data were recorded at 1 Hz in asynchronous mode, and subsequently interpolated to 1 Hz synchronous data on the exact second.

5.5.1. SPECTRAL COMPONENT ANALYSIS

Raw 256-channel spectrometer data were analyzed using noise-adjusted singular value decomposition (NASVD) described by Hovgaard and Grasty (1997). Normalization with respect to the count rate is achieved by dividing each measured spectrum by the square root of the best fit of the mean spectra, i.e., component zero. The NASVD method determines the components in order of significance with respect to the amount of variance in the data they describe. Each component is a spectrum with 256 channels for the Exploranium™ system. In theory, there are as many components as there are channels. Variation in the signal is accounted for by the low-order components, and variation resulting from noise is accounted for by the higher order components. Spectra are reconstructed from the low-order signal–only components, and the count rates in the standard windows are recalculated.

Through such an analysis, it was determined that components 0–6 from the Exploranium™ system contained signal. Only these components were used in the final data. Figure 10 shows charts of the significant NASVD components.

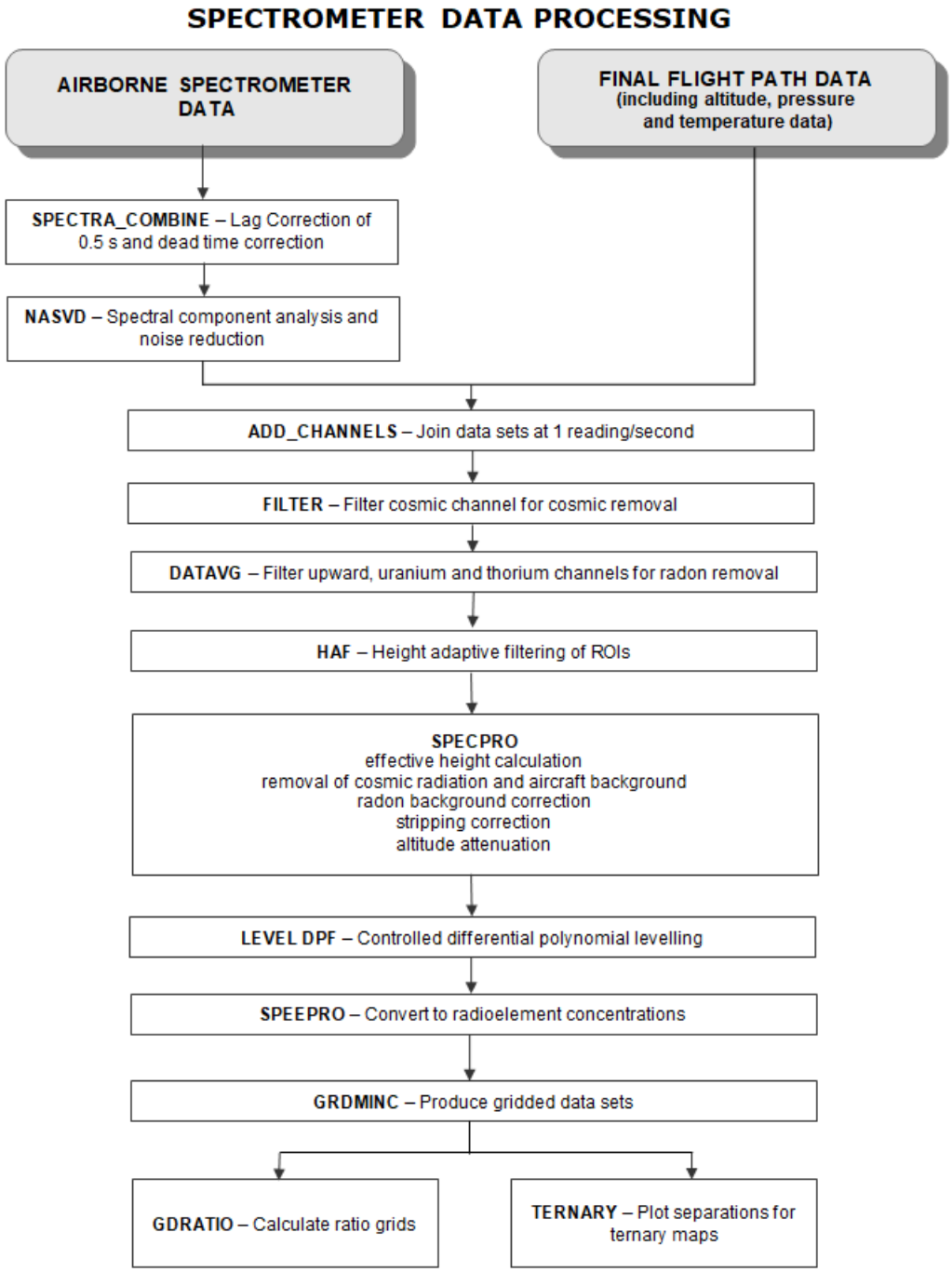

Figure 9. Spectrometer data compilation flow chart.

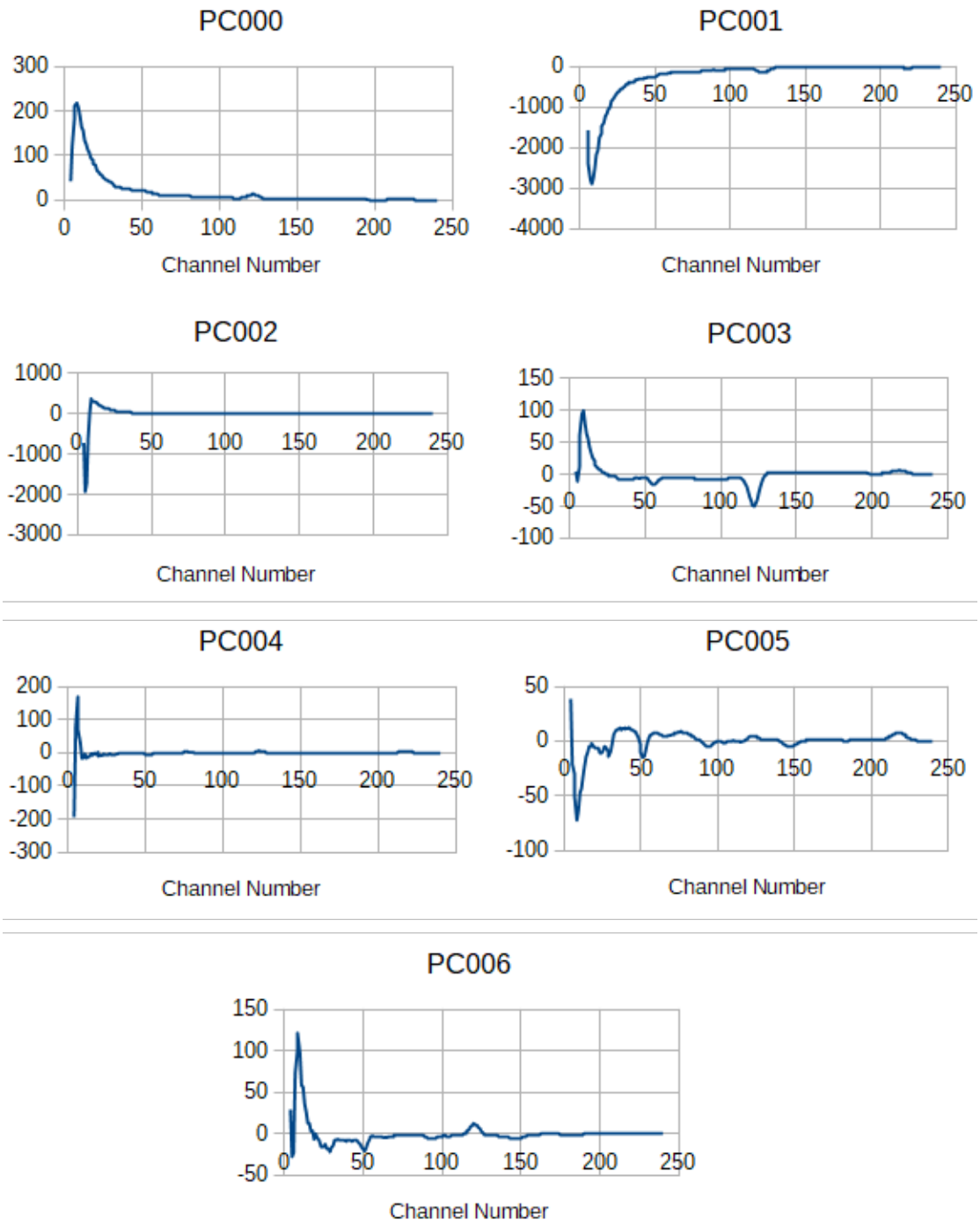

Figure 10. NASVD spectrometer components used in data processing.

5.5.2. STANDARD CORRECTIONS

Spectrometer data were corrected as documented in reports by Grasty (1972) and the International Atomic Energy Agency (1991). The gamma-ray spectroscopy processing parameters are shown in Tables 4, 5 and 6. The parameters are based on the calibrations described in Appendix A, but adjusted as deemed necessary during processing.

Table 4. Spectrometer processing parameters for C-GSGV.

Spectrometer Processing Parameters C-GSGV		
Window	**Cosmic Stripping Ratio (b)**	**Aircraft Background (a)**
Total	0.7331	36.98
Potassium	0.0433	5.81
Uranium	0.0334	0.89
Thorium	0.0363	0.00
Upward	0.0080	0.25
Radon Component	**a**	**b**
Total (I_r)	13.7075	2.9964
Potassium (K_r)	0.7343	0.3025
Thorium (T_r)	0.0368	0.00
Upward (u_r)	0.2159	0.1220
Ground Component	**a_1**	**a_2**
Upward (u_g)	0.0242	0.0187
Stripping Ratios	**Contribution on the Ground**	**Effective Height Adjustment (m^{-1})**
α	0.2414	0.00049
β	0.3719	0.00065
γ	0.7152	0.00069
a	0.0424	
b	0.0014	
g	0.0103	
Attenuation Coefficients (m^{-1})		
Total	−0.006413	
Potassium	−0.007974	
Uranium	−0.006992	
Thorium	−0.006297	
Sensitivities		
Total Counts	26.8838 cps/(nGy/h)	
Potassium	85.3183 cps/%	
Uranium	6.6074 cps/eU ppm	
Thorium	5.2263 cps/eTh ppm	

Table 5. Spectrometer processing parameters for C-GSGW.

Spectrometer Processing Parameters C-GSGW		
Window	**Cosmic Stripping Ratio (b)**	**Aircraft Background (a)**
Total	0.6746	66.49
Potassium	0.0392	11.83
Uranium	0.0297	1.95
Thorium	0.0347	0.00
Upward	0.0074	0.47
Radon Component	**a**	**b**
Total (I_r)	13.7421	16.3564
Potassium (K_r)	0.6986	5.4848
Thorium (T_r)	0.0336	0.00
Upward (u_r)	0.2036	0.0847
Ground Component	**a_1**	**a_2**
Upward (u_g)	0.0242	0.0169
Stripping Ratios	**Contribution on the Ground**	**Effective Height Adjustment (m^{-1})**
α	0.2197	0.00049
β	0.4078	0.00065
γ	0.7051	0.00069
a	0.0413	
b	0.00	
g	0.0018	
Attenuation Coefficients (m^{-1})		
Total	−0.006754	
Potassium	−0.008206	
Uranium	−0.007157	
Thorium	−0.006907	
Sensitivities		
Total Counts	26.8838 cps/(nGy/h)	
Potassium	68.79072 cps/%	
Uranium	7.10198cps/eU ppm	
Thorium	4.58003 cps/eTh ppm	

Table 6. Spectrometer processing parameters for C-GSGL.

Spectrometer Processing Parameters C-GSGL		
Window	**Cosmic Stripping Ratio (b)**	**Aircraft Background (a)**
Total	0.6196	38.47
Potassium	0.0369	7.07
Uranium	0.0285	0.10
Thorium	0.0293	0.00
Upward	0.0070	0.11
Radon Component	**a**	**b**
Total (I_r)	14.0379	6.9613
Potassium (K_r)	0.7220	2.1512
Thorium (T_r)	0.0801	0.00
Upward (u_r)	0.2039	0.0717
Ground Component	**a_1**	**a_2**
Upward (u_g)	0.0249	0.0178
Stripping Ratios	**Contribution on the Ground**	**Effective Height Adjustment (m^{-1})**
α	0.2283	0.00049
β	0.3793	0.00065
γ	0.7075	0.00069
a	0.0387	
b	0.00	
g	0.0029	
Attenuation Coefficients (m^{-1})		
Total	−0.006741	
Potassium	−0.008075	
Uranium	−0.006911	
Thorium	−0.006546	
Sensitivities		
Total Counts	26.8838cps/(nGy/h)	
Potassium	79.3612cps/%	
Uranium	7.5443 cps/eU ppm	
Thorium	4.9875 cps/eTh ppm	

Before gridding, the following corrections were applied to the spectrometer data, in the order described in sections 5.5.3 to 5.5.12.

5.5.3. DEAD-TIME CORRECTION

The system live time was recorded by the Exploranium™ spectrometer and represents the time that the system was available to accept incoming gamma radiation pulses. Live time is reduced, and dead-time increased, as count rates increase and the time taken by the spectrometer to process measured pulses increases. The cosmic channel does not receive a dead-time correction as it is processed by separate circuitry in a GR-820 spectrometer. The dead-time correction was applied to each window in both the upward- and downward-looking detector data using the following equation:

$$N = \frac{n}{t}$$

where, N = the corrected count rate in each channel;
n = the raw count recorded in each second; and
t = the recorded live time (fraction of a second).

5.5.4. CALCULATION OF EFFECTIVE HEIGHT ABOVE GROUND LEVEL (AGL)

A 67-point low-pass filter was applied to 10 Hz radar altimeter data, and all of the 10 Hz barometric altimeter data were filtered with a low-pass frequency domain filter (cosine taper between 42 and 47 seconds). The barometric altimeter data were then converted to equivalent pressure and used with the digitally recorded temperature to convert the radar altimeter data to effective height at standard pressure and temperature (STP) as follows:

$$h_e = h \times \frac{273.15}{T + 273.15} \times \frac{P}{101.325}$$

where, h_e = the effective height;
h = the observed radar altitude in metres;
T = the observed air temperature in degrees Celsius; and
P = the observed barometric pressure in millibars.

5.5.5. HEIGHT ADAPTIVE FILTER

Adaptive filters were applied between 330 m and 380 m effective height to improve the signal-to-noise ratio. A moving average filter was applied to data flown at 330 m and above and the degree of filtering applied increased gradually up to a maximum 3-point average at 380 m.

5.5.6. REMOVAL OF COSMIC RADIATION AND AIRCRAFT BACKGROUND RADIATION

A 67-point low-pass filter was applied to 1 Hz cosmic data to reduce statistical noise. Cosmic radiation and aircraft background radiation were removed from each spectral window using the cosmic coefficients and aircraft background values determined from test flight data using the following equation:

$$N = a + b \times C$$

where, N = the combined cosmic and aircraft background in each spectral window;
a = the aircraft background in the window;
b = the cosmic stripping factor for the window; and
C = the cosmic channel count.

5.5.7. RADON BACKGROUND CORRECTIONS

A 199-point average low-pass filter was applied to 1 Hz downward uranium, downward thorium and upward uranium count data for the purposes of the radon correction only. The radon component in the uranium window was calculated using the radon coefficients determined from the survey data using the following equation:

$$U_r = \frac{u - a_1 U - a_2 T + a_2 b_T - b_u}{a_u - a_1 - a_2 a_T}$$

where, U_r = the radon background measured in the downward uranium window;
u = the filtered observed count in the upward uranium window;
U = the filtered observed count in the downward uranium window;
T = the filtered observed count in the downward thorium window;
a_1 and a_2 = the ground coefficients;
a_u and b_u = the radon coefficients for uranium; and
a_T and b_T = the radon coefficients for thorium.

The radon counts in the uranium upward window and the potassium, thorium and total count downward windows were calculated from U_r using the following equations:

$$\begin{aligned} u_r &= a_u U_r + b_u \\ K_r &= a_K U_r + b_K \\ T_r &= a_T U_r + b_T \\ I_r &= a_I U_r + b_I \end{aligned}$$

where, u_r = the radon component in the upward uranium window;
K_r, U_r, T_r and I_r = the radon components in the various windows of the downward detectors; and
a and b = the radon calibration coefficients.

5.5.8. STRIPPING

The stripping ratios for the spectrometer system were determined experimentally. The stripped count rates for the potassium, uranium and thorium downward windows were calculated using the following equations:

$$N_K = \frac{n_{Th}(\alpha\gamma - \beta) + n_U(\alpha\beta - \gamma) + n_K(1 - a\alpha)}{A}$$

$$N_U = \frac{n_{Th}(g\beta - \alpha) + n_U(1 - b\beta) + n_K(b\alpha - g)}{A}$$

$$N_{Th} = \frac{n_{Th}(1 - g\gamma) + n_U(b\gamma - a) + n_K(ag - b)}{A}$$

where, A has the value:

$$A = 1 - g\gamma - a(\gamma - gb) - b(\beta - \alpha\gamma)$$

and where, n_K, n_U and n_{Th} = the unstripped potassium, uranium and thorium downward windows counts;
N_K, N_U and N_{Th} = the stripped potassium, uranium and thorium downward windows counts;
α, β and γ = the forward stripping ratios; and
a, b and g = the reverse stripping ratios.

Stripping ratios α, β and γ are adjusted for effective height (as calculated above) by standard factors, which are provided in Tables 4, 5 and 6 (spectrometer processing parameters).

5.5.9. ALTITUDE ATTENUATION CORRECTION

This correction normalizes the data to a constant terrain clearance of 100 m above ground level (agl) at standard temperature and pressure (STP). Attenuation coefficients for each of the downward windows were determined from test flights. The measured count rate is related to the actual count rate at the nominal survey altitude by the equation:

$$N_s = N_m(e^{\mu(h_o - h)})$$

where, N_s = the count rate normalized to the nominal survey altitude, h_o;
N_m = the background corrected, stripped count rate at effective height, h;
μ = the attenuation coefficient for that window;
h_o = the nominal survey altitude; and
h = the effective height.

The effective height was determined as described above.

5.5.10. LEVELLING

Following the method of Beiki, Bastani and Pedersen (2010), differential polynomial levelling was used to correct for precipitation and residual radon effects in the measured uranium channel. The algorithm is based on polynomial fitting of data points in 1-D and 2-D sliding windows. The levelling error is taken as the difference between 1-D and 2-D polynomial fitted data at the centre of the windows. Polynomials of order 1 were used along with a search radius of 750 m for all components, and the long wavelength (>200 s) correction for the line was applied to bring each line to the same zero-base level. Upon examining the gridded data together with the test line data, it was determined that some additional levelling corrections to the uranium data for residual radon effects were required. Manual adjustments to the line-by-line levelling were then applied to render the correctly levelled uranium channel. Refer to Table 42 in Appendix C for the lines that were corrected, together with the correction value and range of time applied.

5.5.11. CORRECTIONS FOR HIGH CLEARANCE

An additional correction for high clearance areas was applied to the uranium data collected at a survey height exceeding 200 m. This was done in an effort to minimize the impact of statistical noise and the increased amplification of background determination errors. This was achieved by scaling the levelled uranium channel by 0.70 in areas where the effective height exceeds 200 m and there was insufficient signal. In this case, insufficient signal was defined as a measured count rate below 15 cps.

5.5.12. CONVERSION TO RADIOELEMENT CONCENTRATION

Sensitivities were determined experimentally from the test flight data. The units of the count rates in each spectral window were converted to “apparent radioelement concentrations” using the following equation:

$$C = \frac{N}{S}$$

where, C = the concentration of the element(s);
N = the count rate for the window after correction for dead time, background, radon, stripping and attenuation; and
S = the broad source sensitivity for the window.

Potassium concentration is expressed as a percentage and equivalent uranium (eU) and equivalent thorium (eTh) are expressed as parts per million using instruments that are calibrated with respect to the International Atomic Energy Agency (IAEA) reference materials (International Atomic Energy Agency 2010). Uranium and thorium are described as "equivalent" because their presence is inferred from gamma-ray radiation from daughter elements (^{214}Bi for uranium, ^{208}Tl for thorium). The air absorbed dose rate (ADR) was determined from the concentrations of the radioelements using the following formula:

$$\text{ADR} = (13.078 \times \%\text{K}) + (5.675 \times \text{ppm eU}) + (2.494 \times \text{ppm eTh})$$

The average ADR and total counts rate were determined from the calibration test range and a conversion factor was calculated that was then applied to the survey total count data on a point-by-point basis.

5.5.13. DATA GRIDDING

Grids were made using a minimum curvature algorithm to create a two-dimensional grid equally sampled in the x and y directions. The algorithm produces a smooth grid by iteratively solving a set of difference equations minimizing the total second horizontal derivative while attempting to honour the input data (Briggs 1974). The final grids of the radiometric data were created with 50 m grid cell size appropriate for survey lines spaced at 250 m.

5.5.14. MICROLEVELLING

Some variations in background and in ground conditions persist after all previous adjustments are made. The combination of residual background variations and changes ground conditions are corrected by microlevelling. This was achieved by using a combined directional cosine filter and high-pass Butterworth filter to identify and remove artefacts that are long wavelength parallel to survey lines and short wavelengths perpendicular to survey lines. Microlevelling corrections were limited to ±0.7 nGy/hr (total counts), ±0.05% (potassium), ±0.50 ppm (uranium) and ±0.50 ppm (thorium).

5.5.15. CALCULATION OF THE ELEMENTAL RATIOS

Ratios of potassium to thorium concentrations were calculated, in grid form, using a procedure originally designed by the GSC.

In order to eliminate calculation of ratios at those locations most likely to be over water, an initial standard is required at each grid cell before a ratio is calculated. The potassium concentration must be ≥0.25%. Otherwise, the ratio for that cell is set to null.

In order to reduce fluctuations caused by limited statistical certainty in the final radioelement concentrations, further minimum standards are set for each ratio calculation. These are somewhat arbitrarily selected to equate to a corrected region-of-interest count rate of about 100 counts per second for each element. For this spectrometer survey, these numbers are derived from the average sensitivities of the 3 spectrometers employed and have the following values:

$$K \geq 0.4368\%$$
$$\text{eTh} \geq 8.1235 \text{ ppm}$$

where, K = the concentration of potassium (%); and
eTh = the equivalent concentration of thorium (ppm)

In order to extend ratio values to those grid cells that fall below these minimum standards, a simple variable length filter was applied prior to ratio calculation. This consists of summing data from adjacent cells on each side of the initial grid cell, for both numerator and denominator, and checking to see if both now meet the required minima. If so, the ratio was calculated. If not, this process was continued to the next adjacent cells until a successful check is achieved or until a maximum distance to adjacent cells is reached. This maximum distance to adjacent cells has been set to 500 m for this survey. Any adjacent cells that already failed the 0.25% potassium concentration limit are not considered. If the minimum check fails after the maximum number of cells have been added, the ratio is set to null at the subject grid cell.

The ratio of potassium over equivalent thorium data channel is derived by sampling of the equivalent ratio grid along survey lines.

5.5.16. GENERATION OF THE TERNARY RADIOELEMENT IMAGE

The ternary map was produced by scaling the distribution of potassium, thorium and uranium against red, green and blue, respectively. In this case, the data were processed using the GSC S-Tergen utility, which normalizes the data and applies an optimum colour distribution. The algorithm used is as described in Broome et al. (1987).

6. Final Products

The following products were delivered to the ENDM.

1. Profile Databases

   Databases, in both Geosoft® *.gdb* and ASCII *.xyz* format, of the following, were provided:

   - magnetic line data archive
   - radiometric line data archive
   - radiometric line data array archive (256 channels)
   - Keating coefficient archive

2. Gridded Data

   Grids, in both Geosoft® *.grd* and Grid Exchange *.gxf* formats, gridded from co-ordinates in UTM Zone 17N, NAD83 CSRS, of the following data:

   - digital elevation model from laser altimeter
   - total magnetic field from the tail sensor
   - GSC-levelled, gradient-enhanced residual magnetic field
   - second vertical derivative of the GSC-levelled gradient-enhanced residual magnetic field
   - measured lateral horizontal gradient
   - measured longitudinal horizontal gradient
   - air-absorbed dose rate
   - potassium concentration
   - equivalent uranium concentration
   - equivalent thorium concentration
   - potassium over equivalent thorium ratio

3. Project Report
   Provided in portable document format (*.pdf*) and Word document (*.doc* or *.docx*)

4. Flight Videos
   The digitally recorded video from each survey flight are provided in a compressed binary format on a hard drive.

5. Maps
   Digital 1:50 000 scale maps (NAD83 CSRS UTM Zone 17N) in Geosoft® *.map* format, with a topographic layer, of the following:

   - colour-filled contours of gradient-enhanced residual magnetic field and flight lines (Figure 11) (with the following tile names and layout, where "m829xx" indicates OGS Map 829xx)

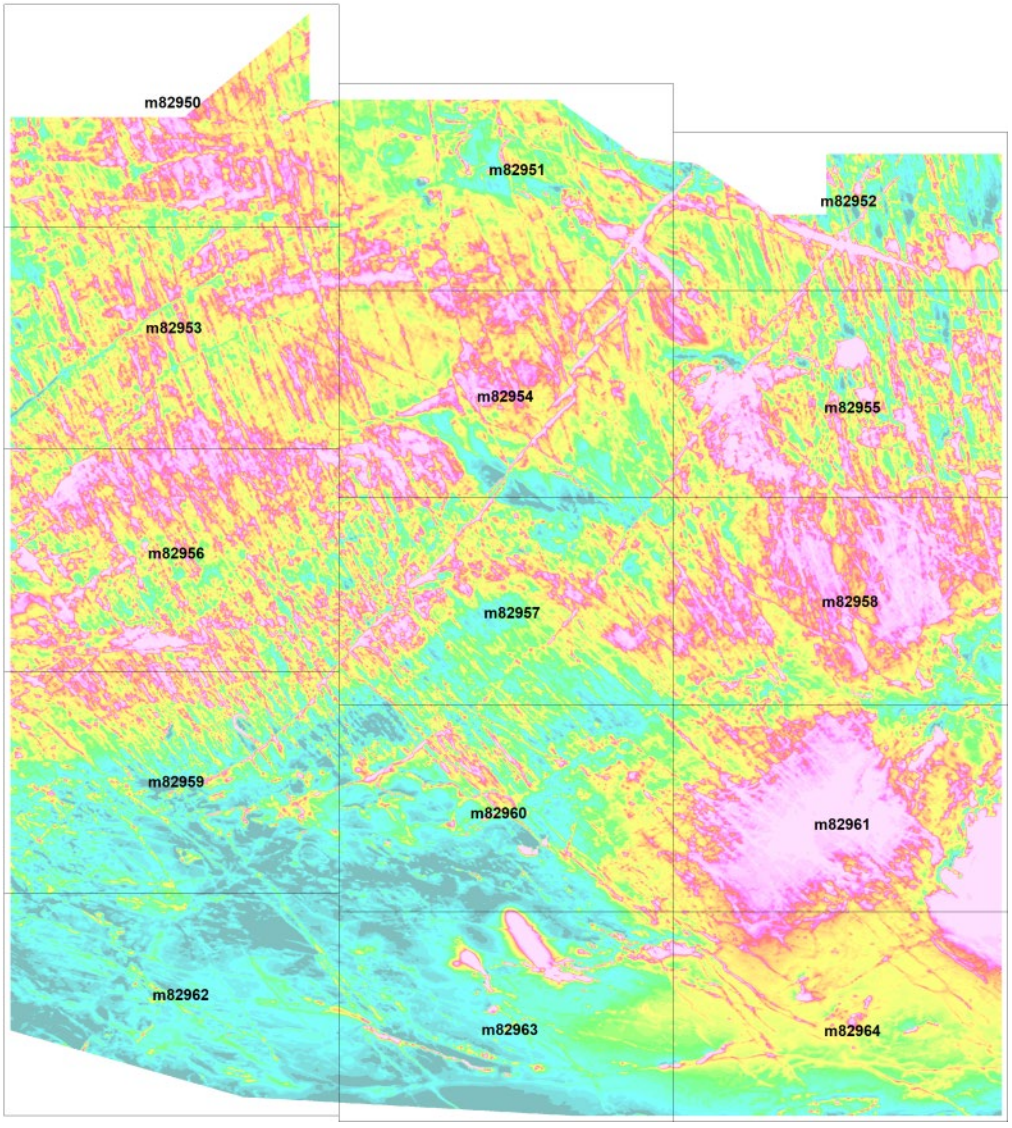

Figure 11. Gradient-enhanced residual magnetic field.

- shaded colour of the second vertical derivative of the gradient-enhanced residual magnetic field with Keating coefficients (Figure 12) (with the following tile names and layout, where "m829xx" indicates OGS Map 829xx)

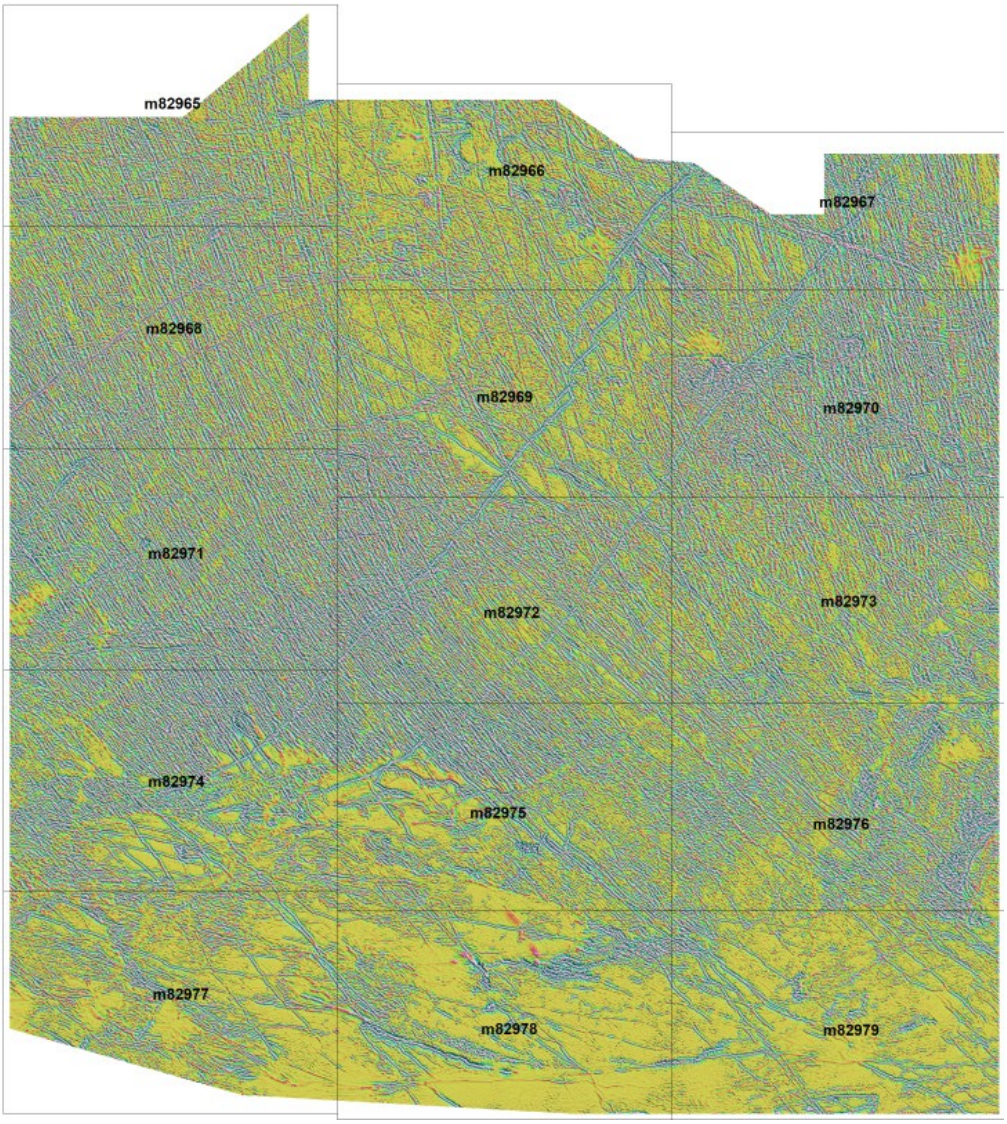

Figure 12. Second vertical derivative of the gradient-enhanced residual magnetic field.

- histogram-equalized ternary red, green and blue radioelement image with inset images of potassium, equivalent uranium, equivalent thorium and dose rate (Figure 13) (with the following tile names and layout, where “m829xx” indicates OGS Map 829xx)

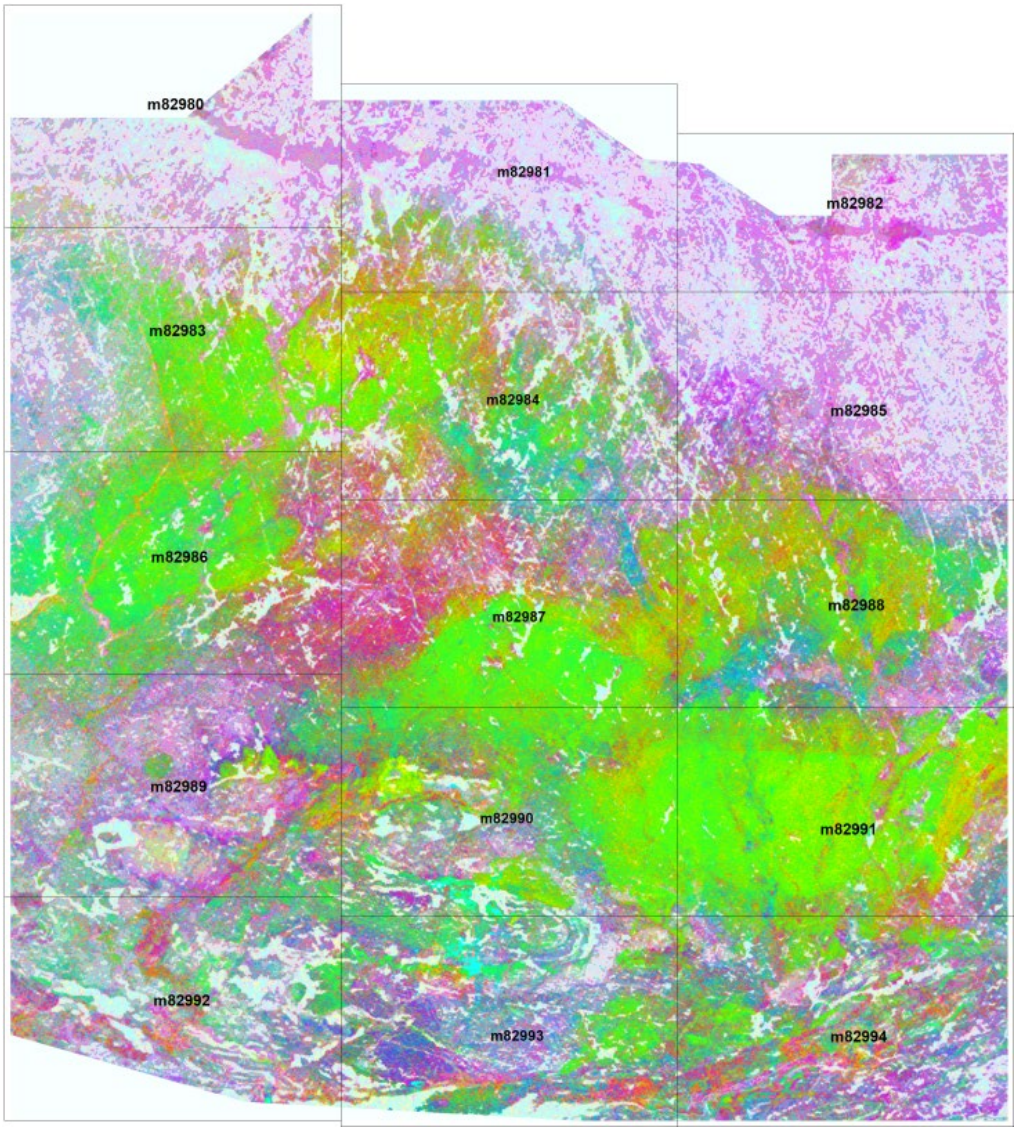

Figure 13. Histogram-equalized ternary red, green and blue radioelement image.

7. Quality Assurance and Quality Control

Quality assurance and quality control (QA/QC) were undertaken by the survey contractor Sander Geophysics Limited and Paterson, Grant & Watson Limited, as well as by ENDM. Stringent QA/QC is emphasized throughout the project so that the optimal geological signal is measured, archived and presented.

7.1. SURVEY CONTRACTOR

Important checks are required during the data acquisition stage to ensure that the data quality is kept within the survey specifications. The following lists, in detail, the standard data quality checks that were performed by SGL during the course of the survey.

7.1.1. TESTS AND CALIBRATIONS

The full results of the tests and calibrations described below are provided in Appendix A.

1. Magnetometer Lag Test (Appendix A: Figures 14 to 31)

   To verify the magnetic system latency, the survey aircraft conducted lag tests. These tests involve flying multiple passes over a known magnetic feature and comparing the position of the observed magnetic peaks with the known position of the target.

   Both prior to commencement and after completion of the survey, aircraft C-GSGL, C-GSGW and C-GSGV flew this test over a railway bridge near Ottawa.

   The calculated system latencies from these tests were determined to be consistent between the pre- and post-survey values and were consistent with previous tests performed by each aircraft.

2. Radar and Laser Altimeter Test (Appendix A: Figures 32 to 37)

   The radar altimeter calibration and verification were performed by acquiring altitude data from several passes of increasing altitude over the Gatineau Airport runway and Lac Dechenes. The radar altimeter of the aircraft was confirmed to have a linear relationship with and within acceptable range of the GPS height.

3. Magnetometer Figure of Merit Test (Appendix A: Figures 38 to 55; Table 7)

   Compensation calibrations determine the magnetic influence of aircraft and its manoeuvres. During the compensation calibration flight, the aircraft performs sets of 3 pitches (±5°), rolls (±10°) and yaws (±5°), while flying in the 4 flight-line directions at high altitude over a magnetically "quiet" area. The coefficients calculated from the calibration are applied to the acquired magnetometer data to measure the effectiveness of the compensation system in mitigating the magnetic interference.

   The total compensated signal noise resulting from the 12 manoeuvres, referred to as the Figure of Merit (FOM), is calculated from the maximum peak-to-peak value resulting from each manoeuvre. A new compensation calibration must be performed after any aircraft or system modifications that may affect the aircraft's magnetic field interference.

   In all calibrations performed by the aircraft, the resultant FOMs for the tail and wingtip sensors were below the specified threshold of 1.5 nT.

4. Magnetometer Heading Test (Appendix A: Figure 56; Tables 8 to 16)

   To verify system accuracy and acceptable heading error, a heading test was performed over the GSC magnetic observatory at Morewood, Ontario, prior to commencement of the survey. The aircraft performed 2 passes in each cardinal direction directly over the observatory and the aircraft measured total field was compared against the observatory data.

   For the calibration performed, the calculated heading errors were minimal, and the absolute accuracies were within the contract threshold of 10 nT.

5. Spectrometer Stripping Calibration (Appendix A: Tables 17 to 25)

   To determine the stripping ratios of each detector, calibrations were done in the SGL hangar using calibrated Geological Survey of Canada pads. Four concrete pads, 3 embedded with the region-of-interest radioelements and 1 "bare" pad for background corrections, were placed beneath detector packs installed in the aircraft. Data were then accumulated for approximately 30 minutes. The averaged count rates can then be used to compute the 6 stripping ratios for each spectrometer.

6. Spectrometer Dynamic Calibration Range (Appendix A: Figures 57 to 59; Tables 26 to 31)

   The aircraft performed a calibration flight over the Breckenridge radiometric test range near Ottawa, Ontario, to determine the radiometric system sensitivities and altitude attenuation factors. The aircraft repeated a 10 km test line and an adjacent over-water line (for background corrections) at altitudes of 60 to 240 m in 30 m increments.

   Simultaneously, actual ground concentrations were measured by a ground crew equipped with a calibrated hand-held Exploranium™ GR-320 spectrometer. At 8 predetermined stations along the survey test line, four 120-second sample accumulations were acquired, each approximately 15 m apart. The processed measurements are then averaged giving the ground concentrations in each window for the test line.

7. Cosmic and Aircraft Background Calibration (Appendix A: Figures 60 to 74; Tables 32 to 34)

   High-altitude cosmic calibration flight was performed by the aircraft after commencement to the survey. In this test, the aircraft climbed from 1500 m to 3500 m in increments of 500 m and accumulated approximately 10 minutes of data at each altitude. The resultant data determined the linear relationship between counts in the cosmic window and each region-of-interest window.

8. Radon Calibration (Appendix A: Figures 75 to 86; Tables 35 to 37)

   Radon background was monitored through the use of 2 upward- looking detectors. Coefficients relating the count rate in the uranium window from the upward detectors to the count rate in the potassium, uranium, thorium and total count windows from the downward-facing detectors were determined using over-water test lines flown over a large lake southwest of the Ramsey–Algoma survey area. The test line was flown 26 times by C-GSGL, 26 times by C-GSGV and 15 times by C-GSGW.

   The cosmic and background corrected data from each of the upward ("Up") (u_r), thorium (T_r), potassium (K_r) and total count (I_r) windows were plotted against the counts in the uranium (U_r) window for each over-water line flown. Linear regressions of these plots provided the radon coefficients used in the radiometric data processing.

7.1.2. DAILY QUALITY CONTROL

1. Navigation Data
    - The differentially corrected GPS flight track was recovered and matched against the theoretical flight path to ensure that any deviations are within the specifications (i.e., deviations not greater than 50 m from the nominal line spacing over a 2 km distance).
    - All altimeter data were checked for consistency and deviations in terrain clearance were monitored closely. The survey was flown in a smooth drape fashion maintaining a nominal terrain clearance of 100 m, whenever possible. A digital elevation trace, calculated from the radar altimeter and the GPS elevation values, was also generated to further control the quality of the altimeter data.
    - The synchronicity of the GPS time and the acquired time of the geophysical data was checked by matching the recorded time fields.
    - A final check on the navigation data was done by computing the point-to-point speed from the corrected UTM X and Y values. The computed values should be free of erratic behaviour showing a nominal ground speed of between 54 m/s and 74 m/s with point-to-point variations not exceeding ±10 m/s.

2. Magnetic Data
    - The diurnal variation was examined for any deviations that exceed the specified 3 nT peak-to-peak over a 60 second chord. Data were re-acquired when this condition was exceeded, with any re-flown line segment crossing a minimum of 2 control lines. Further quality control on the diurnal variation was to examine the data for any man-made disturbances. When noted, these artefacts were graphically removed by a polynomial interpolation so that they are not introduced into the final data when the diurnal values are subtracted from the recorded airborne data.
    - The integrity of the airborne magnetometer data was checked through statistical analysis and graphically viewed in profile form to ensure that there were no gaps and that the noise specifications were met.
    - A fourth difference algorithm was applied to the raw data to help locate and correct any small steps and/or spikes in the data.
    - Any effects of filtering applied to the data were examined by displaying, in profile form, the final processed results against the original raw data, via a graphic screen. This was done to ensure that any noise filtering applied has not compromised the resolution of the geological signal.
    - Ongoing gridding and imaging of the data were also done to control the overall quality of the magnetic data.

3. Radiometric Data
    - Onsite, weather conditions were continuously monitored to ensure that no radiometric survey took place within 4 hours after measurable precipitation or 12 hours after heavy precipitation.
    - Prior to each survey flight, the field crew performed 2 system verification tests. The results of these system verification tests are plotted in Appendix A.
    - Source Tests: While the aircraft was stationary, a ^{232}Th source was placed in a cradle attached to the aircraft beneath the spectrometer detector pack and data were collected for 2 minutes. The sample was then removed, and data were again collected for 2 minutes for background determination. The results analyzed and plotted to ensure consistent sensitivities throughout the survey.

- System Resolution Test: A ^{232}Th source was used determine the full width–half amplitude (FWHM) of the 2615 keV photopeak, expressed as a percentage, as a measure of system performance. In all tests performed, FWHM of the photopeak remained well below the contract specified threshold of 7%.
- Before and after each radiometric survey flight, a repeat line was flown as an additional measure of system consistency throughout the survey, as well as for consistency between aircraft.
- During a survey flight, the flight crew is presented with a diagnostic display of the radiometric acquisition system showing a combined spectra and status of each detector crystal. In the event of anomalous system state or error, a visual alert is displayed.
- Post flight, the radiometric data were viewed in profile format. The data were checked for any gaps, erroneous detector crystal states or stabilization errors. Any records that show an error in detector state were removed and scheduled for reflight if needed. Rough background correction estimates were removed from the region-of-interest channels and the data were displayed in grid format to check for coherence.

7.1.3. NEAR-FINAL FIELD PRODUCTS

Near-final products of the profile and gridded magnetic and radiometric data were made available to the QA/QC Geophysicist during visits to the survey site, for review and approval, prior to demobilization.

7.1.4. QUALITY CONTROL IN THE OFFICE

1. Review of preliminary processed data

   The general results of the preliminary processing were reviewed in the profile database by producing a multichannel stacked display of the data (raw and processed) for every line, using a graphic viewing tool. The magnetic and altimeter data were checked for spikes and residual noise.

2. Review of the final processed data

   The results of the field levelling of the magnetics were reviewed, using imaging and shadowing techniques. Any residual errors noted were corrected and the final microlevelling re-applied to the profile data.

3. Creation of first and second vertical derivative

   The first and second vertical derivatives were created from the final gridded values of the residual field magnetic data and checked for any residual errors using imaging and shadowing techniques.

7.1.5. INTERIM PRODUCTS

Archive files containing the raw and interim processed profile data and the gridded data were provided to the QA/QC Geophysicist for review and approval.

7.1.6. CREATION OF 1:50 000 MAPS

After approval of the interim data, the 1:50 000 maps were created and verified for registration, labelling, dropping weights, general surround information, etc. The corresponding digital files were provided to the QA/QC Data Manager for review and approval.

7.2. QA/QC GEOPHYSICIST

The QA/QC Geophysicist received data on a regular basis throughout the data acquisition, focussing initially on the data acquisition procedures, base station monitoring and instrument calibration. As data were collected, they were reviewed for adherence to the survey specifications and completeness. Any problems encountered during data acquisition were discussed and resolved.

The QA/QC checks included the following:

1. Navigation Data
   - appropriate location of the GPS base station
   - flight-line and control-line separations are maintained, and deviations along lines are minimized
   - verify synchronicity of GPS navigation and flight video
   - all boundary control lines are properly located
   - terrain clearance specifications are maintained
   - aircraft speed remained within the satisfactory range
   - area flown covers the entire specified survey area
   - real-time corrected GPS data does not suffer from satellite induced shifts or dropouts
   - GPS height and radar/laser altimeter data are able to produce an image-quality Digital Elevation Model
   - GPS and geophysical data acquisition systems are properly synchronized
   - GPS data are adequately sampled.

2. Magnetic Data
   - appropriate location of the magnetic base station, and adequate sampling of the diurnal variations
   - heading error and lag tests are satisfactory
   - magnetometer noise levels are within specifications
   - magnetic diurnal variations remain within specifications
   - spikes and/or drop-outs are minimal to non-existent in the raw data
   - filtering of the profile data is minimal to non-existent
   - preliminary levelling produces image-quality grids of total magnetic field and higher order products (e.g., second vertical derivative)

3. Radiometric data
   - consistency between daily test lines
   - consistency between daily fixed source and static background measurements
   - shifts in radioelement concentrations between flights
   - precipitation limitations are observed
   - the energy resolution is confirmed daily with ^{232}Th and, using the 2615 keV photopeak of ^{232}Th, a total system resolution better than 7% is maintained
   - gamma-ray peaks properly located in the energy spectrum

The QA/QC Geophysicist reviewed interim and final digital and map products throughout the data compilation phase, to ensure that noise was minimized and that the products adhered to the QA/QC specifications. This typically resulted in several iterations before all digital products were considered satisfactory. Considerable effort was devoted to specifying the data formats and verifying that the data adhered to these formats.

7.3. MINISTRY OF ENERGY, NORTHERN DEVELOPMENT AND MINES

ENDM prepared all of the base map and map surround information required for the hard-copy maps. This ensured consistency and completeness for all of the geophysical map products. The base map was constructed from digital files of the 1:50 000 NTS map sheet series.

ENDM worked with the QA/QC Geophysicist to ensure that the digital files adhered to the specified ASCII and binary file formats, that the file names and channel names were consistent, and that all required data were delivered on schedule. The map products were carefully reviewed in digital and hard-copy form to ensure legibility and completeness.

ENDM and the QA/QC geophysicist provided the magnetic profile and gridded data guidelines for SGL as part of the GSC-levelling process.

8. References

Beiki, M., Bastani, M. and Pedersen, L.B. 2010. Leveling HEM and aeromagnetic data using differential polynomial fitting; Geophysics, v.75, p.L13-L23.

Bennett, G., Dressler, B.O. and Robertson, J.A. 1991. The Huronian Supergroup and associated intrusive rocks; Chapter 14 *in* Geology of Ontario, Ontario Geological Survey, Special Volume 4, Part 1, p.548-591.

Briggs, I.C. 1974. Machine contouring using minimum curvature; Geophysics, v.39, p.39-48.

Broome, J., Carson, J.M., Grant, J.A. and Ford, K. 1987. A modified ternary radioelement mapping technique and its application to the south coast of Newfoundland; Geological Survey of Canada, Paper 87-14, scale 1:500 000.

Grasty, R.L. 1972. An airborne gamma-ray spectrometry data processing manual giving information of the data collected by the gamma-ray spectrometer system; Geological Survey of Canada, Open File 109, 82p.

Gupta, V., Paterson, N., Reford, S., Kwan, K., Hatch, D. and Macleod, I. 1989. Single master aeromagnetic grid and magnetic colour maps for the province of Ontario; *in* Summary of Field Work and Other Activities, 1989, Ontario Geological Survey, Miscellaneous Paper 146, p.244-250.

Hovgaard, J. and Grasty, R.L. 1997. Reducing statistical noise in airborne gamma-ray data through spectral component analysis; paper 98 *in* Geophysics and Geochemistry at the Millennium, Proceedings of the 4th Decennial International Conference on Mineral Exploration ’97, p.753-764.

International Atomic Energy Agency 1991. Airborne gamma ray spectrometer surveying; International Atomic Energy Agency, Vienna, Austria, Technical Reports Series 323, 97p.

——— 2010. Radioelement mapping; International Atomic Energy Agency, Vienna, Austria, Nuclear Energy Series No.NF-T-1.3, 107p.

Jackson, S.L. and Fyon, J.A. 1991. The western Abitibi Subprovince in Ontario; Chapter 11 *in* Geology of Ontario, Ontario Geological Survey, Special Volume 4, Part 1, p.404-482.

Keating, P.B. 1995. A simple technique to identify magnetic anomalies due to kimberlite pipes; Exploration and Mining Geology, v.4, no.2, p.121-125.

——— 2001. Identification of kimberlite pipes from aeromagnetic surveys; oral presentation, Canadian Geophysical Union, Annual Meeting, May 2001.

Nabighian, M.N. 1984. Toward a three-dimensional automatic interpretation of potential field data via generalized Hilbert transforms: Fundamental relations; Geophysics, v.49, p.780-786.

Naudy, H. and Dreyer, H. 1968. Essai de filtrage nonlinéaire appliqué aux profiles aéromagnétiques; Geophysical Prospecting, v.16, p.171-178.

Ontario Geological Survey 2003a. Ontario airborne magnetic and electromagnetic surveys, processed data and derived products: Archean and Proterozoic "greenstone" belts—Matachewan area; Ontario Geological Survey, Geophysical Data Set 1014.

——— 2003b. Single master gravity and aeromagnetic data for Ontario—Geosoft® format; Ontario Geological Survey, Geophysical Data Set 1036.

——— 2011. 1:250 000-scale bedrock geology of Ontario; Ontario Geological Survey, Miscellaneous Release—Data 126–Revision 1.

Reford, S.W., Gupta, V.K., Paterson, N.R., Kwan, K.C.H. and Macleod, I.N. 1990. Ontario master aeromagnetic grid: A blueprint for detailed compilation of magnetic data on a regional scale; abstract *in* Society of Exploration Geophysicists, 60th Annual Meeting, San Francisco, California, SEG Technical Program, Expanded Abstracts 1990, p.617-619, DOI:10.1190/1.1890282.

Williams, H.R., Stott, G.M., Heather, K.B., Muir, T.L. and Sage, R.P. 1991. Wawa Subprovince; Chapter 12 *in* Geology of Ontario, Ontario Geological Survey, Special Volume 4, Part 1, p.484-546.

Appendix A. Test and Calibration Results

1. MAGNETOMETER LAG TEST

The lag in the magnetic data is a function of 2 components, a static lag resulting from signal processing and a speed-dependent dynamic lag resulting from the physical offset of the magnetometer and the GPS antenna. Both elements of the lag are well known. The static lag is known to be 0.244 s from the filters applied during signal processing. The dynamic lag is equal to the offset of the GPS sensor from the magnetometers as measured along the long axis of the aircraft, divided by the flying speed. For the wingtip sensors #1 and #2 the offset is 1 m, whereas for the tail sensor #3 the offset is 12 m. So, for example, at a speed of 55 m/s, the total lag for the wingtip sensors would be 0.27 s and 0.47 s for the tail sensor.

Lag tests were performed by all aircraft before deployment and after the survey as follows: C-GSGV on June 15 and August 27, 2018; C-GSGW on June 29 and August 23, 2018; and C-GSGL on June 15 and September 12, 2018. The tests were flown close to Ottawa over a railway bridge that crosses the Ottawa River near the township of Pontiac.

Results of the lag tests performed for this survey are provided below. The lag on the geophysical instruments is calculated using a computer program written by SGL. This program uses a statistical comparison of high-pass filtered data from the same line flown in opposite directions.

The program was developed by SGL because we found that it is not possible to determine the lag in an airborne system to an accuracy of better than about one second using a visible ground feature, which causes a distinct anomaly. It is difficult to find the exact centre of the magnetic anomaly, and to locate the precise time on the video flight path record. This method calculates the lag between the GPS data and the magnetometer data, rather than the lag between the magnetometer data and the flight path video. It is important to calculate the lag using the GPS positional data, which is actually used in the compilation process.

The known lag for the airborne magnetometer acquisition system is applied to the airborne magnetic data. The lag test is considered successful if the peaks of the lag corrected magnetic anomaly acquired on passes in opposite directions are not offset by more than one data point as based on data rate and survey speed (0.1 s × 67 m/s = 6.7 m) plus an allowance for the expected differential GPS (“DGPS”) accuracy of ±0.5 m for each data peak, so that the peaks will be within 6.5 m along the direction of flight.

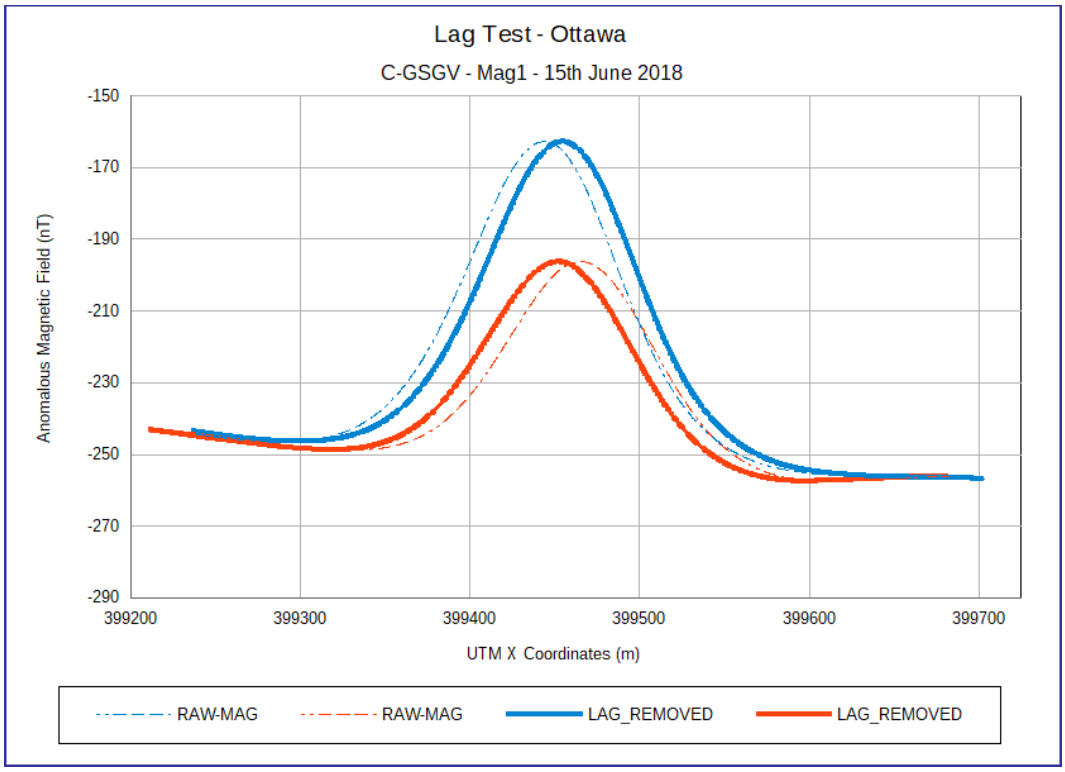

Figure 14. Lag test, Ottawa, C-GSGV, Mag1, June 15, 2018.

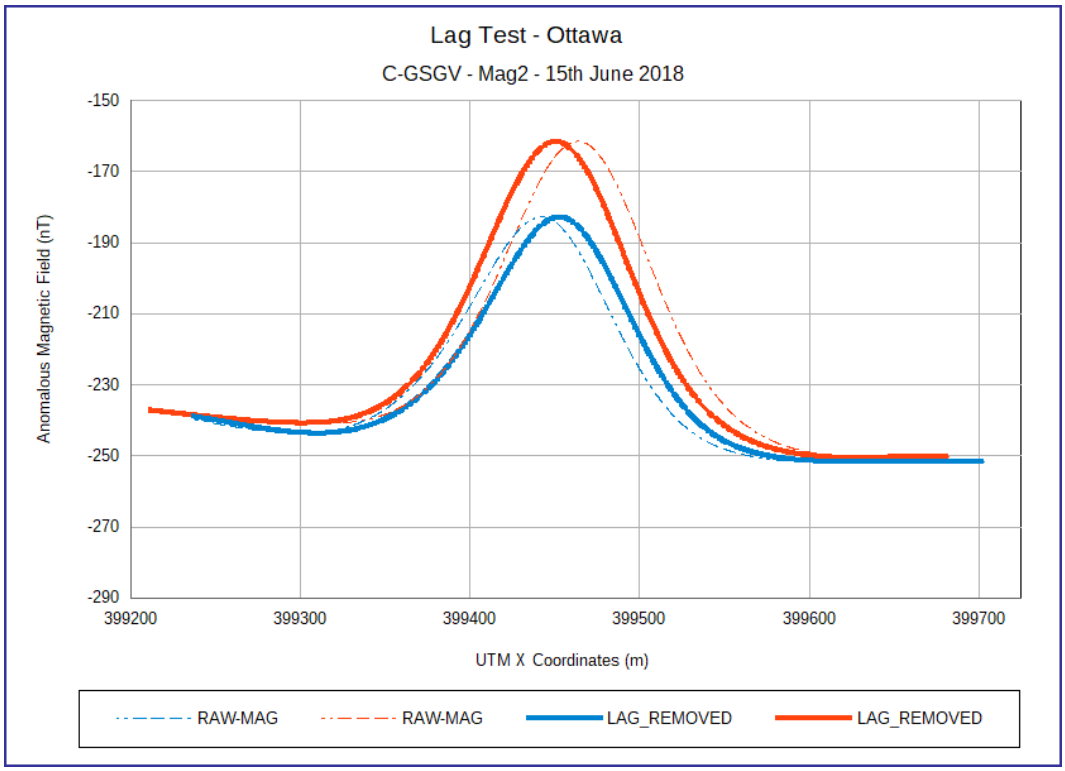

Figure 15. Lag test, Ottawa, C-GSGV, Mag2, June 15, 2018.

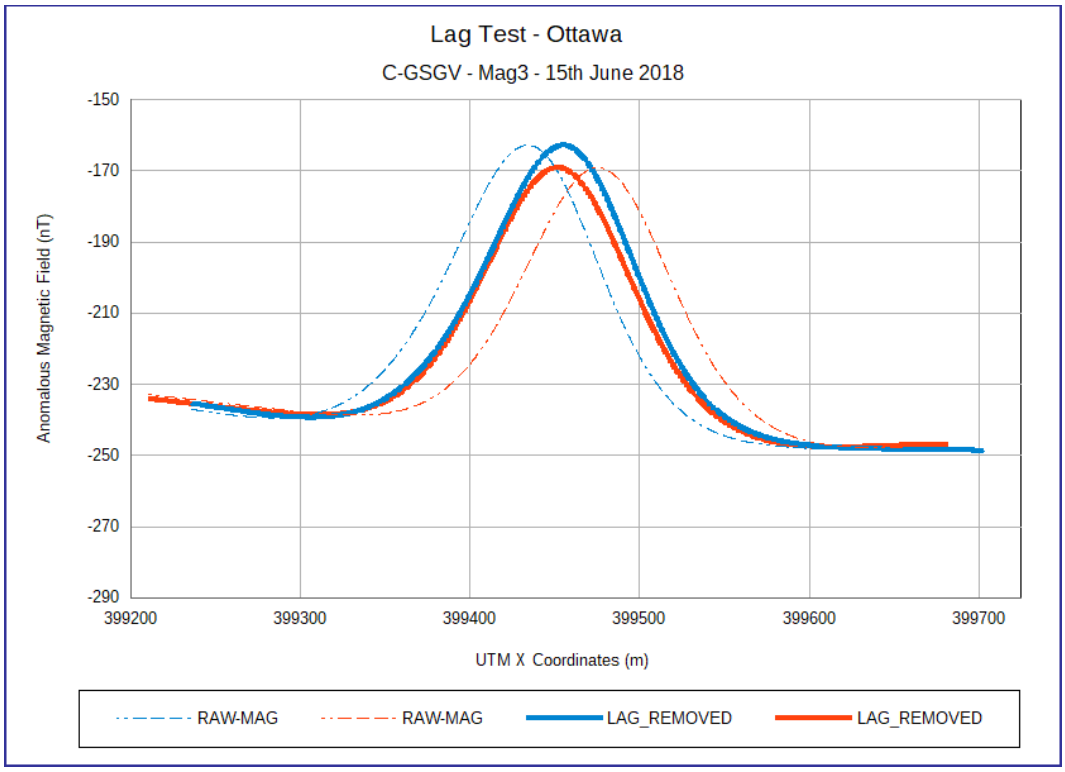

Figure 16. Lag test, Ottawa, C-GSGV, Mag3, June 15, 2018.

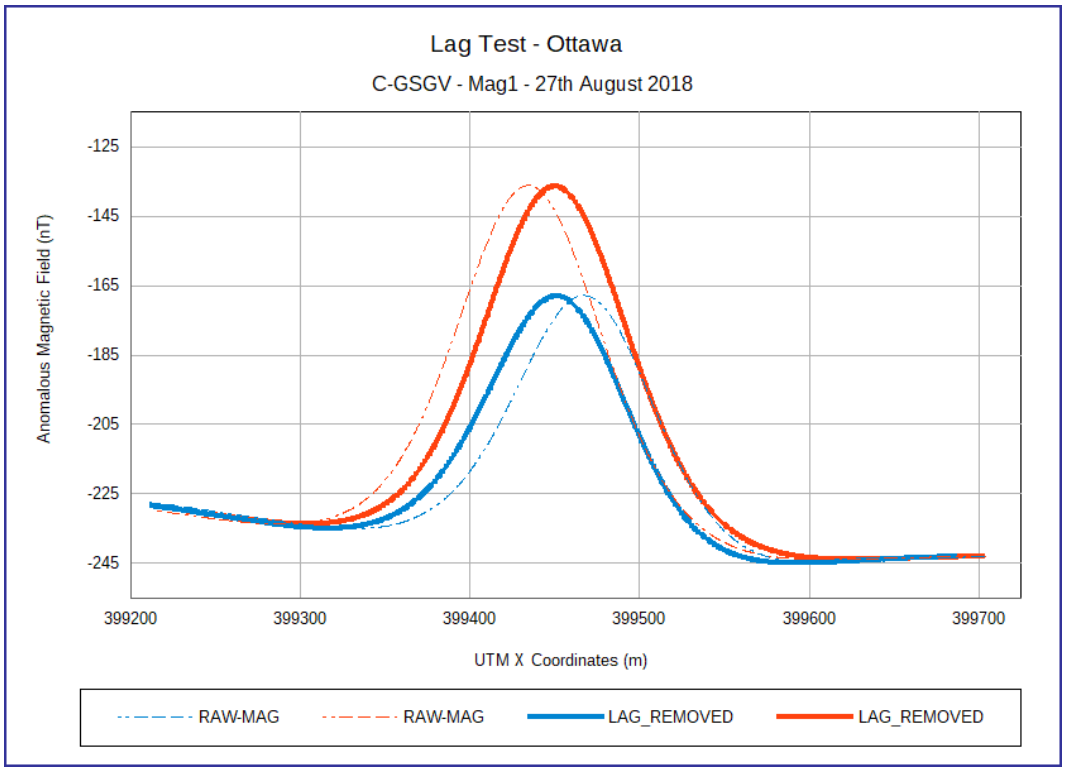

Figure 17. Lag test, Ottawa, C-GSGV, Mag1, August 27, 2018.

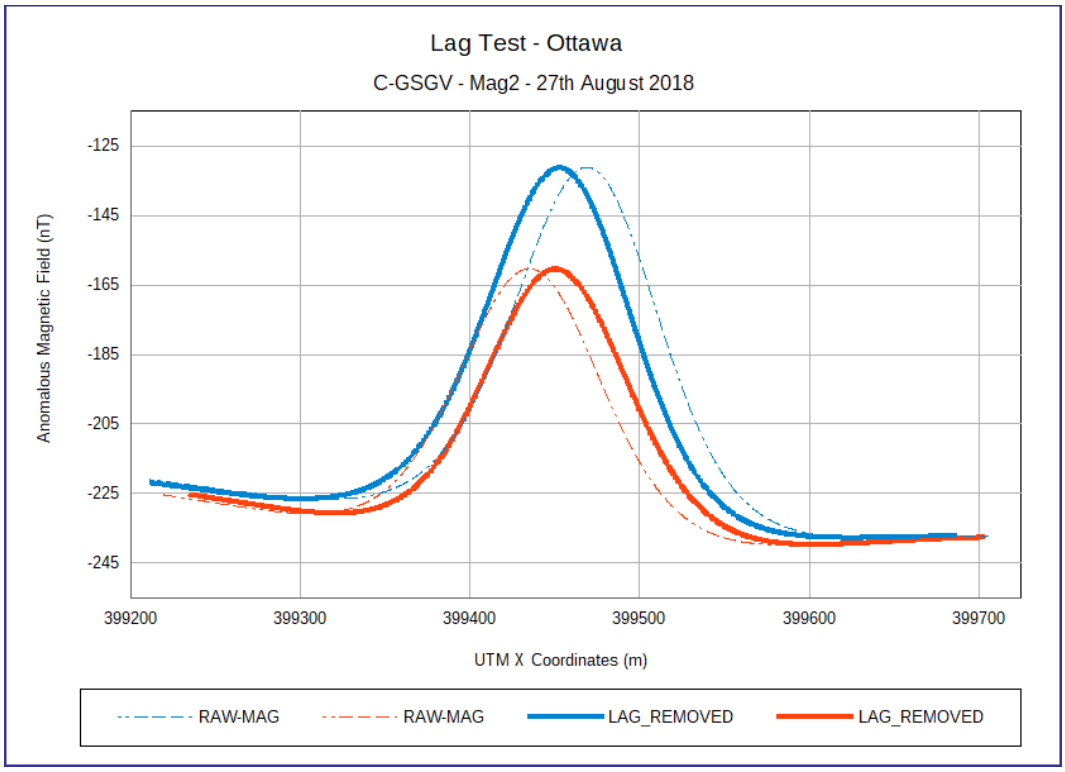

Figure 18. Lag test, Ottawa, C-GSGV, Mag2, August 27, 2018.

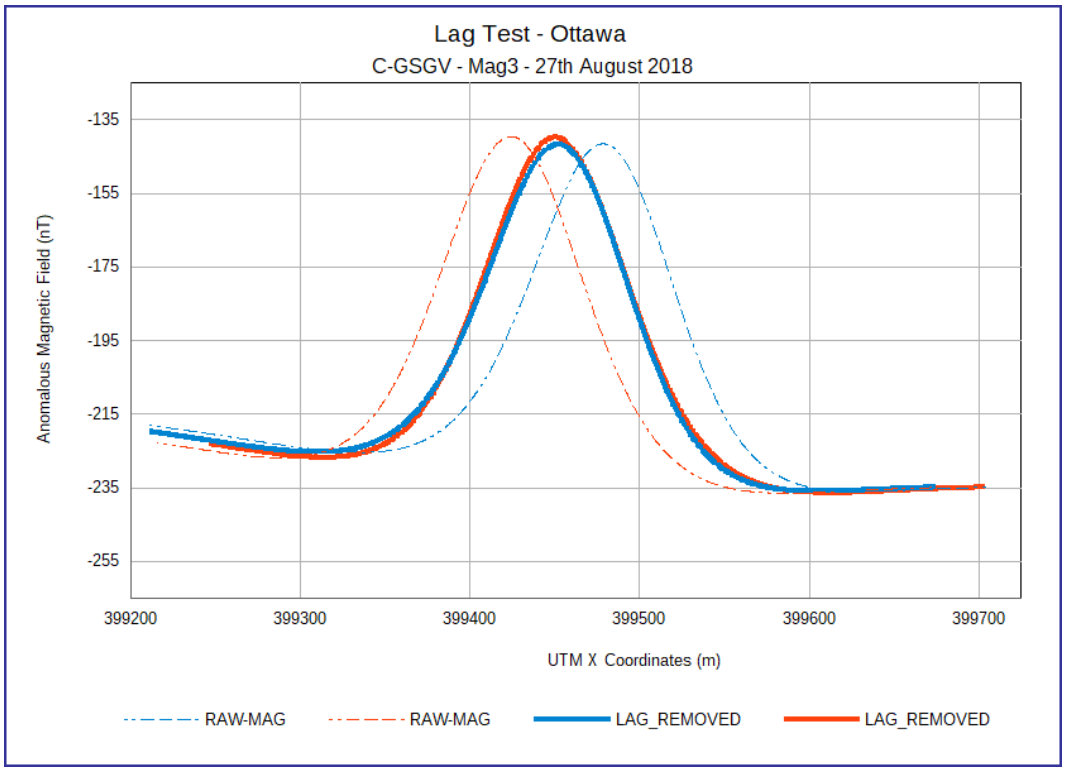

Figure 19. Lag test, Ottawa, C-GSGV, Mag3, August 27, 2018.

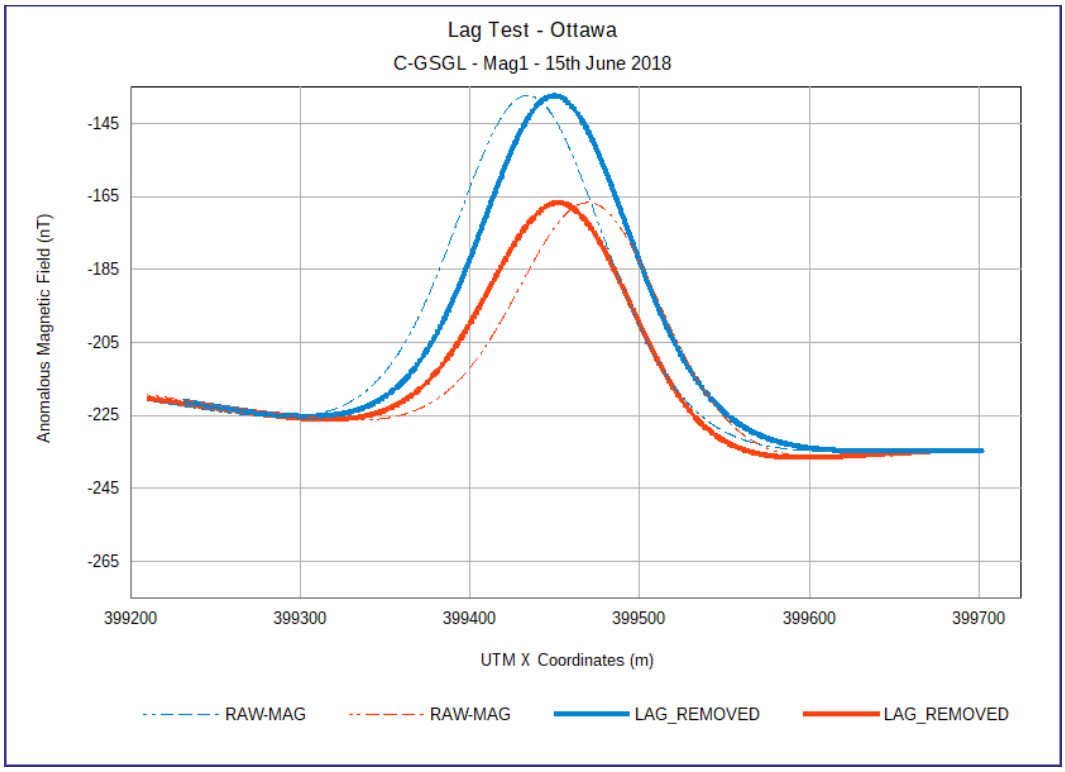

Figure 20. Lag test, Ottawa, C-GSGL, Mag1, June 15, 2018.

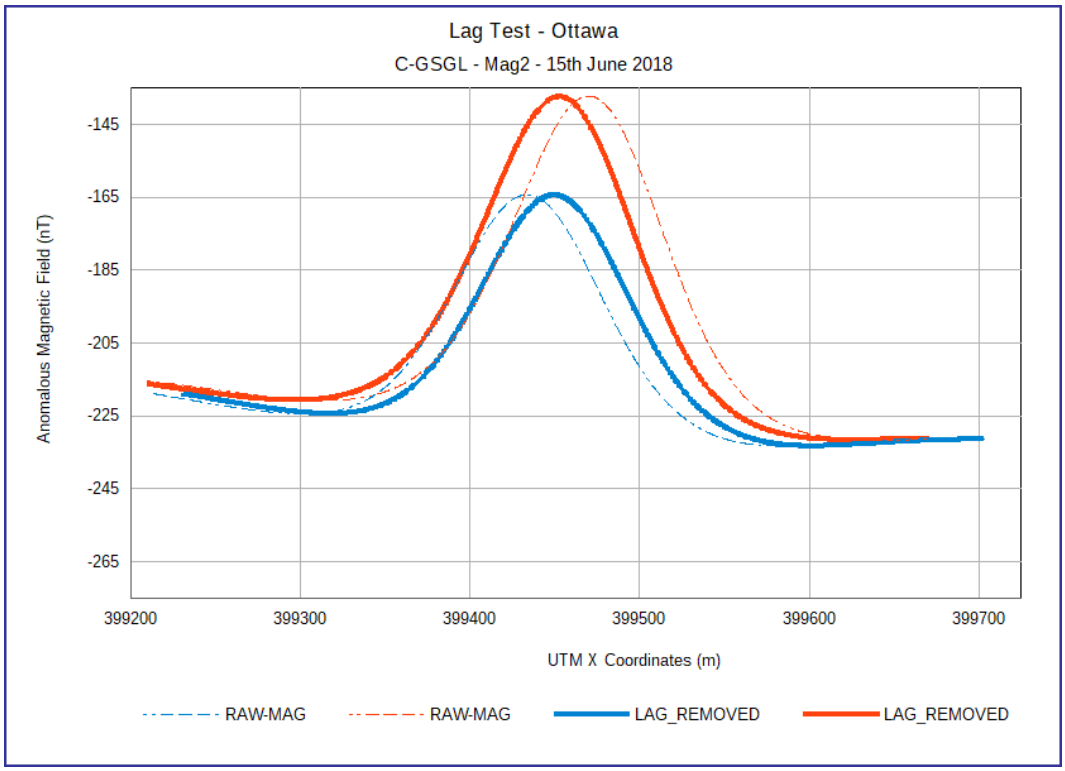

Figure 21. Lag test, Ottawa, C-GSGL, Mag2, June 15, 2018.

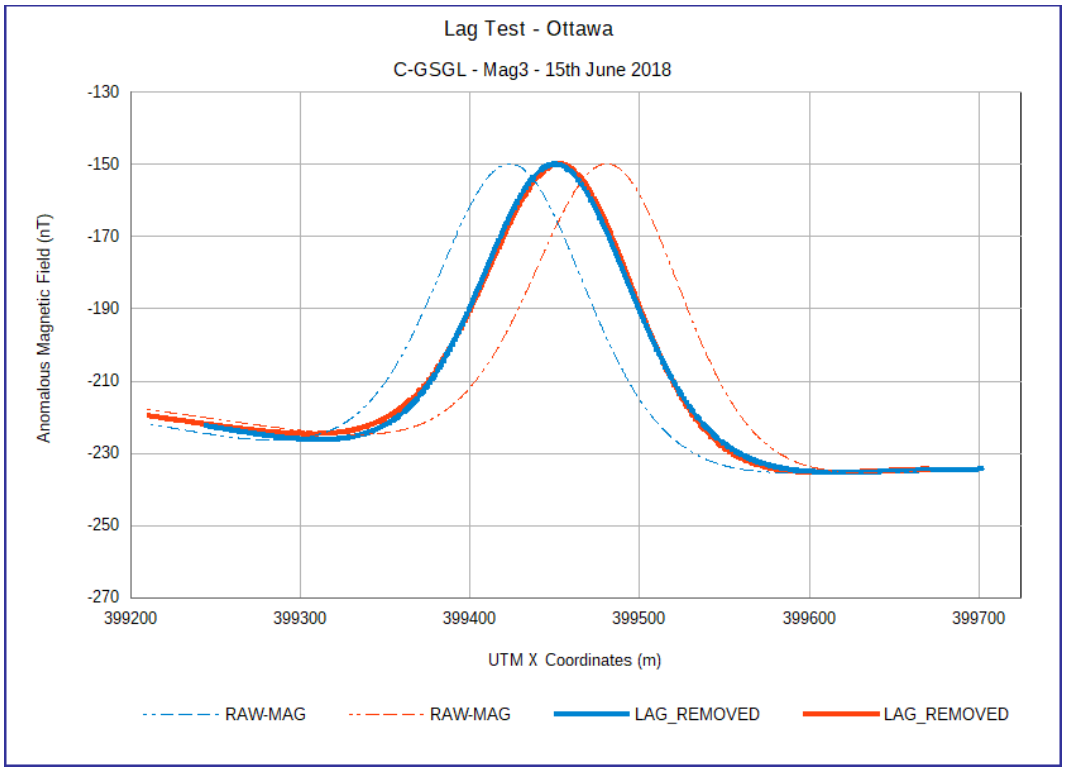

Figure 22. Lag test, Ottawa, C-GSGL, Mag3, June 15, 2018.

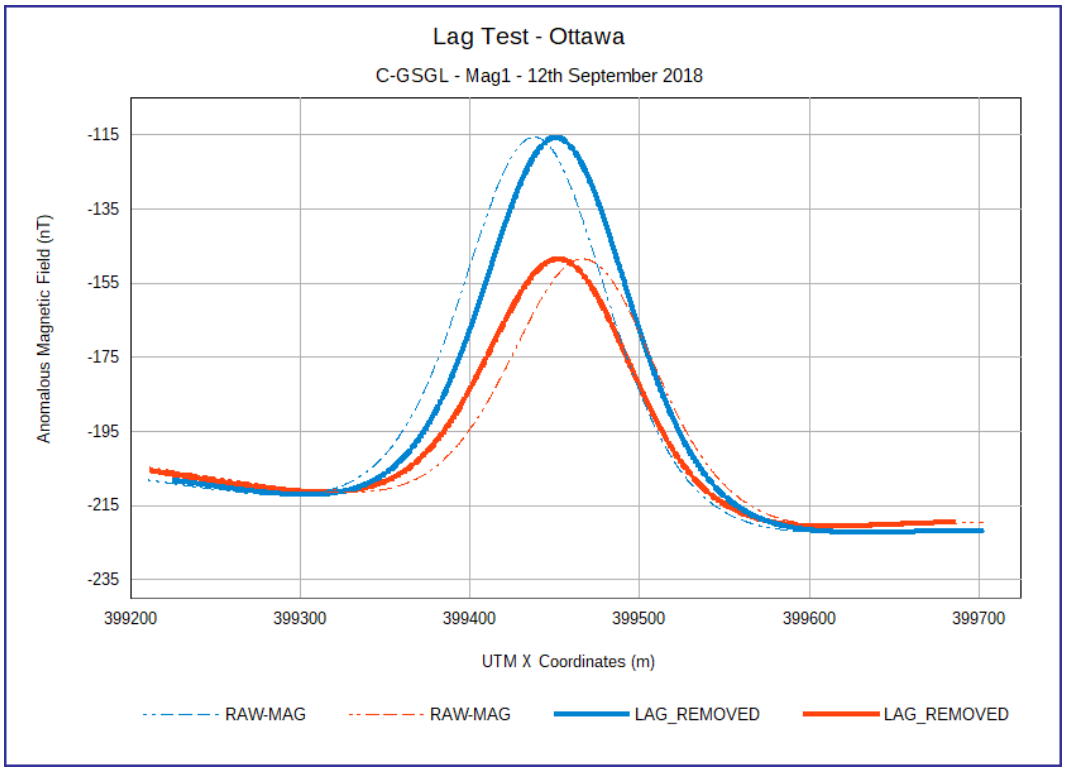

Figure 23. Lag test, Ottawa, C-GSGL, Mag1, September 12, 2018.

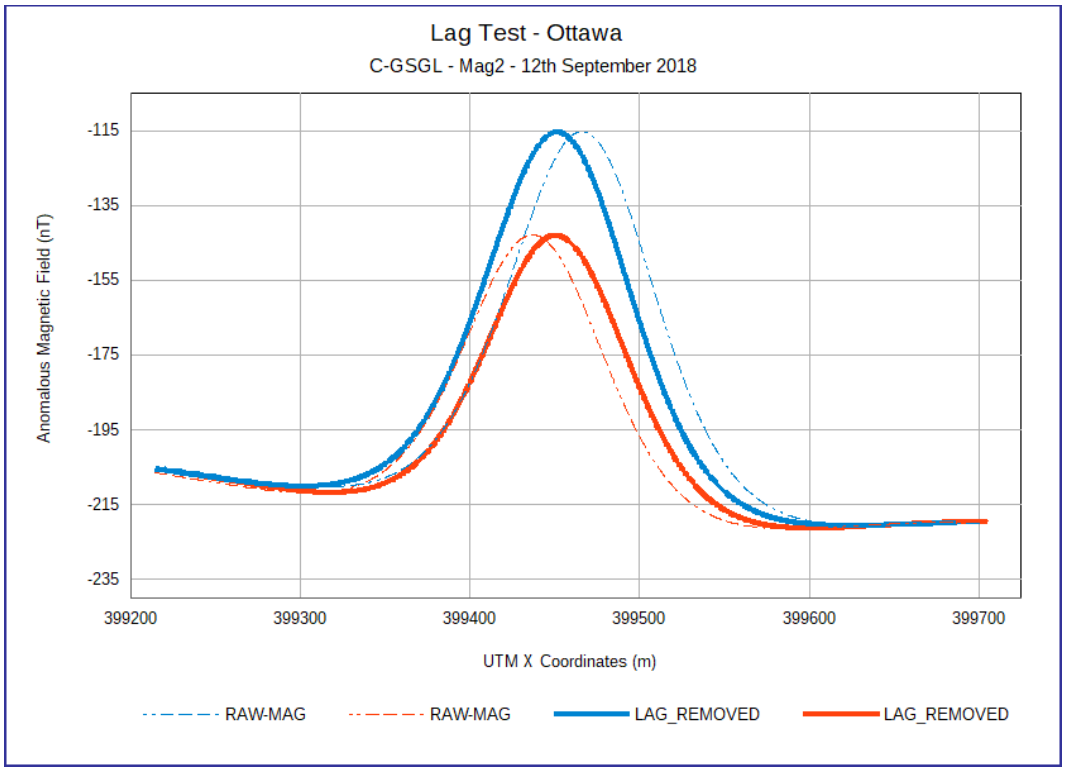

Figure 24. Lag test, Ottawa, C-GSGL, Mag2, September 12, 2018.

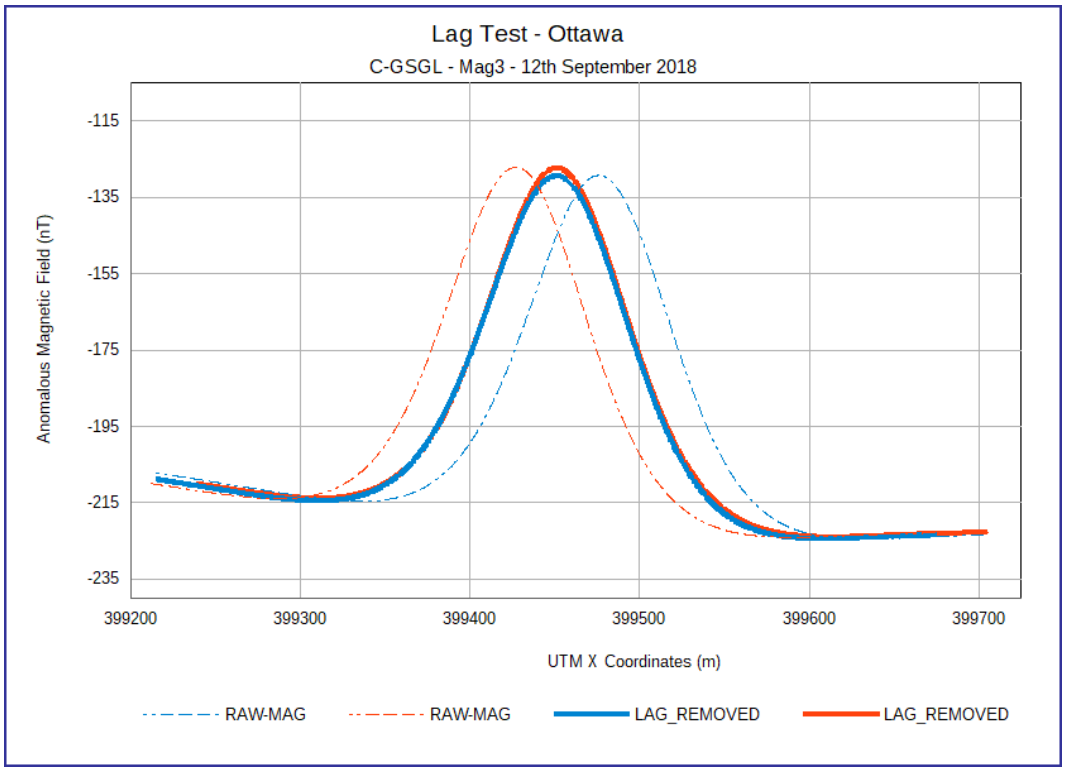

Figure 25. Lag test, Ottawa, C-GSGL, Mag3, September 12, 2018.

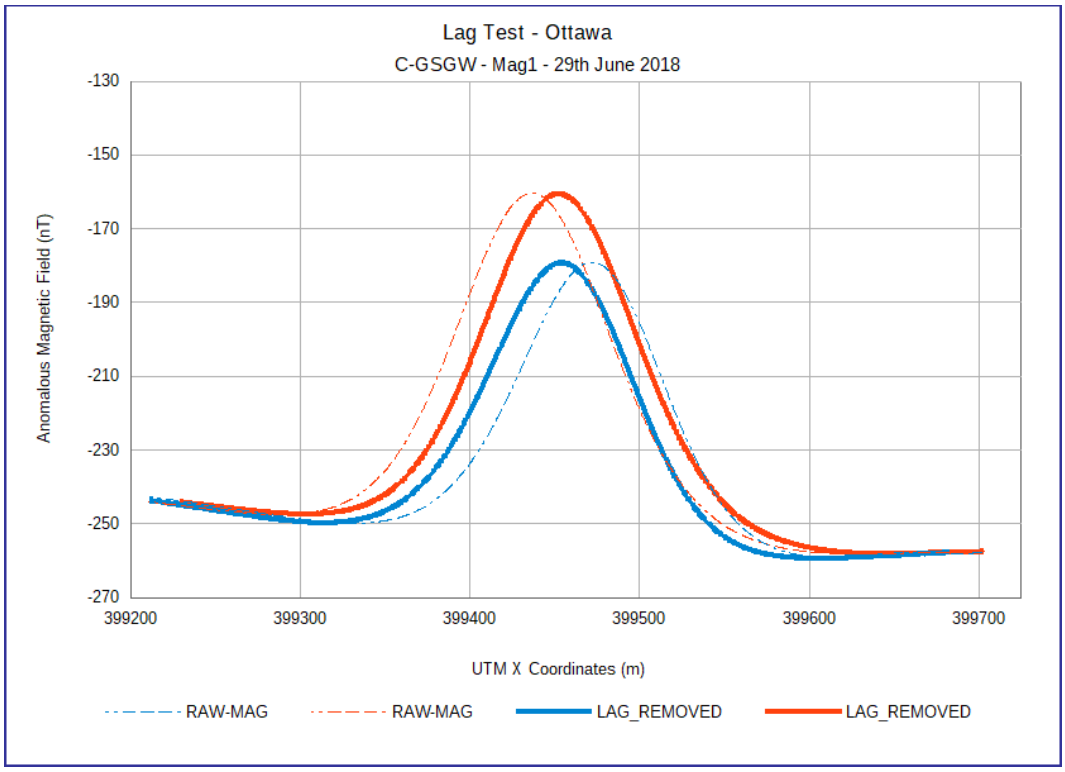

Figure 26. Lag test, Ottawa, C-GSGW, Mag1, June 29, 2018.

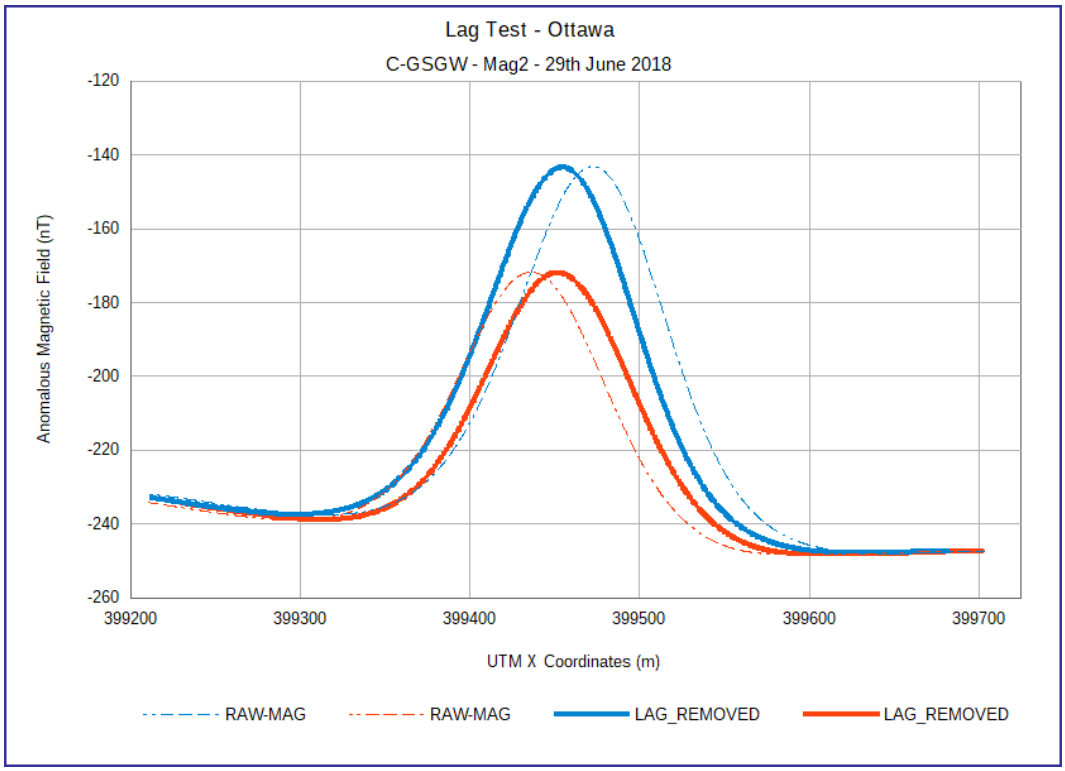

Figure 27. Lag test, Ottawa, C-GSGW, Mag2, June 29, 2018.

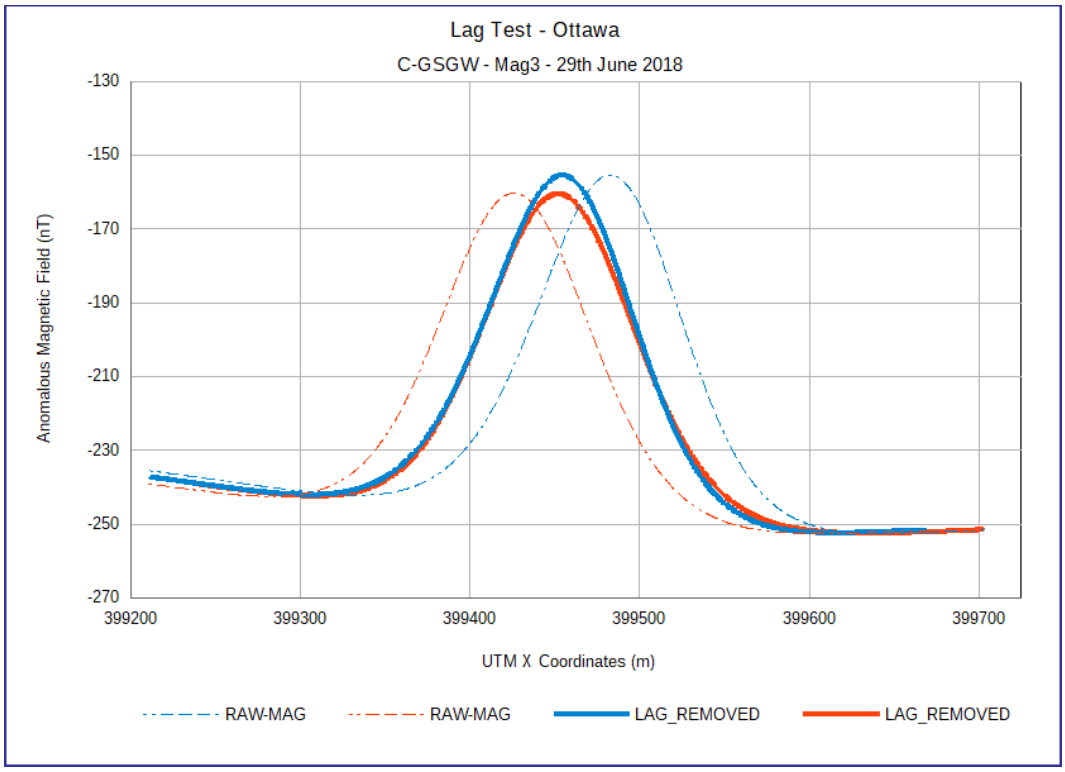

Figure 28. Lag test, Ottawa, C-GSGW, Mag3, June 29, 2018.

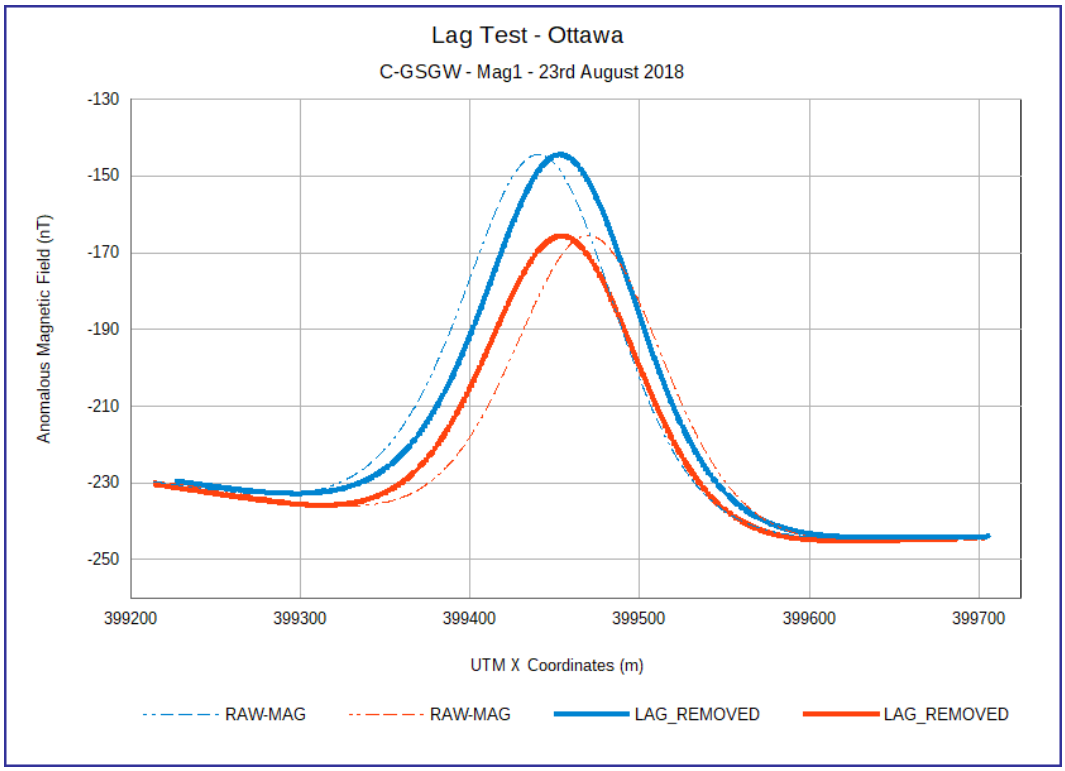

Figure 29. Lag test, Ottawa, C-GSGW, Mag1, August 23, 2018.

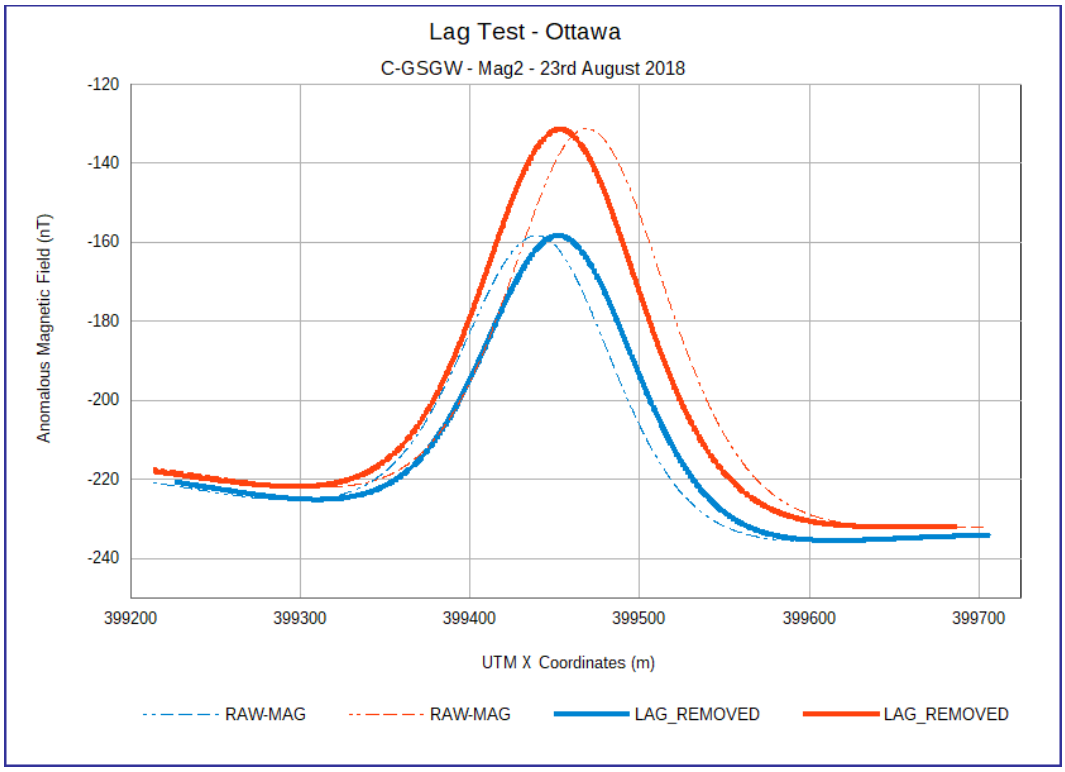

Figure 30. Lag test, Ottawa, C-GSGW, Mag2, August 23, 2018.

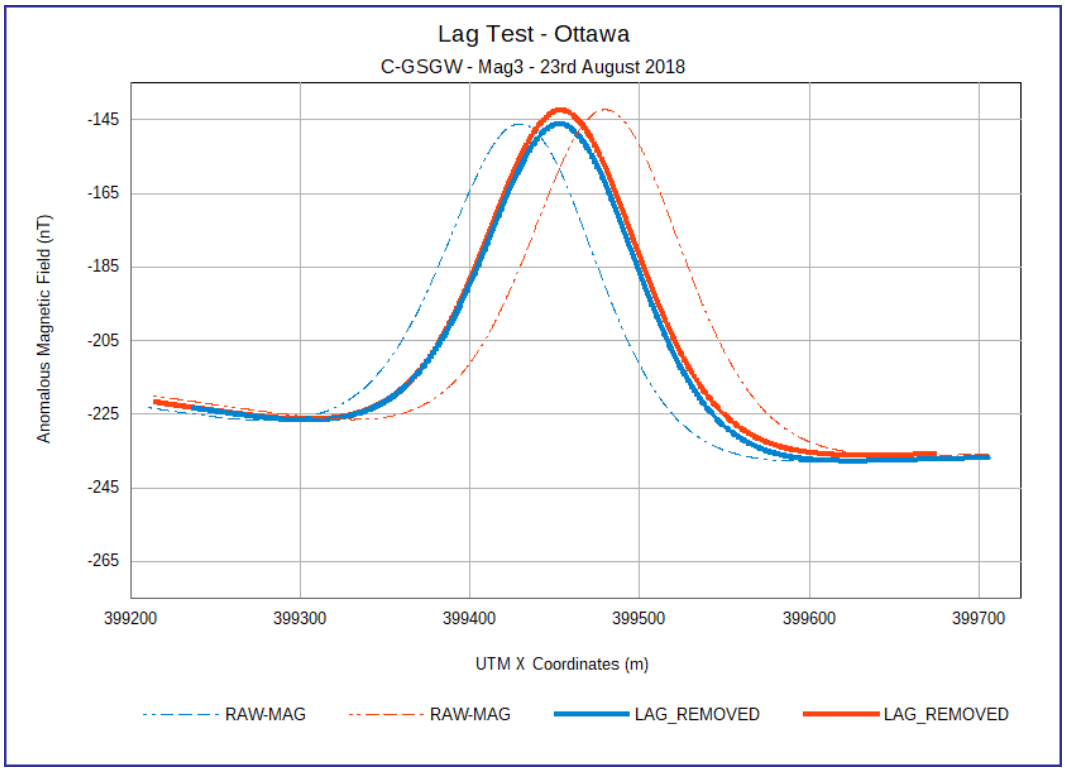

Figure 31. Lag test, Ottawa, C-GSGW, Mag3, August 23, 2018.

2. RADAR AND LASER ALTIMETER TEST

Altimeter calibration test flights were performed by all aircraft before deployment and after the survey. The radar tests were flown for C-GSGL on June 15 and September 12, 2018, over the Gatineau Airport runway. The radar tests for C-GSGW were flown on June 29 over Lac Deschenes and on August 23, 2018, over the Gatineau runway. The radar tests were flown for C-GSGV on June 15 and August 27, 2018, at the Gatineau Airport.

Results of the altimeter tests performed for this survey are provided below. For this test, the survey aircraft flies at pre-established altitudes over an airport runway or a very flat area, so that the corresponding readings of the altimeters can be checked. The aircraft is flown over the runway, once, in either direction at the following heights above ground level: 50 m, 150 m, 250 m, 350 m and 450 m. The passes over Lac Deschenes by C-GSGW were done at the following intervals above the ground: 150 m, 175 m, 190 m, 205 m, 220 m, 270 m, 330 m and 390 m.

Three altimeters are tested: Thomson-CSF ERT 530A radar ("TRT"), Bendix/King® KRA-10A radar ("King") and Riegl® LD90-31K-HiP ("laser"). Calibration coefficients as derived from the altimeter test are applied to all the observed altimeter data. The altimeter test is considered successful if the adjusted data for all passes over the test range fall within accepted accuracy limitations of the altimeter plus an allowance for 0.5 m error in DGPS altitude.

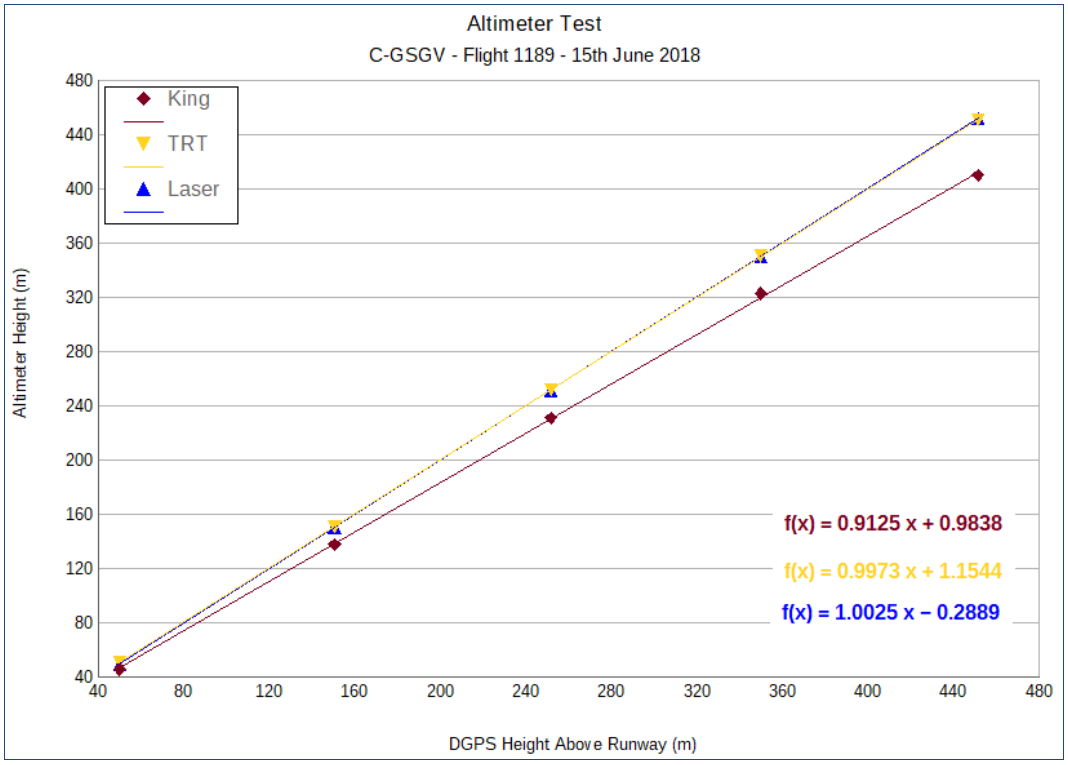

Figure 32. Altimeter test, C-GSGV, flight 1189, June 15, 2018.

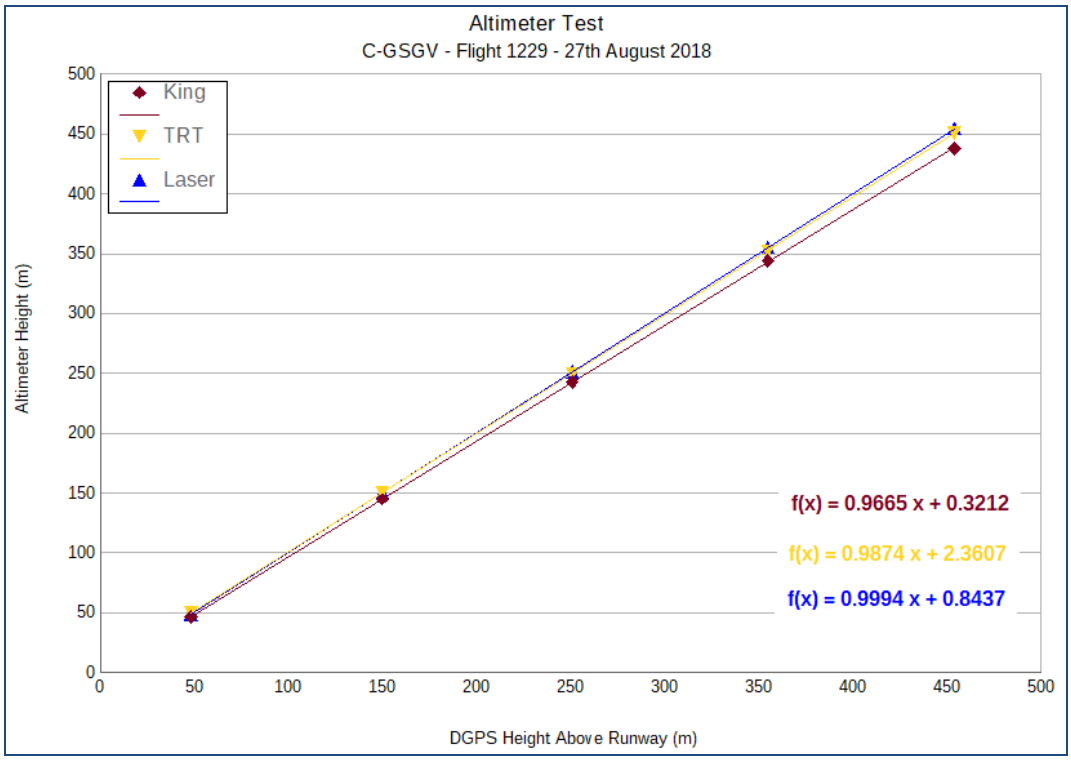

Figure 33. Altimeter test, C-GSGV, flight 1229, August 27, 2018.

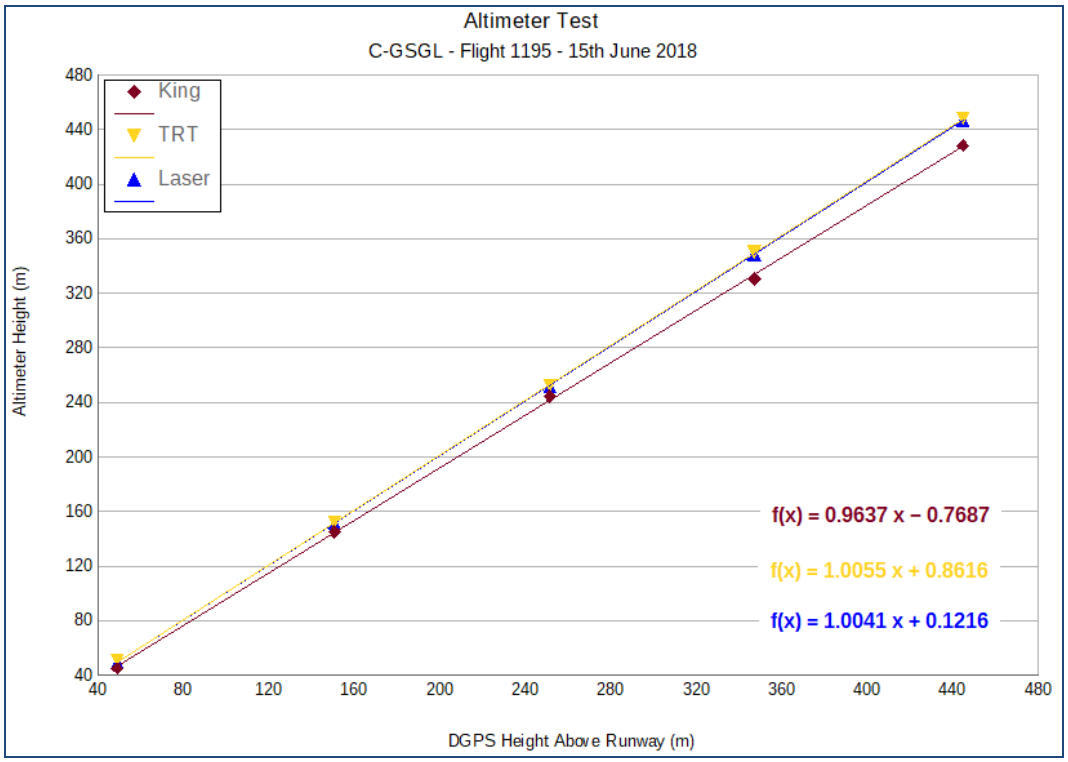

Figure 34. Altimeter test, C-GSGL, flight 1195, June 15, 2018.

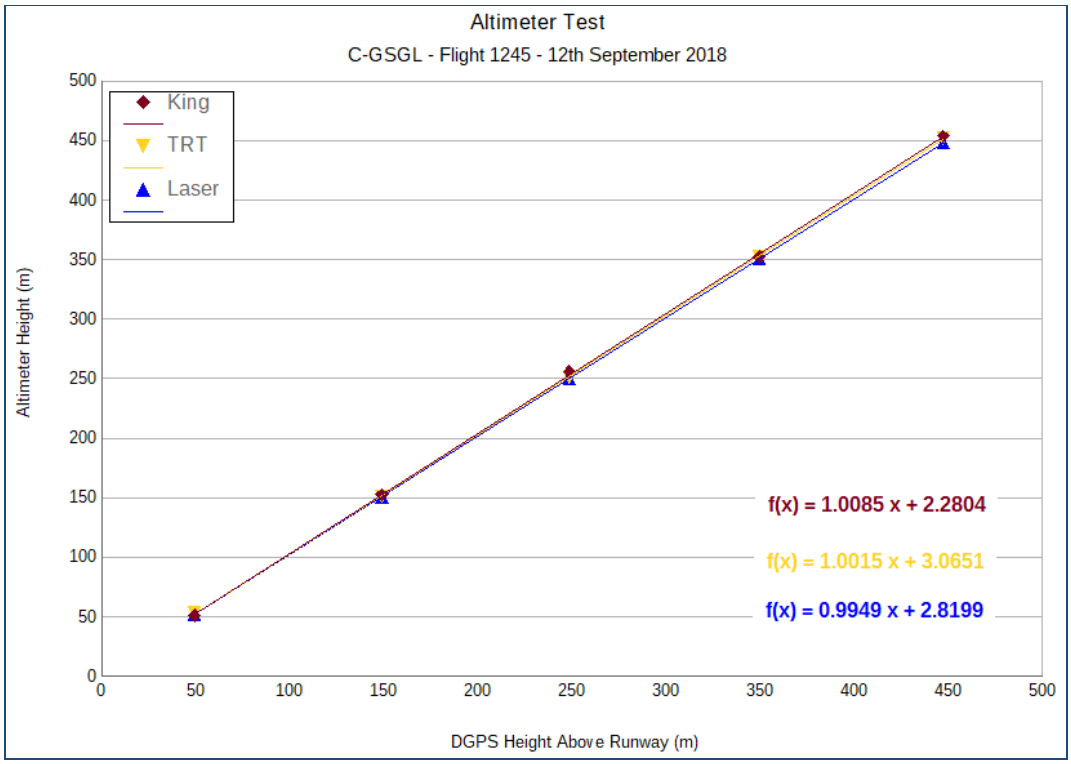

Figure 35. Altimeter test, C-GSGL, flight 1245, September 12, 2018.

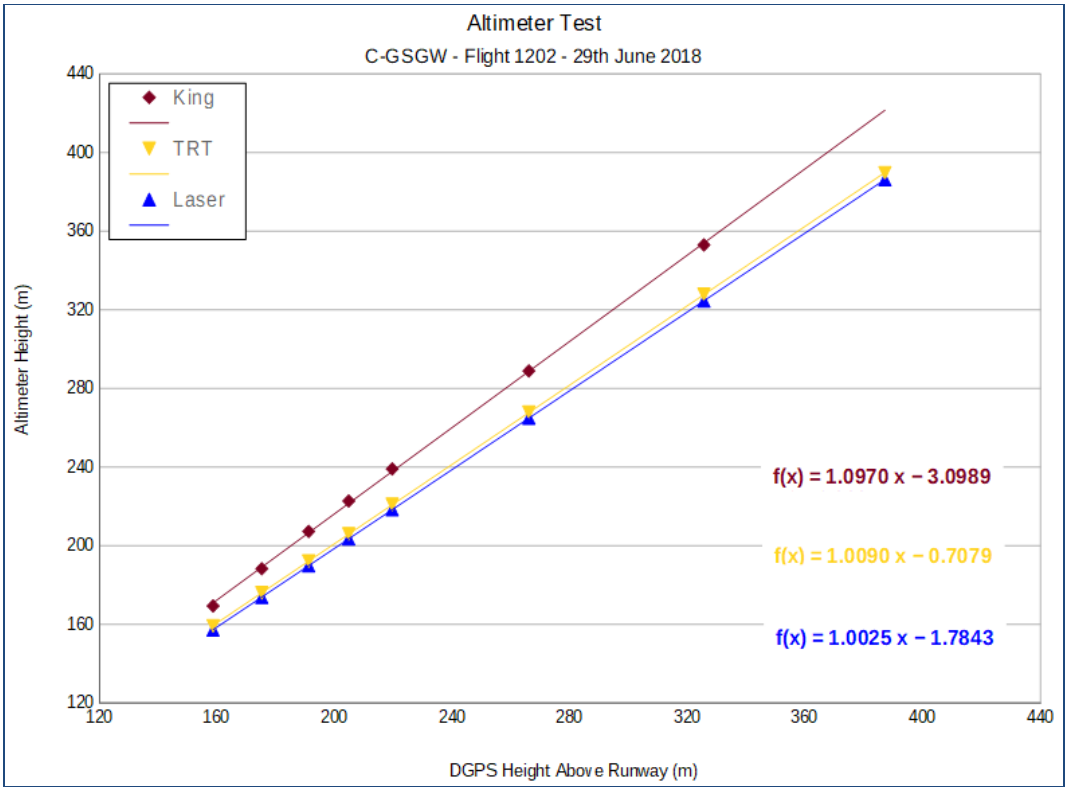

Figure 36. Altimeter test, C-GSGW, flight 1202, June 29, 2018.

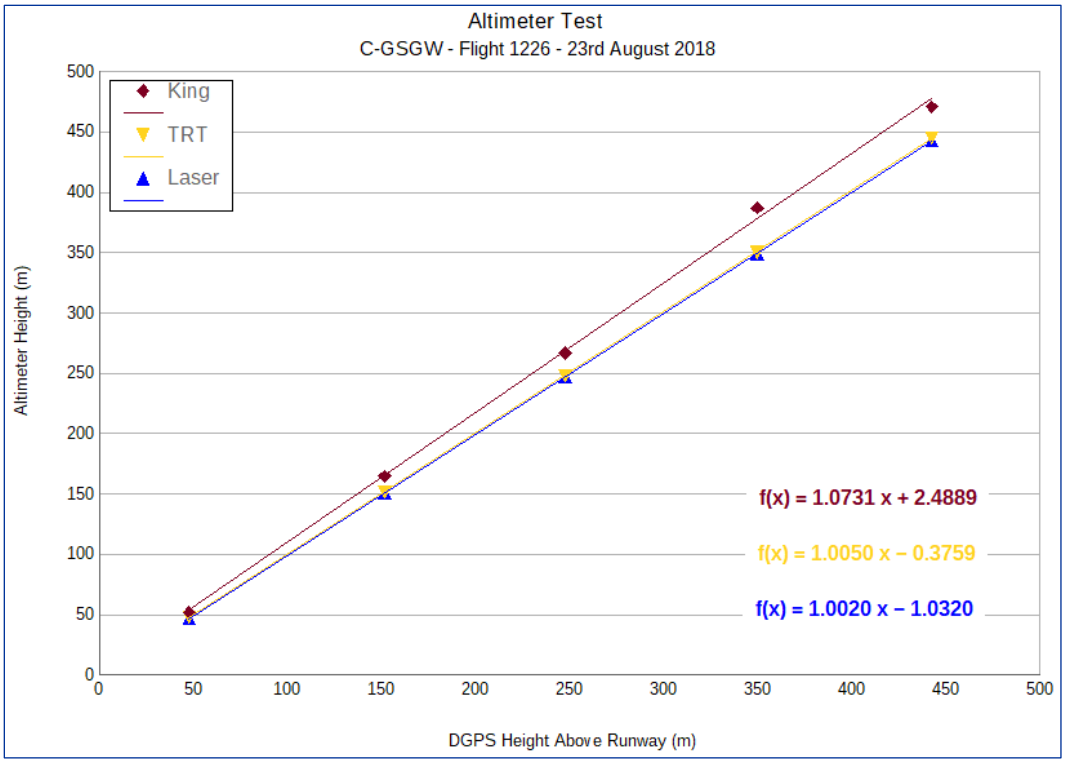

Figure 37. Altimeter test, C-GSGW, flight 1226, August 23, 2018.

3. MAGNETOMETER FIGURE OF MERIT TEST

The compensation calibration determines the magnetic influence of aircraft manoeuvres and the effectiveness of the compensation. The aircraft flies a square pattern in the 4 survey directions at a high altitude over a magnetically quiet area and performs 3 pitches, 3 rolls and 3 yaws. The total compensated signal resulting from the 12 manoeuvres is referred to as the Figure of Merit ("FOM").

In addition to being flown prior to mobilization, the magnetic compensation test is flown prior to data acquisition near the survey base. If any aircraft part is replaced during the survey, and is known to have a distinct magnetic signature, the compensation test is reflown and a new FOM is calculated. Compensation tests are deemed acceptable if the FOM is less than 1.5 nT. Compensation calibration flights were performed by both aircraft before and after the survey at high altitude (roughly 10 000 feet) in the Ottawa area. Separate compensation calibration coefficients are obtained for each magnetometer: #1 on the port wingtip, #2 on the starboard wingtip and #3 in the tail. Test results are illustrated below and summarized in Table 7.

Table 7. Figures of Merit ("FOM") for the 3 survey aircrafts determined at the start and end of operations.

Aircraft	Date	Location	Magnetometer	FOM (nT)
C-GSGV	June 15, 2018	Ottawa	Port #1	1.39
			Starboard #2	1.49
			Tail #3	0.83
	August 27, 2018	Ottawa	Port #1	1.23
			Starboard #2	1.36
			Tail #3	0.73
C-GSGW	June 29, 2018	Ottawa	Port #1	0.78
			Starboard #2	1.41
			Tail #3	0.73
	August 23, 2018	Ottawa	Port #1	0.73
			Starboard #2	0.76
			Tail #3	1.42
C-GSGL	June 19, 2018	Ottawa	Port #1	0.97
			Starboard #2	1.07
			Tail #3	0.84
	September 12, 2018	Ottawa	Port #1	0.67
			Starboard #2	0.70
			Tail #3	0.51

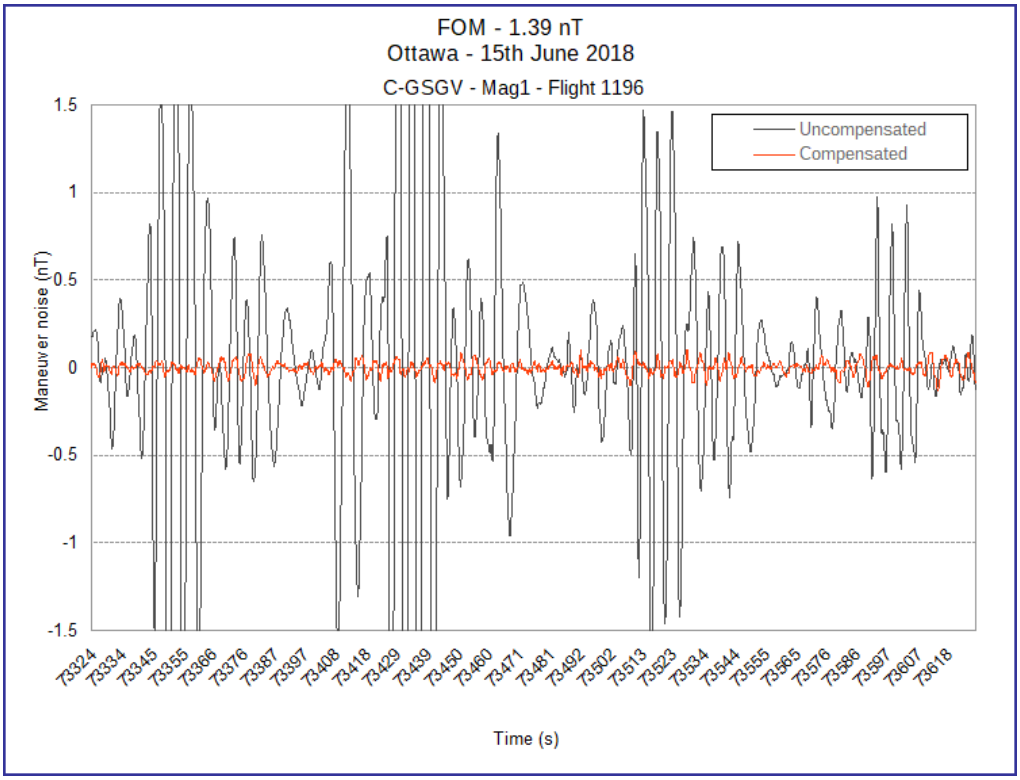

Figure 38. Figure of Merit (FOM) = 1.39 nT, Ottawa, June 15, 2018, C-GSGV, Mag1, flight 1196.

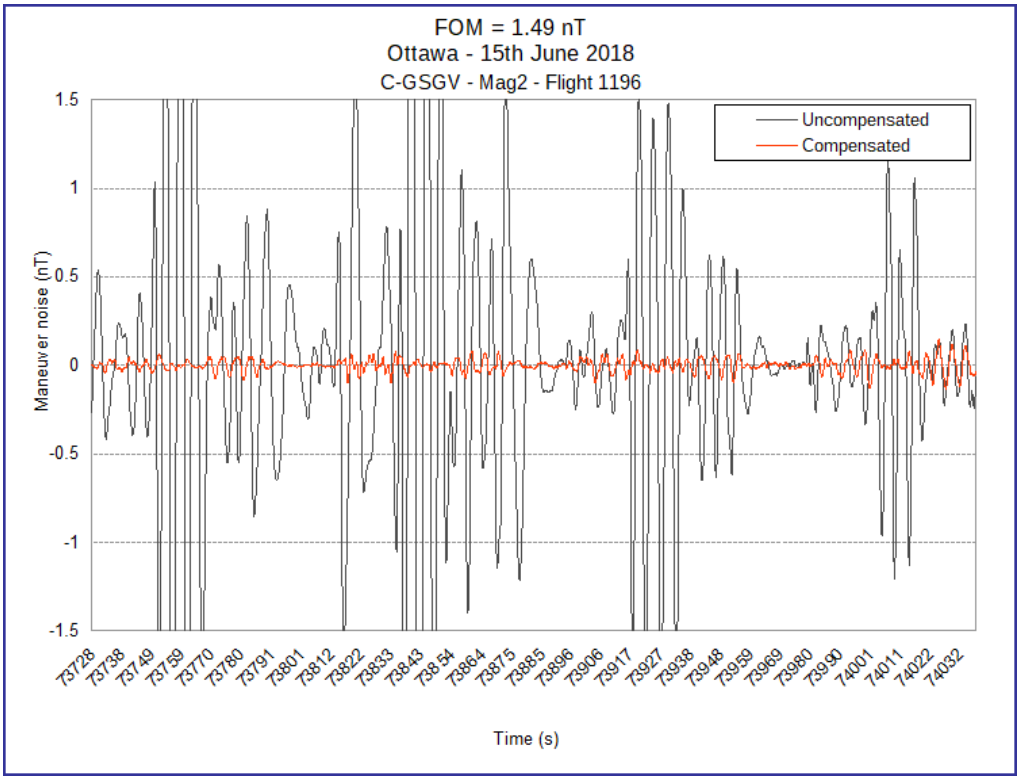

Figure 39. Figure of Merit (FOM) = 1.49 nT, Ottawa, June 15, 2018, C-GSGV, Mag2, flight 1196.

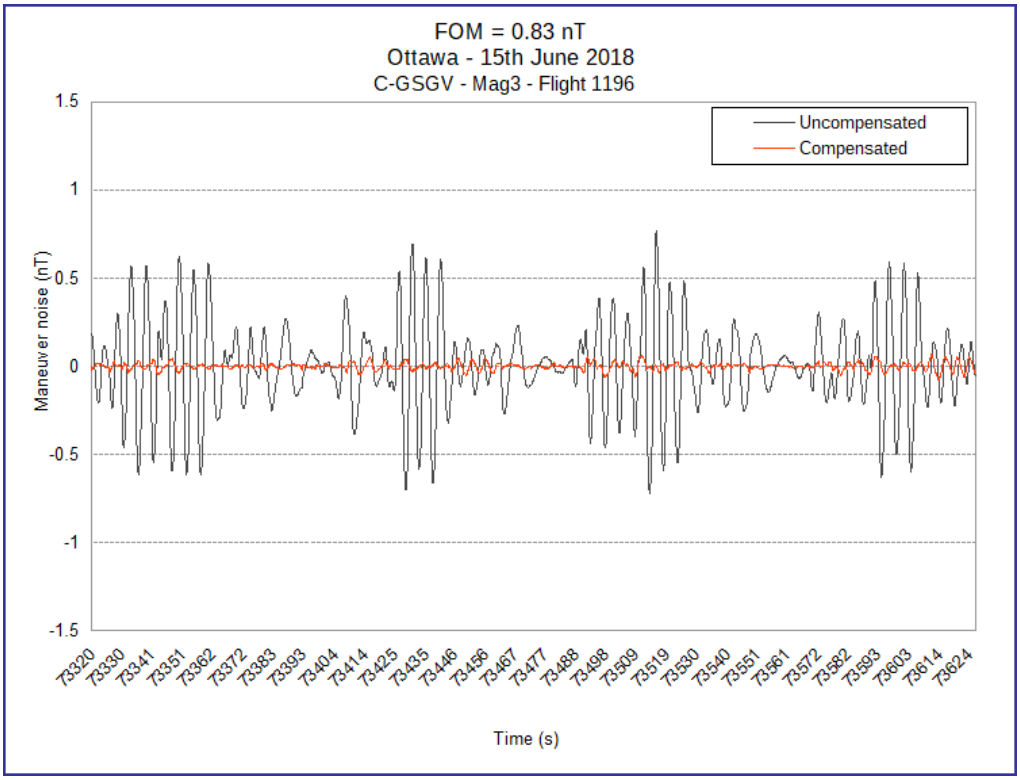

Figure 40. Figure of Merit (FOM) = 0.83 nT, Ottawa, June 15, 2018, C-GSGV, Mag3, flight 1196.

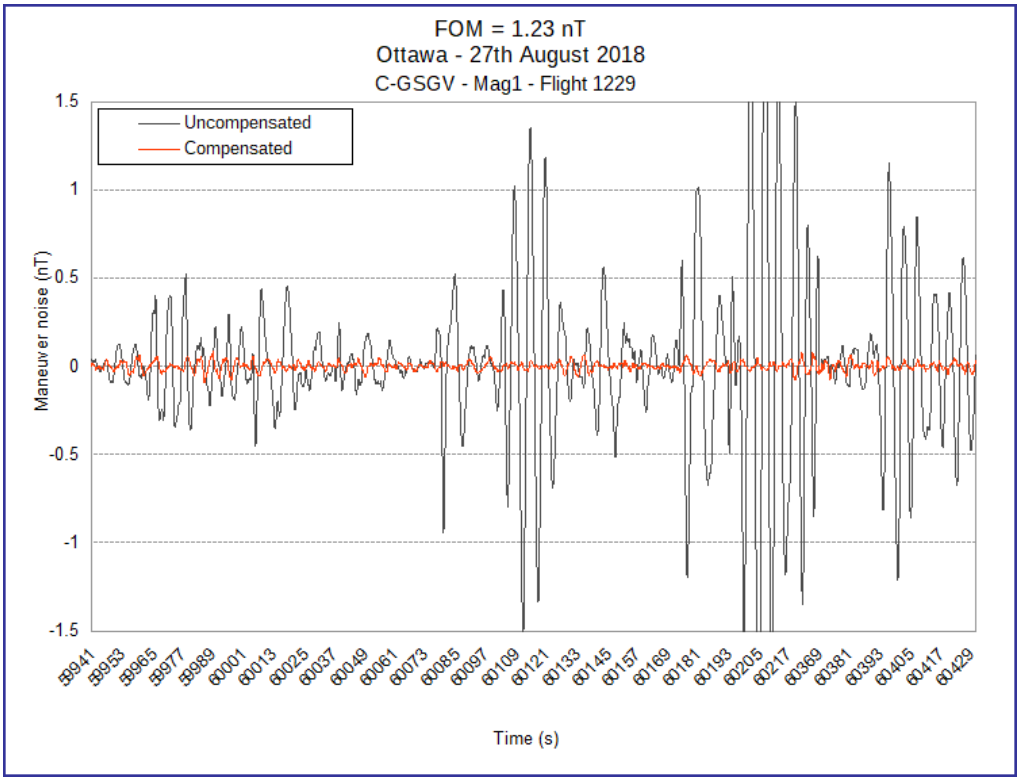

Figure 41. Figure of Merit (FOM) = 1.23 nT, Ottawa, August 27, 2018, C-GSGV, Mag1, flight 1229.

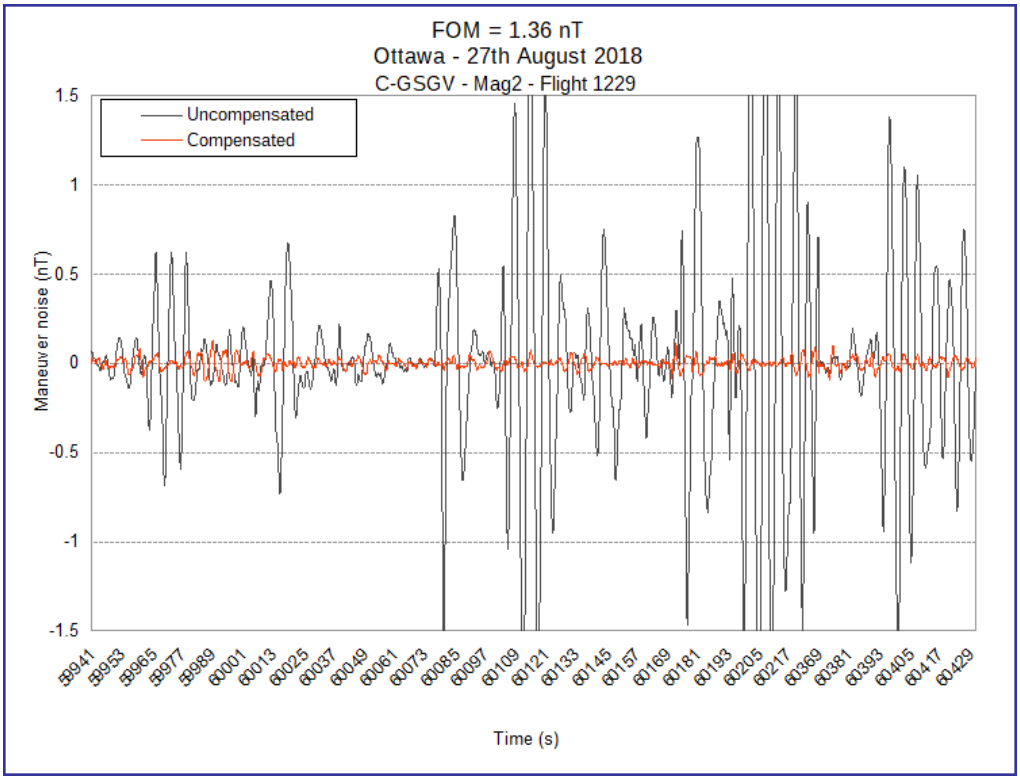

Figure 42. Figure of Merit (FOM) = 1.36 nT, Ottawa, August 27, 2018, C-GSGV, Mag2, flight 1229.

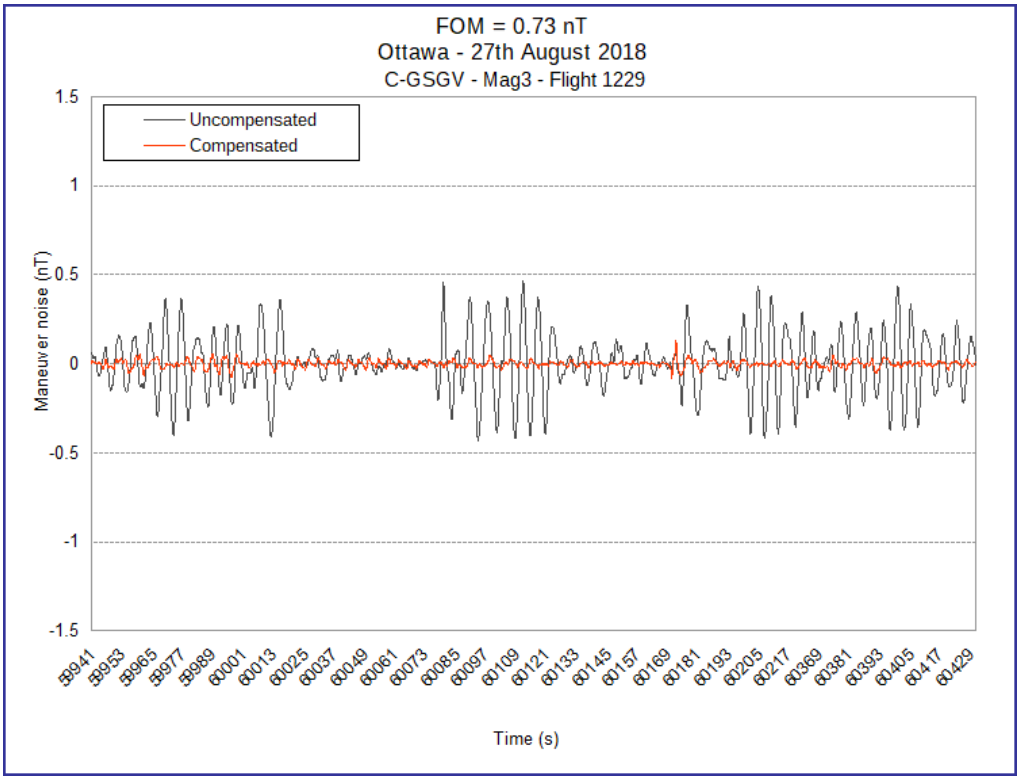

Figure 43. Figure of Merit (FOM) = 0.73 nT, Ottawa, August 27, 2018, C-GSGV, Mag3, flight 1229.

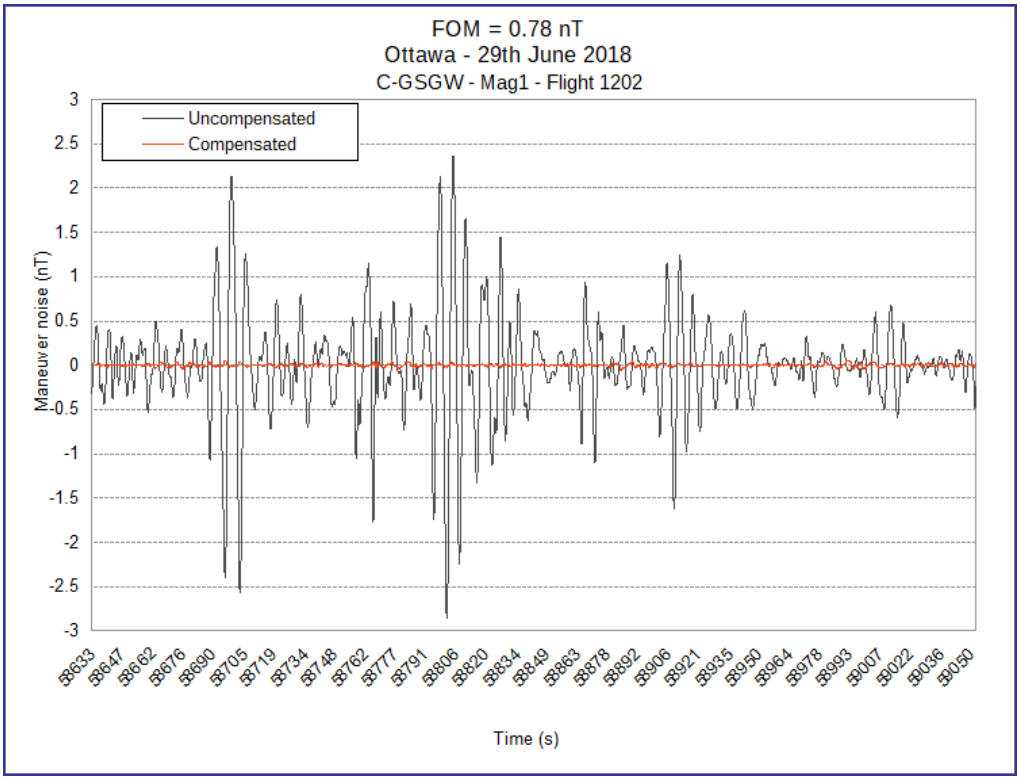

Figure 44. Figure of Merit (FOM) = 0.78 nT, Ottawa, June 29, 2018, C-GSGW, Mag1, flight 1202.

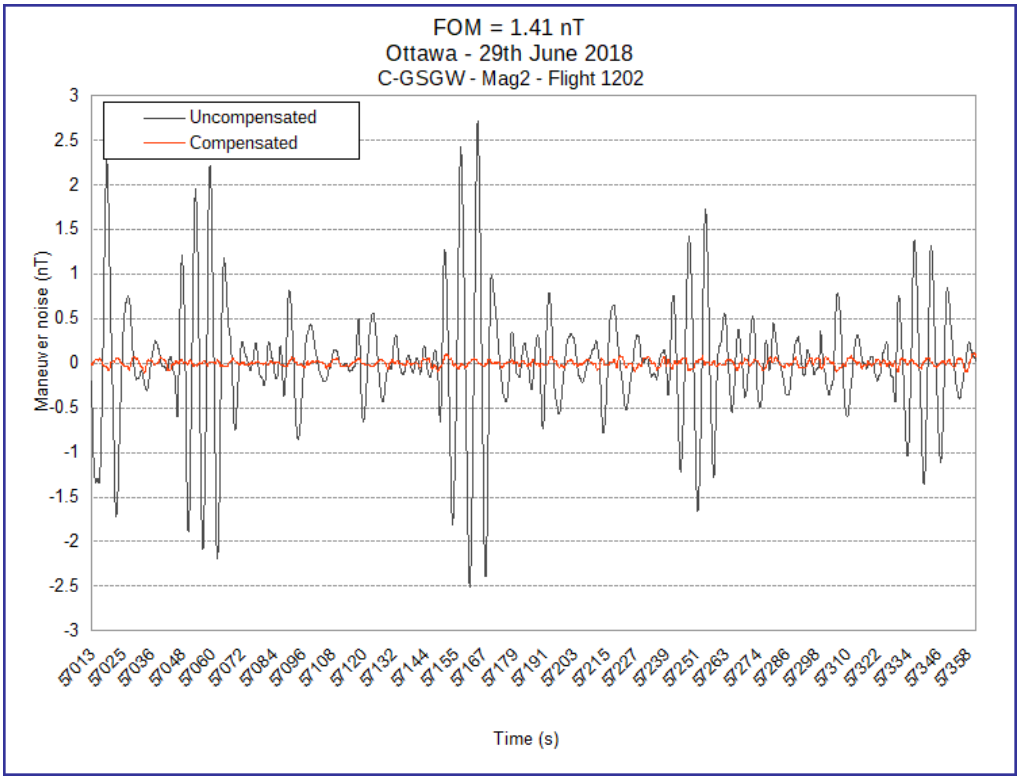

Figure 45. Figure of Merit (FOM) = 1.41 nT, Ottawa, June 29, 2018, C-GSGW, Mag2, flight 1202.

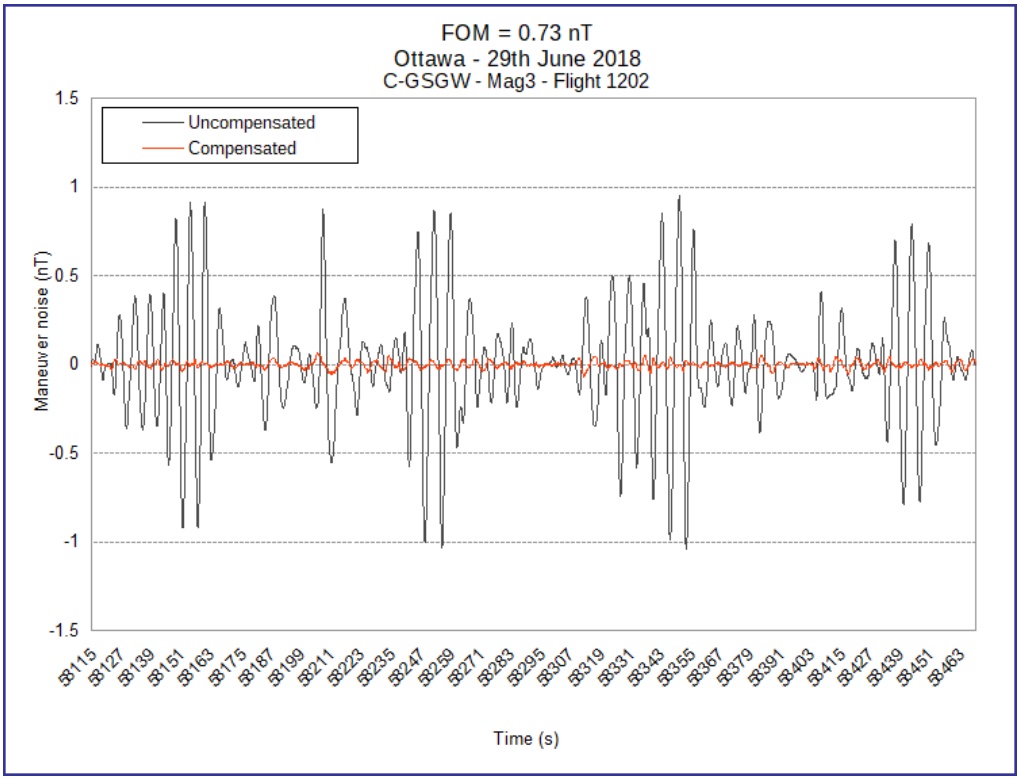

Figure 46. Figure of Merit (FOM) = 0.73 nT, Ottawa, June 29, 2018, C-GSGW, Mag3, flight 1202.

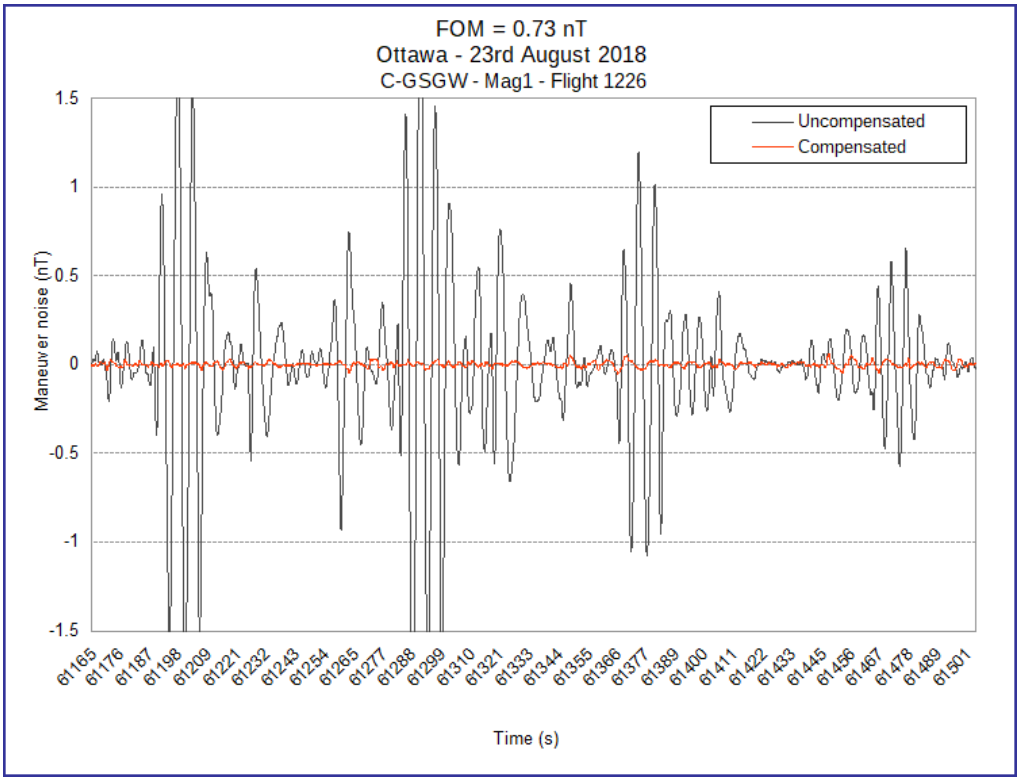

Figure 47. Figure of Merit (FOM) = 0.73 nT, Ottawa, August 23, 2018, C-GSGW, Mag1, flight 1226.

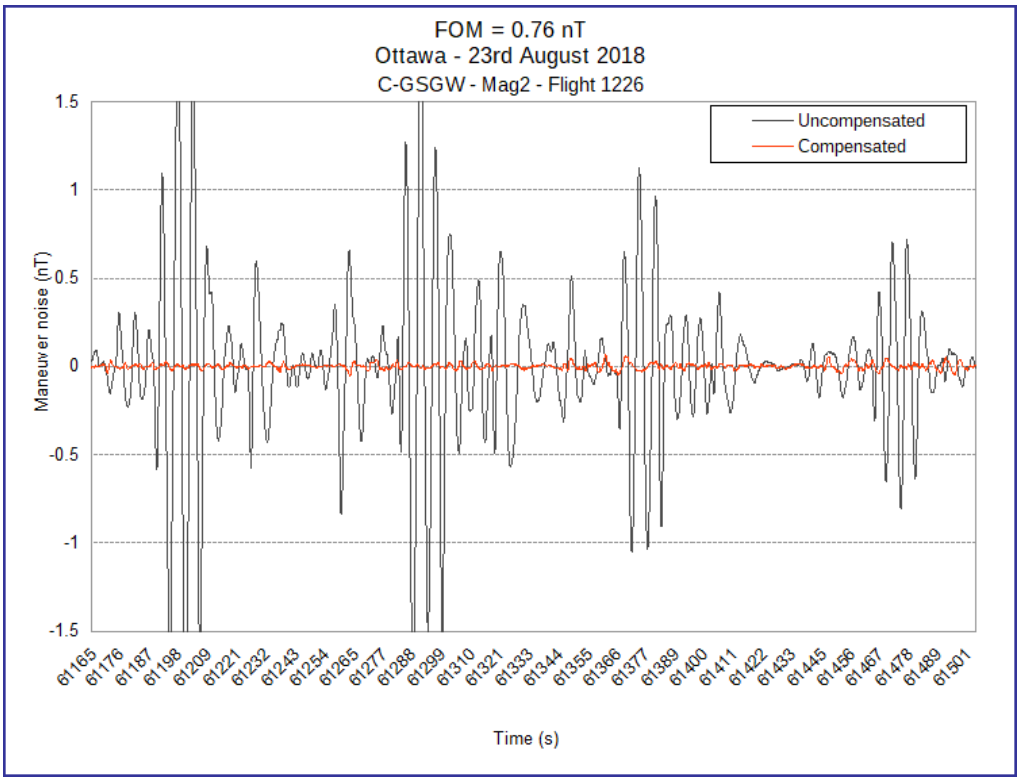

Figure 48. Figure of Merit (FOM) = 0.76 nT, Ottawa, August 23, 2018, C-GSGW, Mag2, flight 1226.

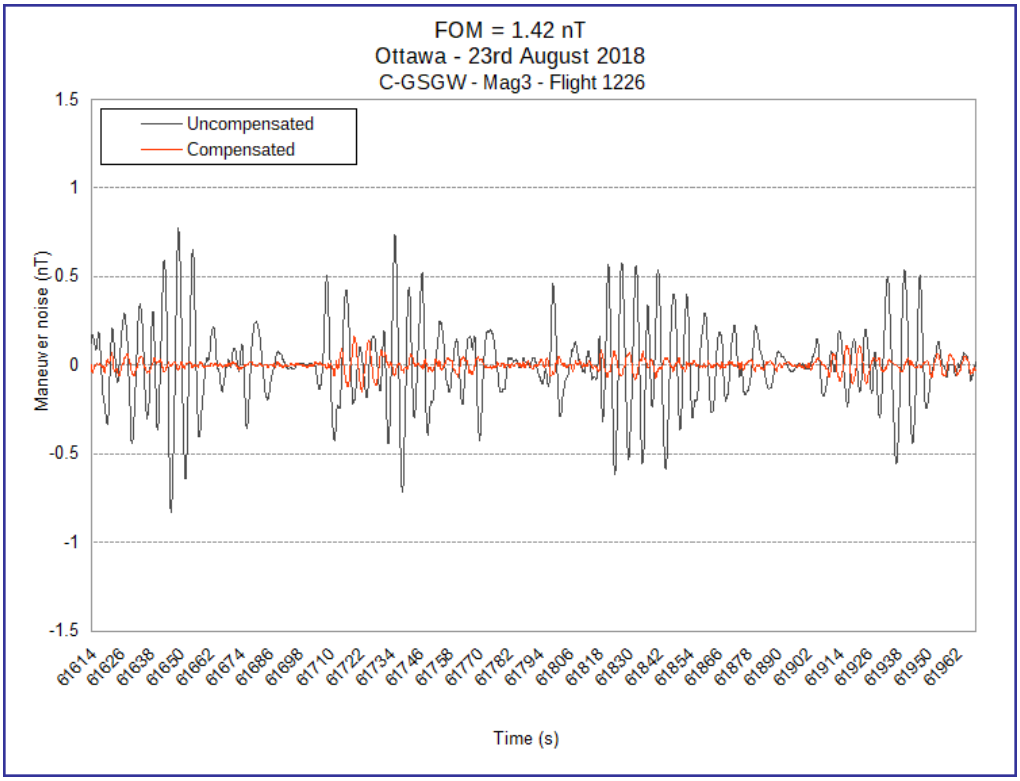

Figure 49. Figure of Merit (FOM) = 1.42 nT, Ottawa, August 23, 2018, C-GSGW, Mag3, flight 1226.

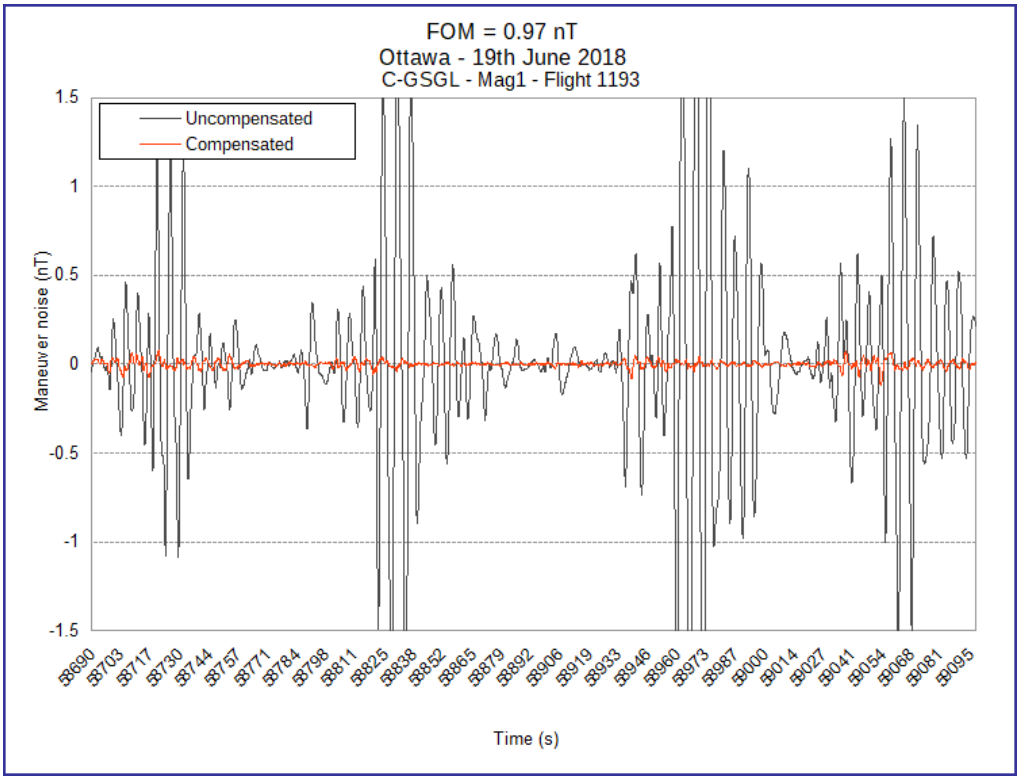

Figure 50. Figure of Merit (FOM) = 0.97 nT, Ottawa, June 19, 2018, C-GSGL, Mag1, flight 1193.

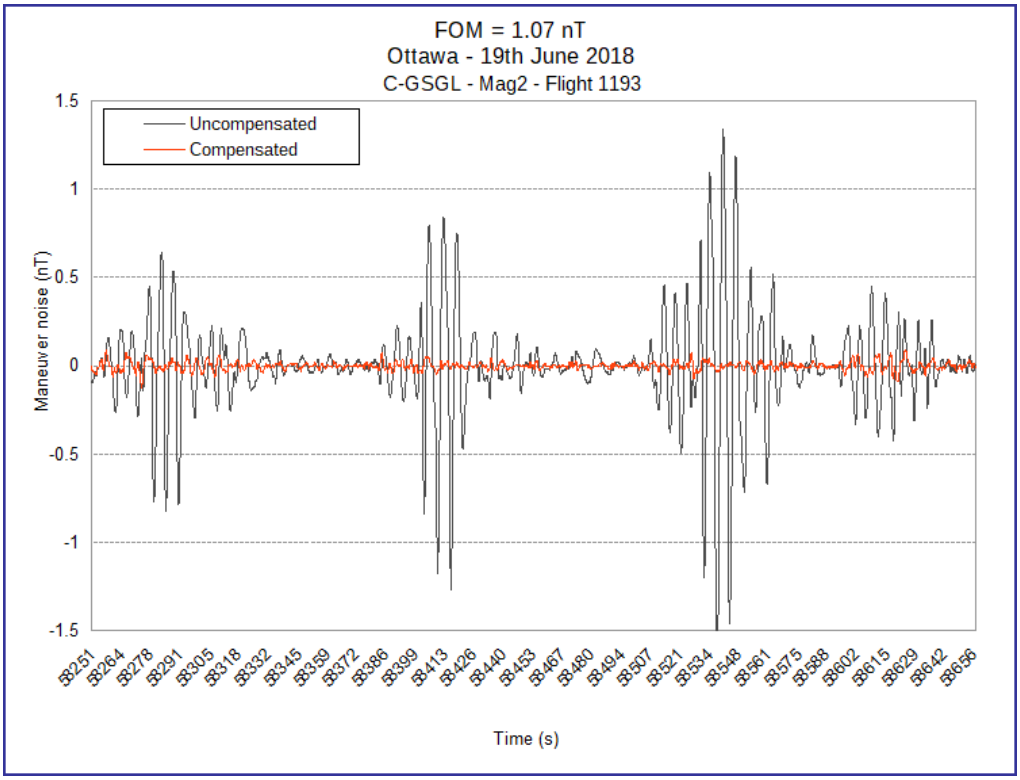

Figure 51. Figure of Merit (FOM) = 1.07 nT, Ottawa, June 19, 2018, C-GSGL, Mag2, flight 1193.

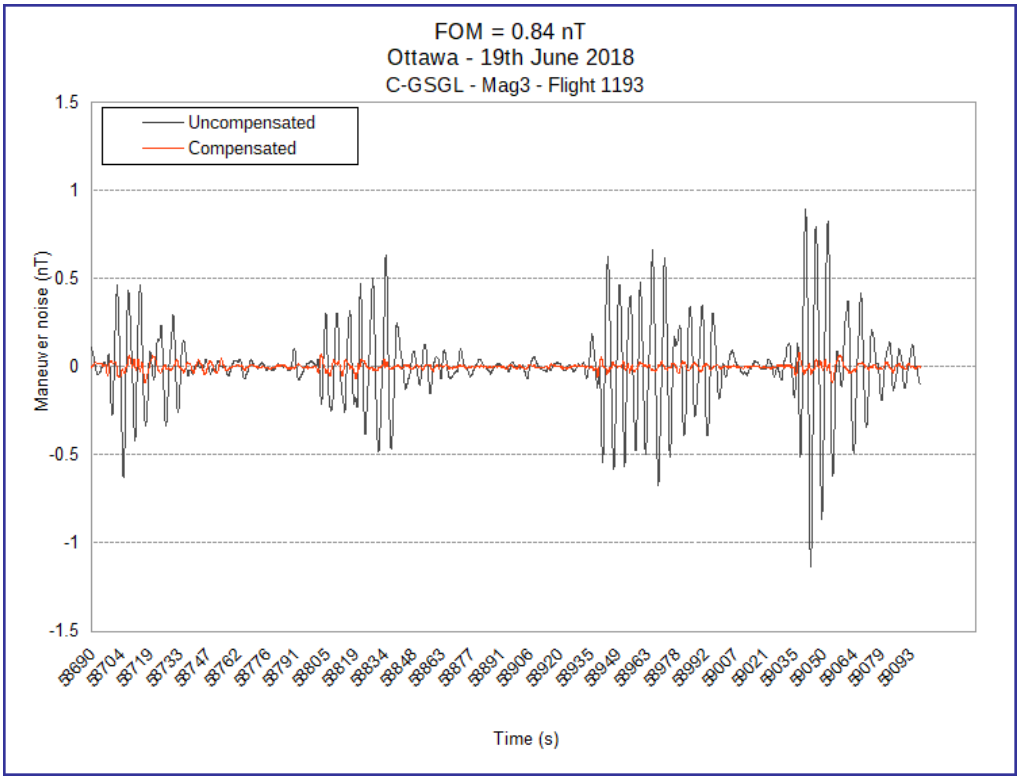

Figure 52. Figure of Merit (FOM) = 0.84 nT, Ottawa, June 19, 2018, C-GSGL, Mag3, flight 1193.

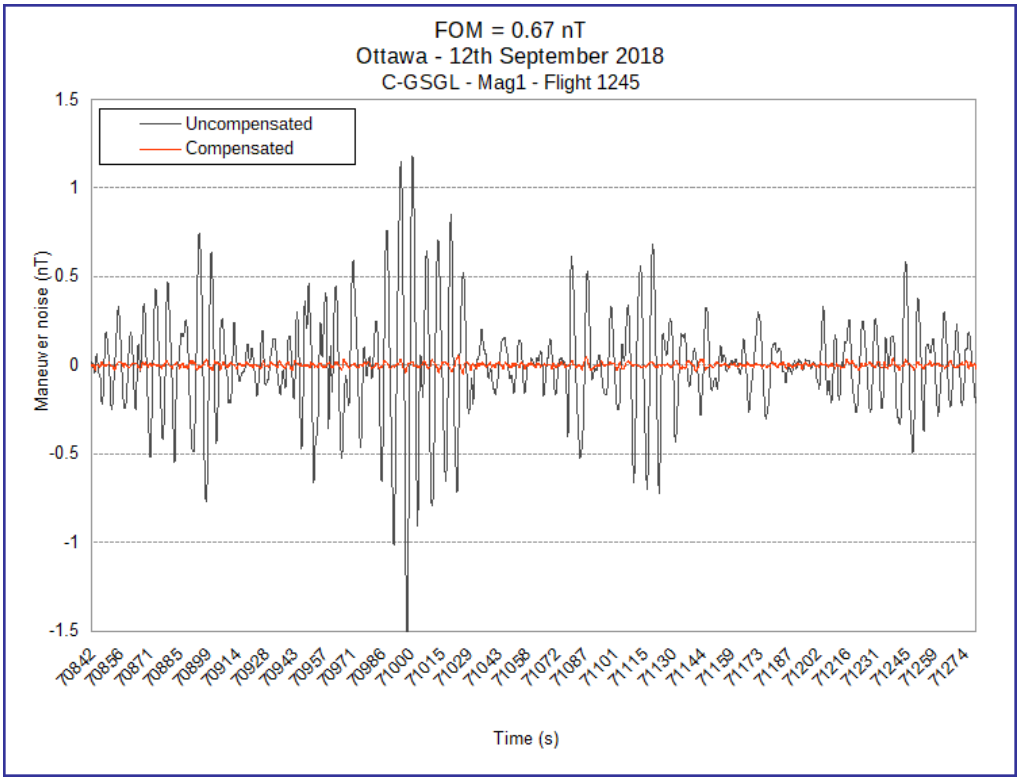

Figure 53. Figure of Merit (FOM) = 0.67 nT, Ottawa, September 12, 2018, C-GSGL, Mag1, flight 1245.

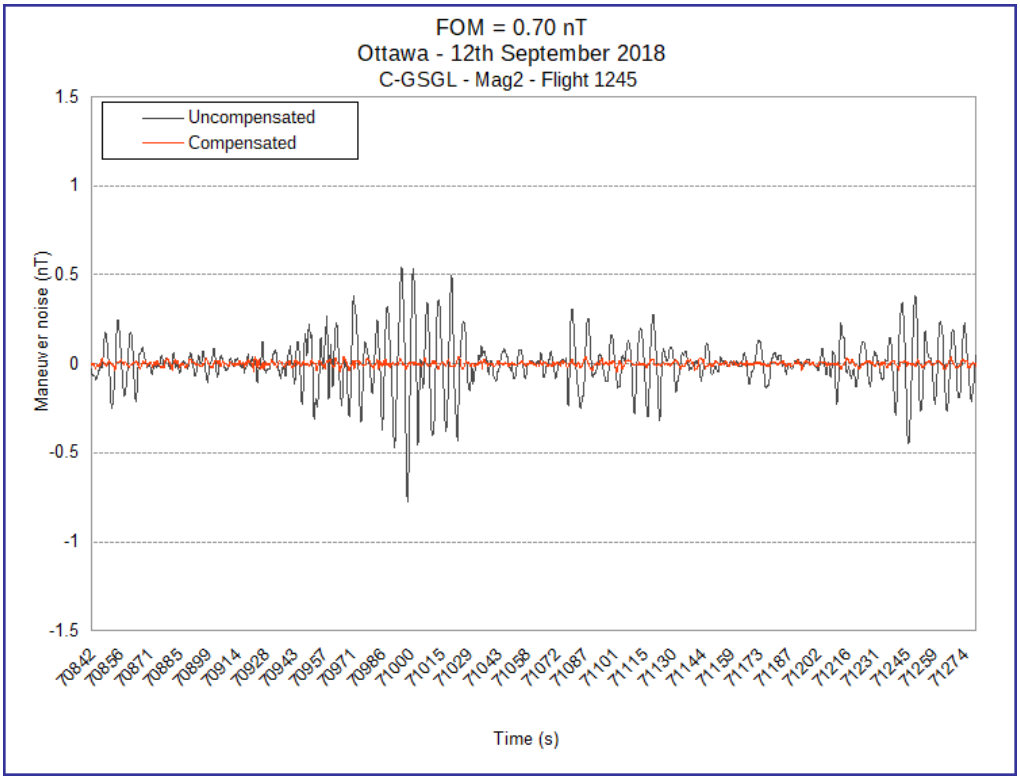

Figure 54. Figure of Merit (FOM) = 0.70 nT, Ottawa, September 12, 2018, C-GSGL, Mag2, flight 1245.

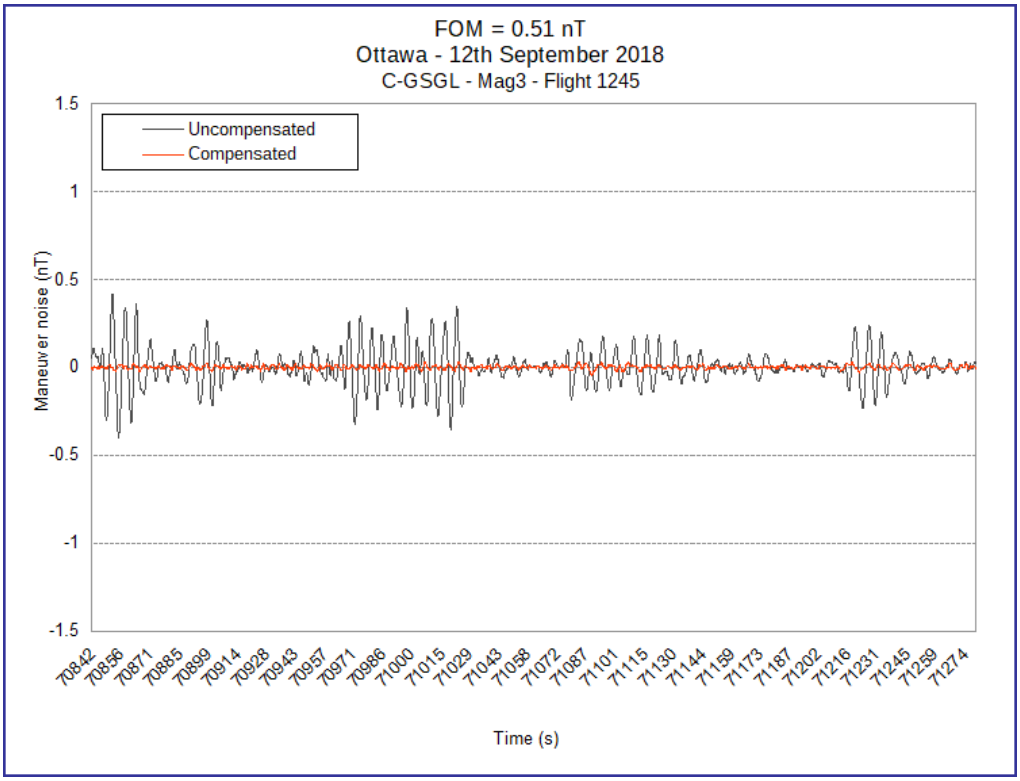

Figure 55. Figure of Merit (FOM) = 0.51 nT, Ottawa, September 12, 2018, C-GSGL, Mag3, flight 1245.

4. MAGNETOMETER HEADING TEST AND GPS NAVIGATION TEST

The heading test for the magnetometer was carried out at the Morewood test site west of Ottawa, established by the Geological Survey of Canada, by flying in a "cloverleaf" pattern over a predetermined location with a known value at 1500 feet above the ground. This pattern allows the airplane to fly 2 passes in 4 directions (NW, SE, NE, SW) while crossing over a single intersection point. For each pass (at the intersection point), magnetic data are recorded for both the airplane and on the ground at the geomagnetic observatory located at Blackburn just east of Ottawa. These data are then used to determine the error values for each magnetometer and the heading error effects. Tests were flown before deployment as follows: C-GSGV and C-GSGL on the June 15, 2018, and C-GSGW on the June 29, 2018. This test also serves to verify the functioning of the GPS Navigation System. Results are provided below.

Figure 56. Flight path of the heading tests flown over the Geological Survey of Canada (GSC) Morewood calibration point, superimposed on an image *from* Google Earth™ mapping service.

Table 8. Aeromagnetic survey system calibration test, Cessna® 208B Grand Caravan® C-GSGV Port, June 15, 2018.

AEROMAGNETIC SURVEY SYSTEM CALIBRATION TEST RANGES AT MOREWOOD, ONTARIO							
AIRCRAFT TYPE AND REGISTRATION: Cessna® 208B Grand Caravan® (C-GSGV) ORGANIZATION (COMPANY): Sander Geophysics Ltd. MAGNETOMETER TYPE: Geometrics G-822A MAGNETOMETER SERIAL NUMBER: 75117-C733 Port COMPILED BY: Jenrené Martel				DATE: June 15, 2018 HEIGHT FLOWN (AGL): 1500 feet SAMPLING RATE: 10 / second DATA ACQUISITION SYSTEM: SGDAS GSC 11/2015			
Direction of flight across the intersection point	**Time that Survey Aircraft was over the intersection point (HH/MM/SS) Greenwich Mean Time**	**Total Field Value (nT) Recorded in Survey Aircraft over the intersection point (T1)**	**Observatory Diurnal Reading at Previous Minute, i.e., Hours + Minutes (T2) from Printout**	**Observatory Diurnal Reading at Subsequent Minute, i.e., H hours + (M + 1) mins. (T3) from Printout**	**Interpolated Observatory Diurnal Reading at Time H hours + M mins + S sec T4 = T2 + S (T3 − T2) ----- 60**	**Calculated Observatory Value T5 = T4 − C***	**Error Value T6 = T1 − T5**
NW	18:49:35	53,532.17	54,180.5	54,180.5	54180.5	53540.4	−8.24
SE	18:37:58	53,529.62	54,178.4	54,178.4	54178.4	53538.3	−8.64
NE	18:54:31	53,531.53	54,179.9	54,179.9	54179.9	53539.8	−8.28
SW	18:43:16	53,531.42	54,179.7	54,179.7	54179.7	53539.6	−8.19
NW	19:09:19	53,534.26	54,182.7	54,182.7	54182.7	53542.6	−8.30
SE	18:59:07	53,532.87	54,181.7	54,181.7	54181.7	53541.6	−8.71
NE	19:14:10	53,534.54	54,183.0	54,183.0	54183.0	53542.9	−8.40
SW	19:04:12	53,534.42	54,182.8	54,182.8	54182.8	53542.7	−8.23

**C is the difference in the total field between the Blackburn, Meanook and Baker Observatories (O) and the value (B) at the test site intersection point above the designated height.*
Ottawa(O)/Morewood(B), Ontario: 1500 feet, C = (O − B) = 640.1 nT

Total = −66.99 nT

Average North-South Heading Error (T6 North – T6 South) = 0.40 nT
Average East-West Heading Error (T6 East – T6 West) = −0.13 nT

Number of Passes for Average = 8 passes *Average = −8.37 nT*

Table 9. Aeromagnetic survey system calibration test, Cessna® 208B Grand Caravan® C-GSGV Starboard, June 15, 2018.

AEROMAGNETIC SURVEY SYSTEM CALIBRATION TEST RANGES AT MOREWOOD, ONTARIO							
AIRCRAFT TYPE AND REGISTRATION: Cessna® 208B Grand Caravan® (C-GSGV) ORGANIZATION (COMPANY): Sander Geophysics Ltd. MAGNETOMETER TYPE: Geometrics G-822A MAGNETOMETER SERIAL NUMBER: 75288-C873 Starboard COMPILED BY: Jenrené Martel				DATE: June 15, 2018 HEIGHT FLOWN (AGL): 1500 feet SAMPLING RATE: 10 / second DATA ACQUISITION SYSTEM: SGDAS GSC 11/2015			
Direction of flight across the intersection point	**Time that Survey Aircraft was over the intersection point (HH/MM/SS) Greenwich Mean Time**	**Total Field Value (nT) Recorded in Survey Aircraft over the intersection point (T1)**	**Observatory Diurnal Reading at Previous Minute, i.e., Hours + Minutes (T2) from Printout**	**Observatory Diurnal Reading at Subsequent Minute, i.e., H hours + (M + 1) mins. (T3) from Printout**	**Interpolated Observatory Diurnal Reading at Time H hours + M mins + S sec T4 = T2 + S (T3 − T2) ----- 60**	**Calculated Observatory Value T5 = T4 − C***	**Error Value T6 = T1 − T5**
NW	18:49:35	53,538.16	54,180.5	54,180.5	54180.5	53540.4	−2.25
SE	18:37:58	53,534.88	54,178.4	54,178.4	54178.4	53538.3	−3.38
NE	18:54:31	53,537.42	54,179.9	54,179.9	54179.9	53539.8	−2.39
SW	18:43:16	53,536.77	54,179.7	54,179.7	54179.7	53539.6	−2.84
NW	19:09:19	53,540.04	54,182.7	54,182.7	54182.7	53542.6	−2.52
SE	18:59:07	53,538.17	54,181.7	54,181.7	54181.7	53541.6	−3.41
NE	19:14:10	53,540.35	54,183.0	54,183.0	54183.0	53542.9	−2.59
SW	19:04:12	53,539.68	54,182.8	54,182.8	54182.8	53542.7	−2.97

**C is the difference in the total field between the Blackburn, Meanook and Baker Observatories (O) and the value (B) at the test site intersection point above the designated height.*
Ottawa(O)/Morewood(B), Ontario: 1500 feet, C = (O − B) = 640.1 nT

Total = −22.35 nT

Average North-South Heading Error (T6 North – T6 South) = 1.01 nT
Average East-West Heading Error (T6 East – T6 West) = 0.41 nT

Number of Passes for Average = 8 passes *Average = −2.79 nT*

Table 10. Aeromagnetic survey system calibration test, Cessna® 208B Grand Caravan® C-GSGV Tail, June 15, 2018.

AEROMAGNETIC SURVEY SYSTEM CALIBRATION TEST RANGES AT MOREWOOD, ONTARIO							
AIRCRAFT TYPE AND REGISTRATION: Cessna® 208B Grand Caravan® (C-GSGV) ORGANIZATION (COMPANY): Sander Geophysics Ltd. MAGNETOMETER TYPE: Geometrics G-822A MAGNETOMETER SERIAL NUMBER: 75189-C248 Tail COMPILED BY: Jenrené Martel				DATE: June 15, 2018 HEIGHT FLOWN (AGL): 1500 feet SAMPLING RATE: 10 / second DATA ACQUISITION SYSTEM: SGDAS GSC 11/2015			
Direction of flight across the intersection point	**Time that Survey Aircraft was over the intersection point (HH/MM/SS) Greenwich Mean Time**	**Total Field Value (nT) Recorded in Survey Aircraft over the intersection point (T1)**	**Observatory Diurnal Reading at Previous Minute, i.e., Hours + Minutes (T2) from Printout**	**Observatory Diurnal Reading at Subsequent Minute, i.e., H hours + (M + 1) mins. (T3) from Printout**	**Interpolated Observatory Diurnal Reading at Time H hours + M mins + S sec T4 = T2 + S (T3 − T2) ----- 60**	**Calculated Observatory Value T5 = T4 − C***	**Error Value T6 = T1 − T5**
NW	18:49:35	53,541.42	54,180.5	54,180.5	54180.5	53540.4	1.01
SE	18:37:58	53,538.21	54,178.4	54,178.4	54178.4	53538.3	−0.05
NE	18:54:31	53,540.66	54,179.9	54,179.9	54179.9	53539.8	0.85
SW	18:43:16	53,540.14	54,179.7	54,179.7	54179.7	53539.6	0.53
NW	19:09:19	53,543.39	54,182.7	54,182.7	54182.7	53542.6	0.83
SE	18:59:07	53,541.45	54,181.7	54,181.7	54181.7	53541.6	−0.13
NE	19:14:10	53,543.67	54,183.0	54,183.0	54183.0	53542.9	0.73
SW	19:04:12	53,543.18	54,182.8	54,182.8	54182.8	53542.7	0.53

**C is the difference in the total field between the Blackburn, Meanook and Baker Observatories (O) and the value (B) at the test site intersection point above the designated height.*
Ottawa(O)/Morewood(B), Ontario: 1500 feet, C = (O − B) = 640.1 nT

Total = 4.30 nT

Average North-South Heading Error (T6 North – T6 South) = 1.01 nT
Average East-West Heading Error (T6 East – T6 West) = 0.26 nT

Number of Passes for Average = 8 passes *Average = 0.54 nT*

Table 11. Aeromagnetic survey system calibration test, Cessna® 208B Grand Caravan® C-GSGW Port, June 29, 2018.

AEROMAGNETIC SURVEY SYSTEM CALIBRATION TEST RANGES AT MOREWOOD, ONTARIO							
AIRCRAFT TYPE AND REGISTRATION: Cessna® 208B Grand Caravan® (C-GSGW) ORGANIZATION (COMPANY): Sander Geophysics Ltd. MAGNETOMETER TYPE: Geometrics G-822A MAGNETOMETER SERIAL NUMBER: 75300-C4925 Port COMPILED BY: Jenrené Martel				DATE: June 29, 2018 HEIGHT FLOWN (AGL): 1500 feet SAMPLING RATE: 10 / second DATA ACQUISITION SYSTEM: SGDAS GSC 11/2015			
Direction of flight across the intersection point	**Time that Survey Aircraft was over the intersection point (HH/MM/SS) Greenwich Mean Time**	**Total Field Value (nT) Recorded in Survey Aircraft over the intersection point (T1)**	**Observatory Diurnal Reading at Previous Minute, i.e., Hours + Minutes (T2) from Printout**	**Observatory Diurnal Reading at Subsequent Minute, i.e., H hours + (M + 1) mins. (T3) from Printout**	**Interpolated Observatory Diurnal Reading at Time H hours + M mins + S sec T4 = T2 + S (T3 − T2) ----- 60**	**Calculated Observatory Value T5 = T4 − C***	**Error Value T6 = T1 − T5**
NW	17:35:16	53,528.73	54,171.3	54,171.3	54171.3	53531.2	−2.43
SE	17:25:19	53,528.55	54,172.3	54,172.3	54172.3	53532.2	−3.62
NE	17:39:43	53,528.44	54,171.8	54,171.8	54171.8	53531.7	−3.21
SW	17:29:55	53,528.69	54,171.7	54,171.7	54171.7	53531.6	−2.90
NW	17:54:12	53,528.49	54,172.2	54,172.2	54172.2	53532.1	−3.58
SE	17:44:38	53,528.17	54,172.2	54,172.2	54172.2	53532.1	−3.96
NE	17:58:08	53,528.87	54,172.9	54,172.9	54172.9	53532.8	−3.97
SW	17:49:24	53,528.91	54,172.7	54,172.7	54172.7	53532.6	−3.68

**C is the difference in the total field between the Blackburn, Meanook and Baker Observatories (O) and the value (B) at the test site intersection point above the designated height.*
Ottawa(O)/Morewood(B), Ontario: 1500 feet, C = (O − B) = 640.1 nT

Total = −27.35 nT

Average North-South Heading Error (T6 North – T6 South) = 0.78 nT
Average East-West Heading Error (T6 East – T6 West) = −0.30 nT

Number of Passes for Average = 8 passes *Average = −3.42 nT*

Table 12. Aeromagnetic survey system calibration test, Cessna® 208B Grand Caravan® C-GSGW Starboard, June 29, 2018.

AEROMAGNETIC SURVEY SYSTEM CALIBRATION TEST RANGES AT MOREWOOD, ONTARIO							
AIRCRAFT TYPE AND REGISTRATION: Cessna® 208B Grand Caravan® (C-GSGW) ORGANIZATION (COMPANY): Sander Geophysics Ltd. MAGNETOMETER TYPE: Geometrics G-822A MAGNETOMETER SERIAL NUMBER: 75246-C517 Starboard COMPILED BY: Jenrené Martel				DATE: June 29, 2018 HEIGHT FLOWN (AGL): 1500 feet SAMPLING RATE: 10 / second DATA ACQUISITION SYSTEM: SGDAS GSC 11/2015			
Direction of flight across the intersection point	**Time that Survey Aircraft was over the intersection point (HH/MM/SS) Greenwich Mean Time**	**Total Field Value (nT) Recorded in Survey Aircraft over the intersection point (T1)**	**Observatory Diurnal Reading at Previous Minute, i.e., Hours + Minutes (T2) from Printout**	**Observatory Diurnal Reading at Subsequent Minute, i.e., H hours + (M + 1) mins. (T3) from Printout**	**Interpolated Observatory Diurnal Reading at Time H hours + M mins + S sec T4 = T2 + S (T3 − T2) ----- 60**	**Calculated Observatory Value T5 = T4 − C***	**Error Value T6 = T1 − T5**
NW	17:35:16	53,537.99	54,171.3	54,171.3	54171.3	53531.2	6.83
SE	17:25:19	53,538.75	54,172.3	54,172.3	54172.3	53532.2	6.58
NE	17:39:43	53,538.76	54,171.8	54,171.8	54171.8	53531.7	7.11
SW	17:29:55	53,538.79	54,171.7	54,171.7	54171.7	53531.6	7.20
NW	17:54:12	53,538.12	54,172.2	54,172.2	54172.2	53532.1	6.05
SE	17:44:38	53,538.46	54,172.2	54,172.2	54172.2	53532.1	6.33
NE	17:58:08	53,538.08	54,172.9	54,172.9	54172.9	53532.8	5.24
SW	17:49:24	53,539.54	54,172.7	54,172.7	54172.7	53532.6	6.95

**C is the difference in the total field between the Blackburn, Meanook and Baker Observatories (O) and the value (B) at the test site intersection point above the designated height.*
Ottawa(O)/Morewood(B), Ontario: 1500 feet, C = (O − B) = 640.1 nT

Total = 52.29 nT

Average North-South Heading Error (T6 North – T6 South) = −0.01 nT
Average East-West Heading Error (T6 East – T6 West) = −0.90 nT

Number of Passes for Average = 8 passes *Average = 6.54 nT*

Table 13. Aeromagnetic survey system calibration test, Cessna® 208B Grand Caravan® C-GSGW Tail, June 29, 2018.

AEROMAGNETIC SURVEY SYSTEM CALIBRATION TEST RANGES AT MOREWOOD, ONTARIO							
AIRCRAFT TYPE AND REGISTRATION: Cessna® 208B Grand Caravan® (C-GSGW) ORGANIZATION (COMPANY): Sander Geophysics Ltd. MAGNETOMETER TYPE: Geometrics G-822A MAGNETOMETER SERIAL NUMBER: 75231-C020 Tail COMPILED BY: Jenrené Martel				DATE: June 29, 2018 HEIGHT FLOWN (AGL): 1500 feet SAMPLING RATE: 10 / second DATA ACQUISITION SYSTEM: SGDAS GSC 11/2015			
Direction of flight across the intersection point	**Time that Survey Aircraft was over the intersection point (HH/MM/SS) Greenwich Mean Time**	**Total Field Value (nT) Recorded in Survey Aircraft over the intersection point (T1)**	**Observatory Diurnal Reading at Previous Minute, i.e., Hours + Minutes (T2) from Printout**	**Observatory Diurnal Reading at Subsequent Minute, i.e., H hours + (M + 1) mins. (T3) from Printout**	**Interpolated Observatory Diurnal Reading at Time H hours + M mins + S sec T4 = T2 + S (T3 − T2) ----- 60**	**Calculated Observatory Value T5 = T4 − C***	**Error Value T6 = T1 − T5**
NW	17:35:16	53,535.47	54,171.3	54,171.3	54171.3	53531.2	4.31
SE	17:25:19	53,534.67	54,172.3	54,172.3	54172.3	53532.2	2.50
NE	17:39:43	53,534.97	54,171.8	54,171.8	54171.8	53531.7	3.32
SW	17:29:55	53,534.89	54,171.7	54,171.7	54171.7	53531.6	3.30
NW	17:54:12	53,535.09	54,172.2	54,172.2	54172.2	53532.1	3.02
SE	17:44:38	53,534.25	54,172.2	54,172.2	54172.2	53532.1	2.12
NE	17:58:08	53,535.46	54,172.9	54,172.9	54172.9	53532.8	2.62
SW	17:49:24	53,535.13	54,172.7	54,172.7	54172.7	53532.6	2.54

**C is the difference in the total field between the Blackburn, Meanook and Baker Observatories (O) and the value (B) at the test site intersection point above the designated height.*
Ottawa(O)/Morewood(B), Ontario: 1500 feet, C = (O − B) = 640.1 nT

Total = 23.73 nT

Average North-South Heading Error (T6 North – T6 South) = 1.35 nT
Average East-West Heading Error (T6 East – T6 West) = 0.05 nT

Number of Passes for Average = 8 passes *Average = 2.97 nT*

Table 14. Aeromagnetic survey system calibration test, Cessna® 208B Grand Caravan® C-GSGL Port, June 15, 2018.

AEROMAGNETIC SURVEY SYSTEM CALIBRATION TEST RANGES AT MOREWOOD, ONTARIO							
AIRCRAFT TYPE AND REGISTRATION: Cessna® 208B Grand Caravan® (C-GSGL) ORGANIZATION (COMPANY): Sander Geophysics Ltd. MAGNETOMETER TYPE: Geometrics G-822A MAGNETOMETER SERIAL NUMBER: 75423-C1931 Port COMPILED BY: Jenrené Martel				DATE: June 15, 2018 HEIGHT FLOWN (AGL): 1500 feet SAMPLING RATE: 10 / second DATA ACQUISITION SYSTEM: SGDAS GSC 11/2015			
Direction of flight across the intersection point	**Time that Survey Aircraft was over the intersection point (HH/MM/SS) Greenwich Mean Time**	**Total Field Value (nT) Recorded in Survey Aircraft over the intersection point (T1)**	**Observatory Diurnal Reading at Previous Minute, i.e., Hours + Minutes (T2) from Printout**	**Observatory Diurnal Reading at Subsequent Minute, i.e., H hours + (M + 1) mins. (T3) from Printout**	**Interpolated Observatory Diurnal Reading at Time H hours + M mins + S sec T4 = T2 + S (T3 − T2) ----- 60**	**Calculated Observatory Value T5 = T4 − C***	**Error Value T6 = T1 − T5**
NW	16:35:54	53,528.00	54,163.6	54,163.6	54163.6	53523.5	4.55
SE	16:45:26	53,530.80	54,168.0	54,168.0	54168.0	53527.9	2.91
NE	16:40:30	53,530.24	54,166.3	54,166.3	54166.3	53526.2	4.08
SW	16:50:10	53,532.63	54,169.1	54,169.1	54169.1	53529.0	3.60
NW	16:55:15	53,534.44	54,170.0	54,170.0	54170.0	53529.9	4.53
SE	17:04:34	53,533.82	54,170.7	54,170.7	54170.7	53530.6	3.25
NE	16:59:42	53,535.11	54,170.8	54,170.8	54170.8	53530.7	4.37
SW	17:09:18	53,532.60	54,169.1	54,169.1	54169.1	53529.0	3.64

**C is the difference in the total field between the Blackburn, Meanook and Baker Observatories (O) and the value (B) at the test site intersection point above the designated height.*
Ottawa(O)/Morewood(B), Ontario: 1500 feet, C = (O − B) = 640.1 nT

Total = 30.93 nT

Average North-South Heading Error (T6 North – T6 South) = 1.46 nT
Average East-West Heading Error (T6 East – T6 West) = 0.60 nT

Number of Passes for Average = 8 passes *Average = 3.87 nT*

Table 15. Aeromagnetic survey system calibration test, Cessna® 208B Grand Caravan® C-GSGL Starboard, June 15, 2018.

AEROMAGNETIC SURVEY SYSTEM CALIBRATION TEST RANGES AT MOREWOOD, ONTARIO							
AIRCRAFT TYPE AND REGISTRATION: Cessna® 208B Grand Caravan® (C-GSGL) ORGANIZATION (COMPANY): Sander Geophysics Ltd. MAGNETOMETER TYPE: Geometrics G-822A MAGNETOMETER SERIAL NUMBER: 75304-C1015 Starboard COMPILED BY: Jenrené Martel				DATE: June 15, 2018 HEIGHT FLOWN (AGL): 1500 feet SAMPLING RATE: 10 / second DATA ACQUISITION SYSTEM: SGDAS GSC 11/2015			
Direction of flight across the intersection point	**Time that Survey Aircraft was over the intersection point (HH/MM/SS) Greenwich Mean Time**	**Total Field Value (nT) Recorded in Survey Aircraft over the intersection point (T1)**	**Observatory Diurnal Reading at Previous Minute, i.e., Hours + Minutes (T2) from Printout**	**Observatory Diurnal Reading at Subsequent Minute, i.e., H hours + (M + 1) mins. (T3) from Printout**	**Interpolated Observatory Diurnal Reading at Time H hours + M mins + S sec T4 = T2 + S (T3 − T2) ----- 60**	**Calculated Observatory Value T5 = T4 − C***	**Error Value T6 = T1 − T5**
NW	16:35:54	53,526.67	54,163.6	54,163.6	54163.6	53523.5	3.22
SE	16:45:26	53,531.12	54,168.0	54,168.0	54168.0	53527.9	3.23
NE	16:40:30	53,528.88	54,166.3	54,166.3	54166.3	53526.2	2.72
SW	16:50:10	53,533.41	54,169.1	54,169.1	54169.1	53529.0	4.38
NW	16:55:15	53,533.26	54,170.0	54,170.0	54170.0	53529.9	3.35
SE	17:04:34	53,534.11	54,170.7	54,170.7	54170.7	53530.6	3.54
NE	16:59:42	53,533.75	54,170.8	54,170.8	54170.8	53530.7	3.01
SW	17:09:18	53,533.57	54,169.1	54,169.1	54169.1	53529.0	4.61

**C is the difference in the total field between the Blackburn, Meanook and Baker Observatories (O) and the value (B) at the test site intersection point above the designated height.*
Ottawa(O)/Morewood(B), Ontario: 1500 feet, C = (O − B) = 640.1 nT

Total = 28.06 nT

Average North-South Heading Error (T6 North – T6 South) = −0.10 nT
Average East-West Heading Error (T6 East – T6 West) = −1.63 nT

Number of Passes for Average = 8 passes *Average = 3.51 nT*

Table 16. Aeromagnetic survey system calibration test, Cessna® 208B Grand Caravan® C-GSGL Tail, June 15, 2018.

AEROMAGNETIC SURVEY SYSTEM CALIBRATION TEST RANGES AT MOREWOOD, ONTARIO							
AIRCRAFT TYPE AND REGISTRATION: Cessna® 208B Grand Caravan® (C-GSGL) ORGANIZATION (COMPANY): Sander Geophysics Ltd. MAGNETOMETER TYPE: Geometrics G-822A MAGNETOMETER SERIAL NUMBER: 75307-C1325 Tail COMPILED BY: Jenrené Martel				DATE: June 15, 2018 HEIGHT FLOWN (AGL): 1500 feet SAMPLING RATE: 10 / second DATA ACQUISITION SYSTEM: SGDAS GSC 11/2015			
Direction of flight across the intersection point	**Time that Survey Aircraft was over the intersection point (HH/MM/SS) Greenwich Mean Time**	**Total Field Value (nT) Recorded in Survey Aircraft over the intersection point (T1)**	**Observatory Diurnal Reading at Previous Minute, i.e., Hours + Minutes (T2) from Printout**	**Observatory Diurnal Reading at Subsequent Minute, i.e., H hours + (M + 1) mins. (T3) from Printout**	**Interpolated Observatory Diurnal Reading at Time H hours + M mins + S sec T4 = T2 + S (T3 − T2) ----- 60**	**Calculated Observatory Value T5 = T4 − C***	**Error Value T6 = T1 − T5**
NW	16:35:54	53,529.68	54,163.6	54,163.6	54163.6	53523.5	6.23
SE	16:45:26	53,534.22	54,168.0	54,168.0	54168.0	53527.9	6.33
NE	16:40:30	53,533.07	54,166.3	54,166.3	54166.3	53526.2	6.91
SW	16:50:10	53,535.34	54,169.1	54,169.1	54169.1	53529.0	6.31
NW	16:55:15	53,536.43	54,170.0	54,170.0	54170.0	53529.9	6.52
SE	17:04:34	53,537.49	54,170.7	54,170.7	54170.7	53530.6	6.92
NE	16:59:42	53,538.03	54,170.8	54,170.8	54170.8	53530.7	7.29
SW	17:09:18	53,535.32	54,169.1	54,169.1	54169.1	53529.0	6.36

**C is the difference in the total field between the Blackburn, Meanook and Baker Observatories (O) and the value (B) at the test site intersection point above the designated height.*
Ottawa(O)/Morewood(B), Ontario: 1500 feet, C = (O − B) = 640.1 nT

Total = 52.87 nT

Average North-South Heading Error (T6 North – T6 South) = −0.25 nT
Average East-West Heading Error (T6 East – T6 West) = 0.76 nT

Number of Passes for Average = 8 passes *Average = 6.61 nT*

5. SPECTROMETER STRIPPING CALIBRATION

The stripping ratios for the gamma-ray spectrometer were determined before mobilization as follows: C-GSGL on June 15, 2018; C-GSGV on June 13, 2018; and C-GSGW on June 27, 2018. The GSC mobile calibration pads, which are stored at the SGL hangar in Ottawa, were used. The tests were performed with the detectors installed in survey configuration on board the aircraft. Each detector was tested separately and the test results were averaged to create stripping ratios for this system.

The following procedure was carried out:

- cesium stabilization
- thorium stabilization
- pre-pads source test, one thorium source below pack
- stabilization on thorium taken off
- pads test carried out in order: background, potassium (6 minutes recording each)
- re-stabilize on thorium
- stabilization on thorium taken off
- pads test carried out in order: uranium, thorium and background (6 minutes recording each)
- stabilization on thorium put on
- post-pads source test, one thorium source below pack

See Tables 17 to 25 for a list of stripping ratios.

Table 17. Stripping ratios – crystal pack A, C-GSGV.

Crystal Pack A, S/N 2558, C-GSGV	ratio
Th into U (ALPHA = A23/A33):	0.2394
Th into K (BETA = A13/A33):	0.3694
U into K (GAMMA = A12/A22):	0.7153
U into Th (A = A32/A22):	0.0468
K into Th (B = A31/A11):	0.0028
K into U (G = A21/A11):	0.0140

Table 18. Stripping ratios – crystal pack B, C-GSGV.

Crystal Pack B, S/N 2645, C-GSGV	ratio
Th into U (ALPHA = A23/A33):	0.2434
Th into K (BETA = A13/A33):	0.3744
U into K (GAMMA = A12/A22):	0.7151
U into Th (A = A32/A22):	0.0380
K into Th (B = A31/A11):	0.0000
K into U (G = A21/A11):	0.0066

Table 19. Average system stripping ratios, C-GSGV.

System Stripping Ratios (C-GSGV)	ratio
Th into U (ALPHA = A23/A33):	0.2414
Th into K (BETA = A13/A33):	0.3719
U into K (GAMMA = A12/A22):	0.7152
U into Th (A = A32/A22):	0.0424
K into Th (B = A31/A11):	0.0014
K into U (G = A21/A11):	0.0103

Table 20. Stripping ratios – crystal pack A, C-GSGW.

Crystal Pack A, S/N 2664, C-GSGW	ratio
Th into U (ALPHA = A23/A33):	0.2214
Th into K (BETA = A13/A33):	0.4050
U into K (GAMMA = A12/A22):	0.7280
U into Th (A = A32/A22):	0.0421
K into Th (B = A31/A11):	0.0000
K into U (G = A21/A11):	0.0002

Table 21. Stripping ratios – crystal pack B, C-GSGW.

Crystal Pack B, S/N 2538, C-GSGW	ratio
Th into U (ALPHA = A23/A33):	0.2180
Th into K (BETA = A13/A33):	0.4106
U into K (GAMMA = A12/A22):	0.6822
U into Th (A = A32/A22):	0.0404
K into Th (B = A31/A11):	0.0000
K into U (G = A21/A11):	0.0033

Table 22. Average system stripping ratios, C-GSGW.

System Stripping Ratios (C-GSGW)	ratio
Th into U (ALPHA = A23/A33):	0.2197
Th into K (BETA = A13/A33):	0.4078
U into K (GAMMA = A12/A22):	0.7051
U into Th (A = A32/A22):	0.0413
K into Th (B = A31/A11):	0.0000
K into U (G = A21/A11):	0.0018

Table 23. Stripping ratios – crystal pack A, C-GSGL.

Crystal Pack A, S/N 2669, C-GSGL	ratio
Th into U (ALPHA = A23/A33):	0.2268
Th into K (BETA = A13/A33):	0.3857
U into K (GAMMA = A12/A22):	0.7007
U into Th (A = A32/A22):	0.0402
K into Th (B = A31/A11):	0.0000
K into U (G = A21/A11):	0.0058

Table 24. Stripping ratios – crystal pack B, C-GSGL.

Crystal Pack B, S/N 2670, C-GSGL	ratio
Th into U (ALPHA = A23/A33):	0.2298
Th into K (BETA = A13/A33):	0.3729
U into K (GAMMA = A12/A22):	0.7142
U into Th (A = A32/A22):	0.0371
K into Th (B = A31/A11):	0.0000
K into U (G = A21/A11):	0.0000

Table 25. Average system stripping ratios, C-GSGL.

System Stripping Ratios (C-GSGL)	ratio
Th into U (ALPHA = A23/A33):	0.2283
Th into K (BETA = A13/A33):	0.3793
U into K (GAMMA = A12/A22):	0.7075
U into Th (A = A32/A22):	0.0387
K into Th (B = A31/A11):	0.0000
K into U (G = A21/A11):	0.0029

6. SPECTROMETER DYNAMIC CALIBRATION RANGE

The exponential height attenuation coefficients for the spectrometer were calculated using the data acquired during pre-survey test flights over the GSC test range at Breckenridge, Quebec: C-GSGL on June 15, 2018; C-GSGV on June 15, 2018; and C-GSGW on June 29, 2018. The calibration flights were carried out from approximately 130 m to 275 m mean terrain clearance at 25 m intervals. A series of background measurements were made by flying the same altitudes over the Ottawa River to determine the background resulting from cosmic radiation, radon decay products in the air and the radioactivity of the aircraft and equipment. After correction for background and stripping, the variation in count rate with effective height was used to determine the attenuation coefficients.

At the same time the attenuation tests were flown, the spectrometer sensitivities were determined through comparison of airborne data with data acquired on the ground. The ground measurements made using an Exploranium™ portable gamma-ray spectrometer, were acquired at 32 different sites along the 10 km length of the calibration range. Measurements were also made using the portable spectrometer on the Ottawa River to determine background radiation resulting from cosmic radiation, radon decay products in the air and any radioactivity of the equipment. The background was subtracted from the ground measurements and the ground concentrations of potassium, uranium and thorium were determined by calibration of the portable spectrometer using the GSC calibration pads located at Ottawa Airport.

The sensitivities of the airborne system for potassium, equivalent uranium and equivalent thorium were calculated by dividing the average count rates corrected to an effective height of 100 m above ground by the measured ground concentrations.

The results of the attenuation and sensitivity tests are shown in Tables 26 to 31. In each chart (Figures 57 to 59), the data before correction for attenuation is shown as a thick, sloped line, and after correction by a thin, approximately flat line.

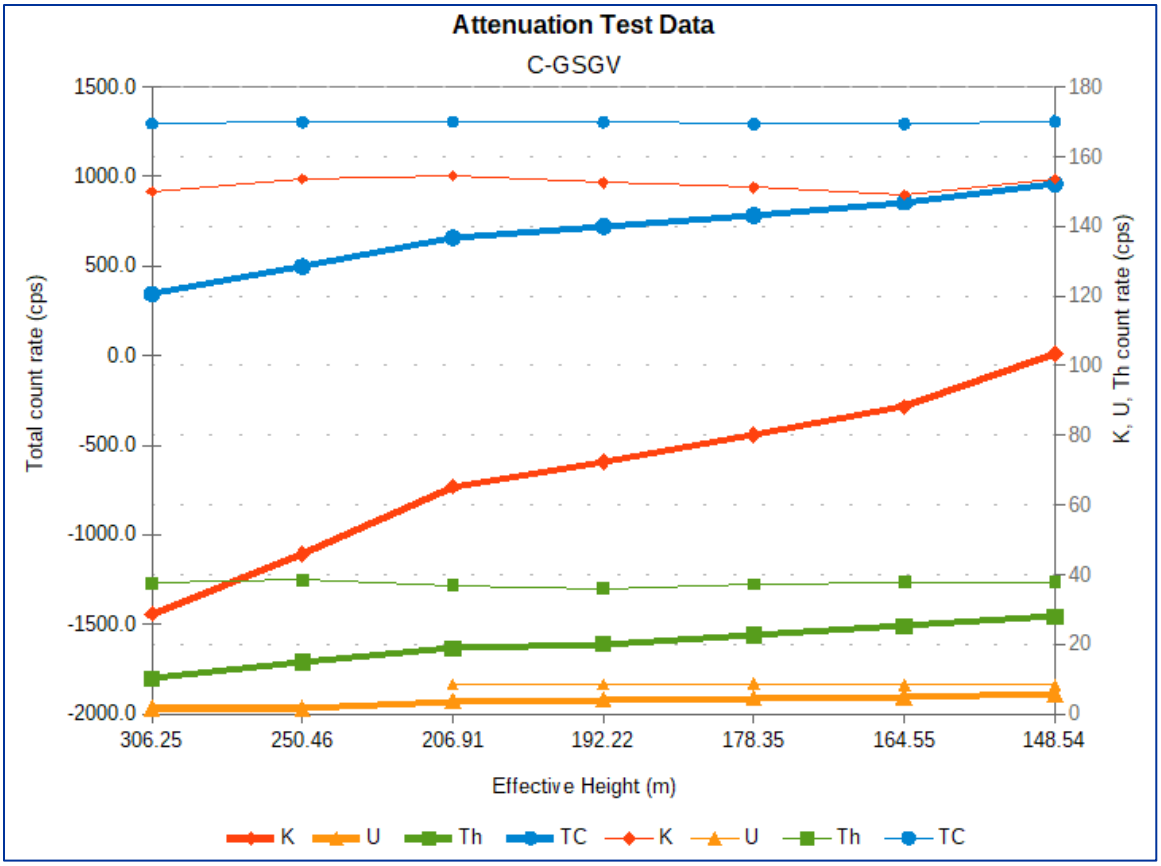

Figure 57. Attenuation test data C-GSGV.

Table 26. Attenuation coefficients – C-GSGV.

Total Count	−0.006413
Potassium	−0.007974
Uranium	−0.007492
Thorium	−0.006297

Table 27. System sensitivities – C-GSGV.

Potassium	85.3183 cps/%K
Uranium	6.6074 cps/eU ppm
Thorium	5.2263 cps/eTh ppm

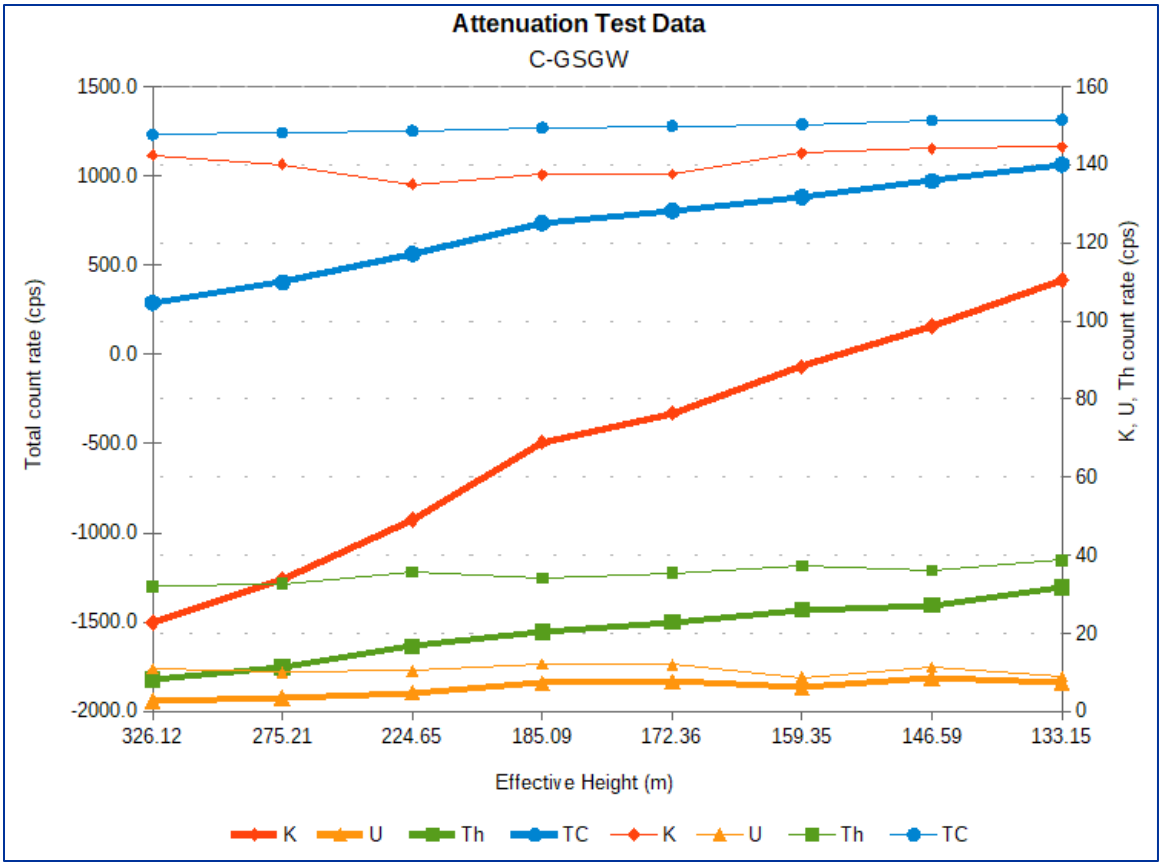

Figure 58. Attenuation test data C-GSGW.

Table 28. Attenuation coefficients – C-GSGW.

Total Count	−0.006754
Potassium	−0.008206
Uranium	−0.007557
Thorium	−0.006907

Table 29. System sensitivities – C-GSGW.

Potassium	68.7907 cps/%K
Uranium	9.102 cps/eU ppm
Thorium	4.58 cps/eTh ppm

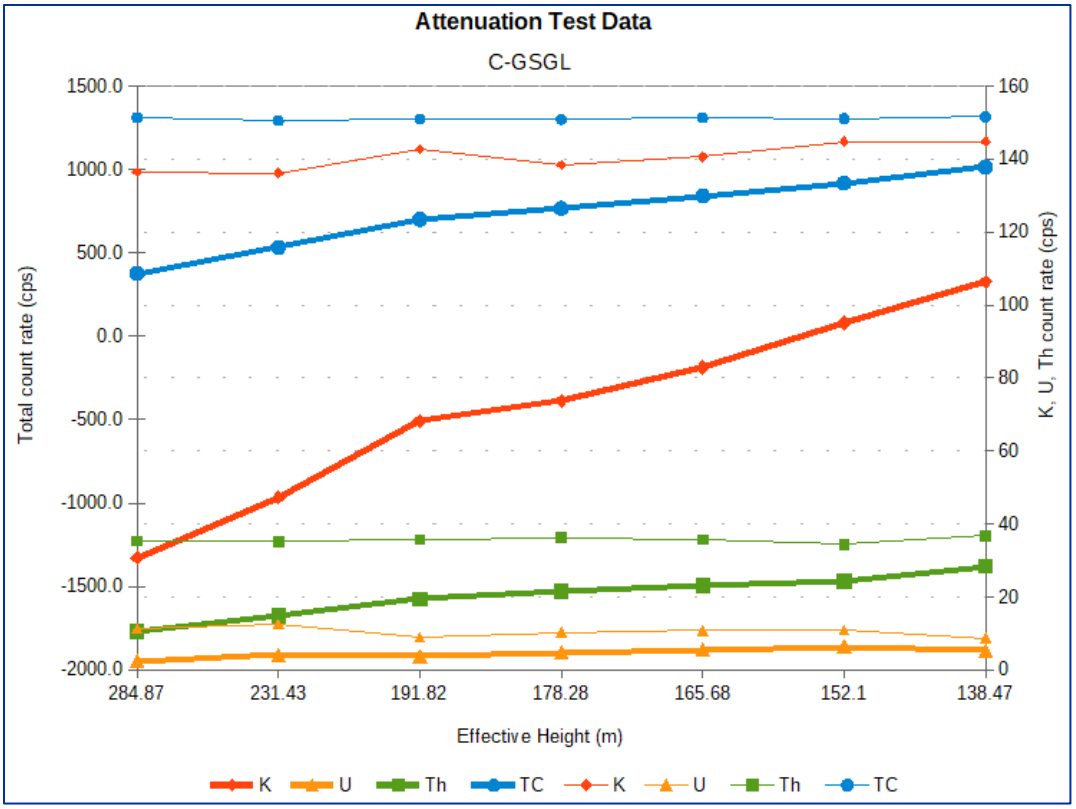

Figure 59. Attenuation test data C-GSGL.

Table 30. Attenuation coefficients – C-GSGL.

Total Count	−0.006741
Potassium	−0.008075
Uranium	−0.008927
Thorium	−0.006546

Table 31. System sensitivities – C-GSGL.

Potassium	79.3612 cps/%K
Uranium	7.8443 cps/eU ppm
Thorium	4.9875 cps/eTh ppm

7. COSMIC AND AIRCRAFT BACKGROUND CALIBRATION

A cosmic and aircraft background test was performed for the spectrometer on June 21, 2018, for both C-GSGL and C-GSGV and on June 30, 2018, for C-GSGW close to the base of operations in the Ramsey–Algoma survey area. The test flight consisted of flying at heights of 1500 m to 3500 m above ground level at 500 m intervals, recording approximately 10 minutes of data at each altitude. Coefficients are determined by linear regression of cosmic counts versus each spectral window as described in the International Atomic Energy Agency (1991). Cosmic coefficients are determined from the slope, whereas the aircraft background values are determined from the y-intercept of the graphs. The results of the cosmic and aircraft background test are provided below.

Table 32. Cosmic and aircraft background coefficients – C-GSGV.

Windows	Background	Linear
Total	38.37	0.7305
Potassium	5.84	0.0435
Uranium	0.91	0.0335
Thorium	0.12	0.0355
Uranium upward	0.15	0.0090

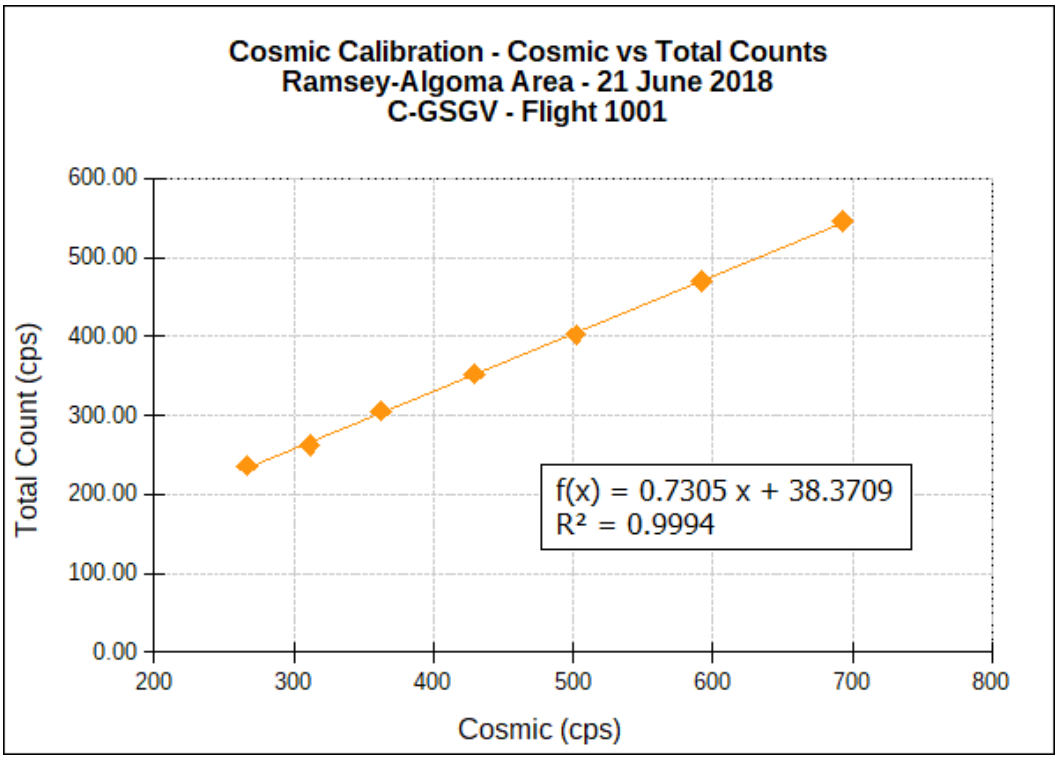

Figure 60. Cosmic calibration, cosmic versus total counts, June 21, 2018, C-GSGV, flight 1001.

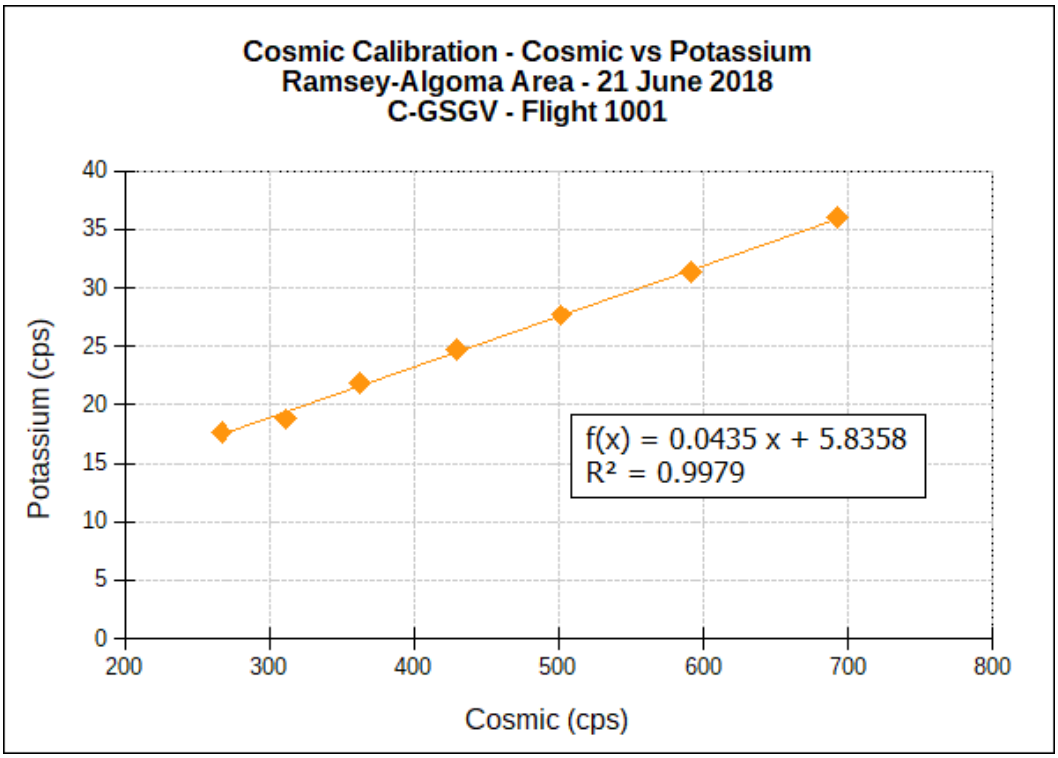

Figure 61. Cosmic calibration, cosmic versus potassium, June 21, 2018, C-GSGV, flight 1001.

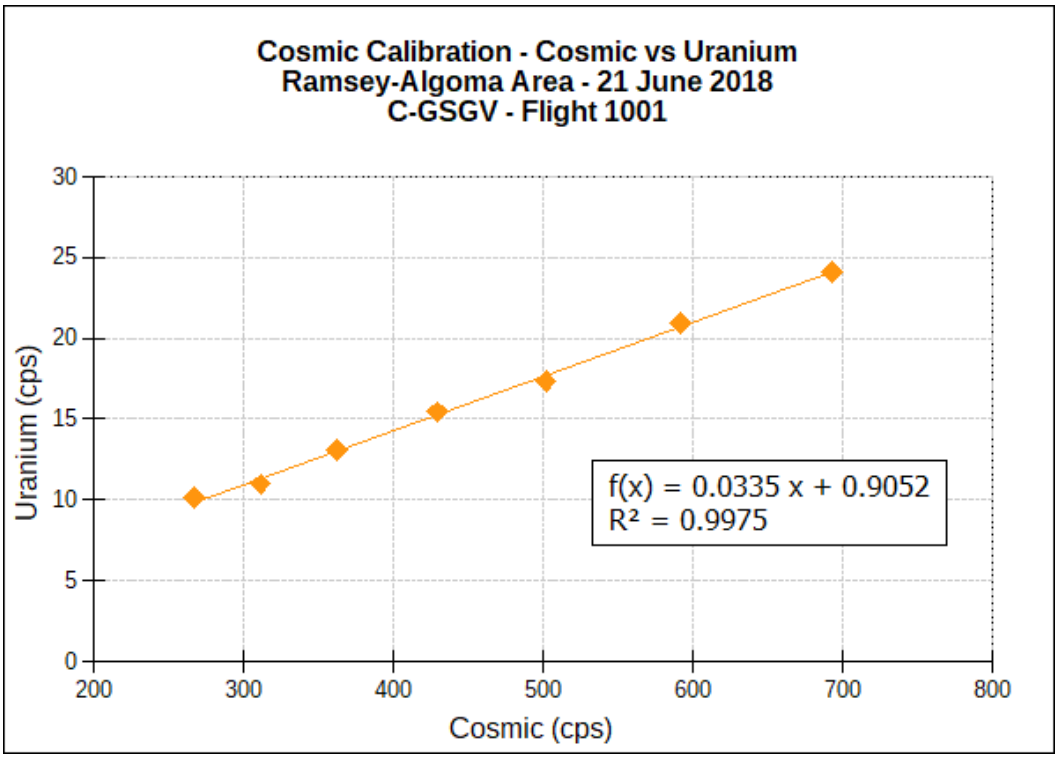

Figure 62. Cosmic calibration, cosmic versus uranium, June 21, 2018, C-GSGV, flight 1001.

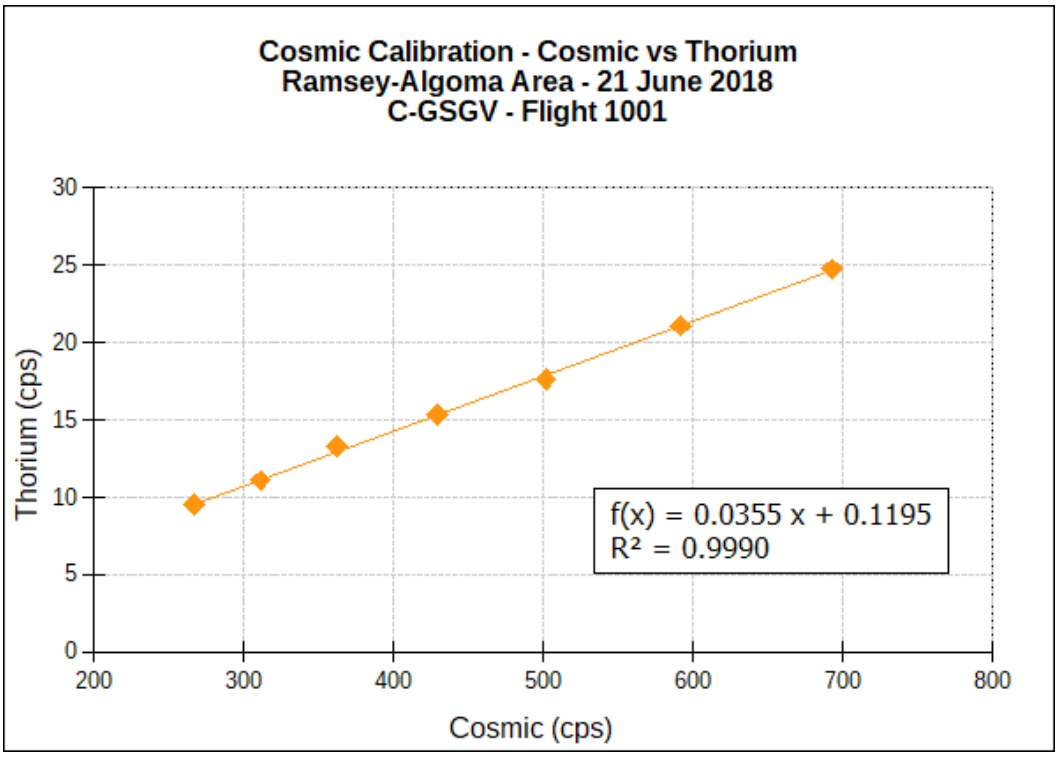

Figure 63. Cosmic calibration, cosmic versus thorium, June 21, 2018, C-GSGV, flight 1001.

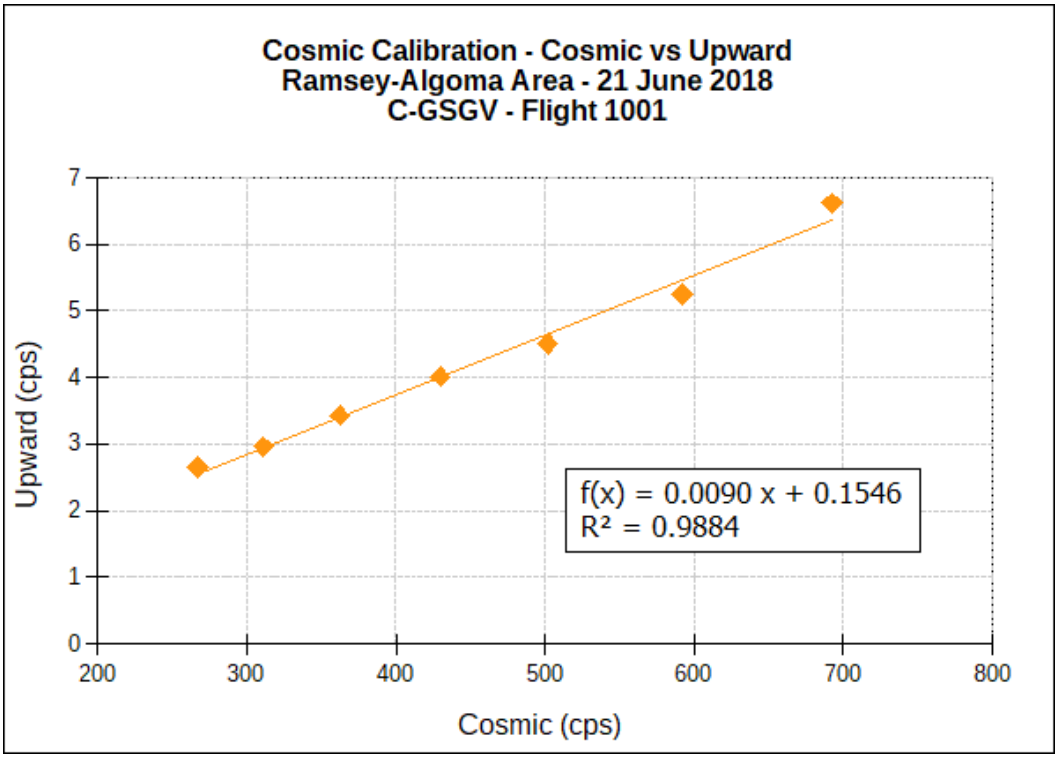

Figure 64. Cosmic calibration, cosmic versus upward, June 21, 2018, C-GSGV, flight 1001.

Table 33. Cosmic and aircraft background coefficients – C-GSGW.

Windows	Background	Linear
Total	66.28	0.6749
Potassium	11.86	0.0391
Uranium	1.98	0.0296
Thorium	−0.46	0.0347
Uranium upward	0.40	0.0082

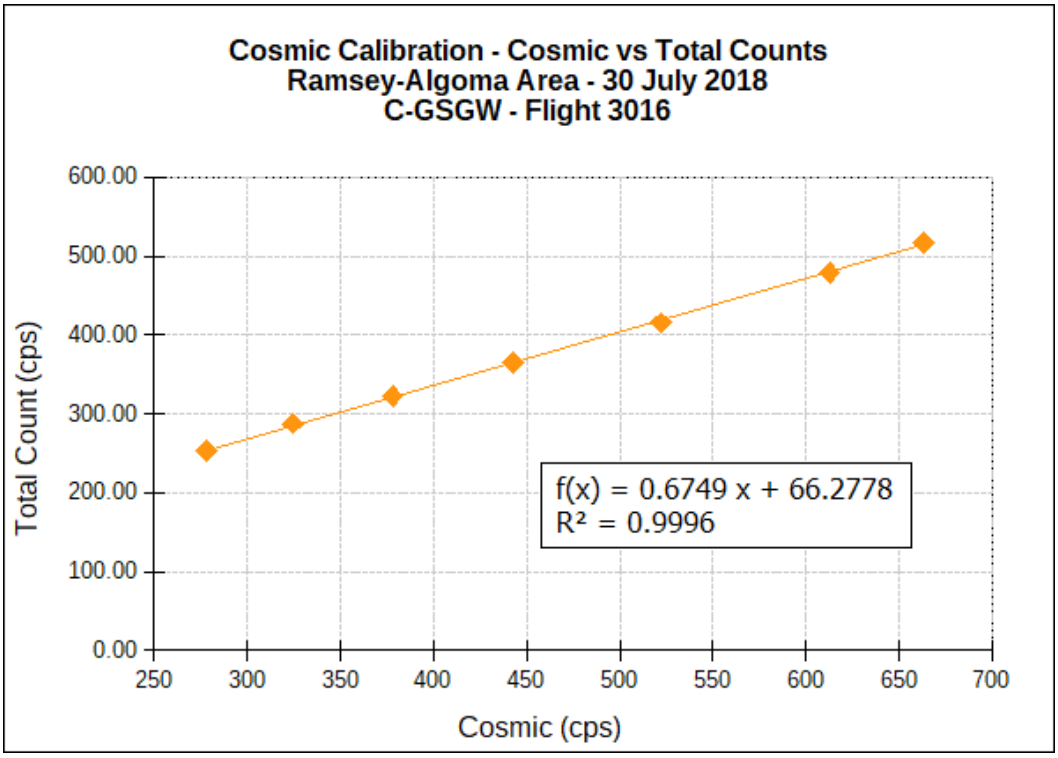

Figure 65. Cosmic calibration, cosmic versus total counts, July 30, 2018, C-GSGW, flight 3016.

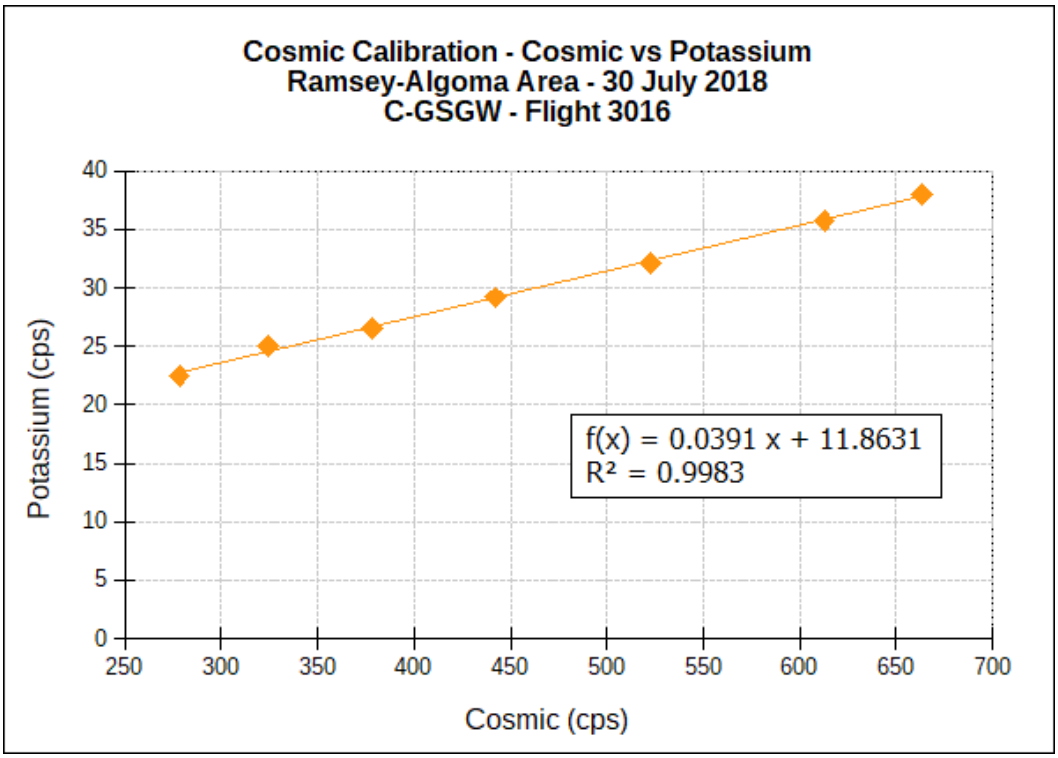

Figure 66. Cosmic calibration, cosmic versus potassium, July 30, 2018, C-GSGW, flight 3016.

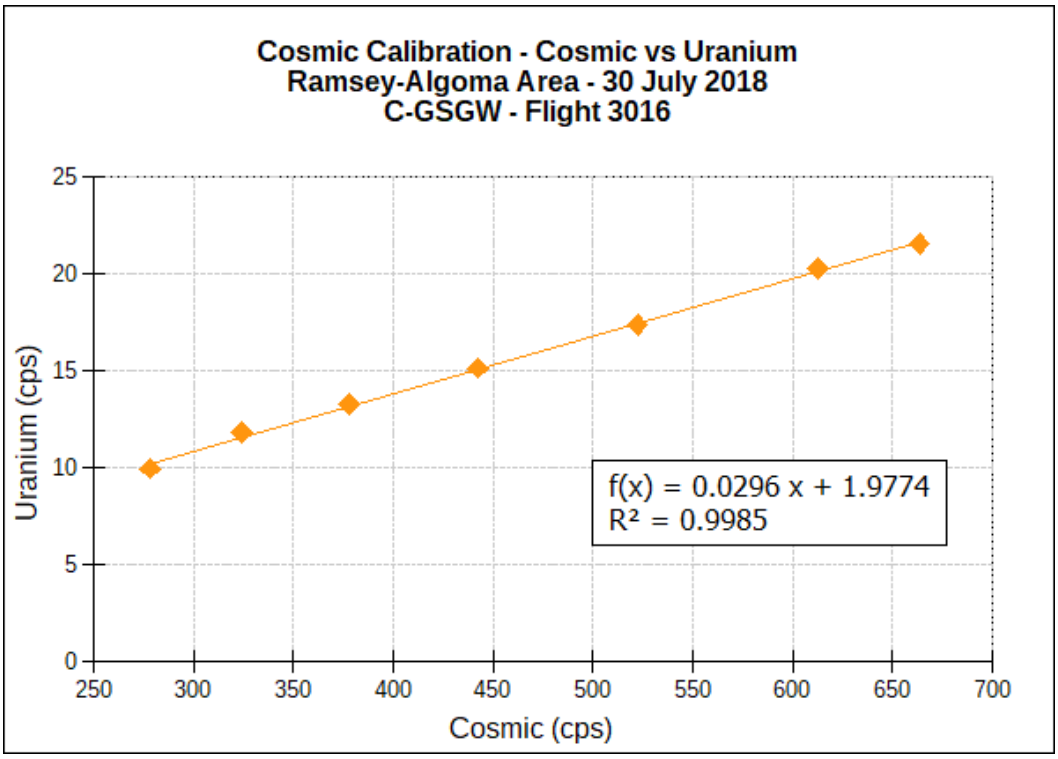

Figure 67. Cosmic calibration, cosmic versus uranium, July 30, 2018, C-GSGW, flight 3016.

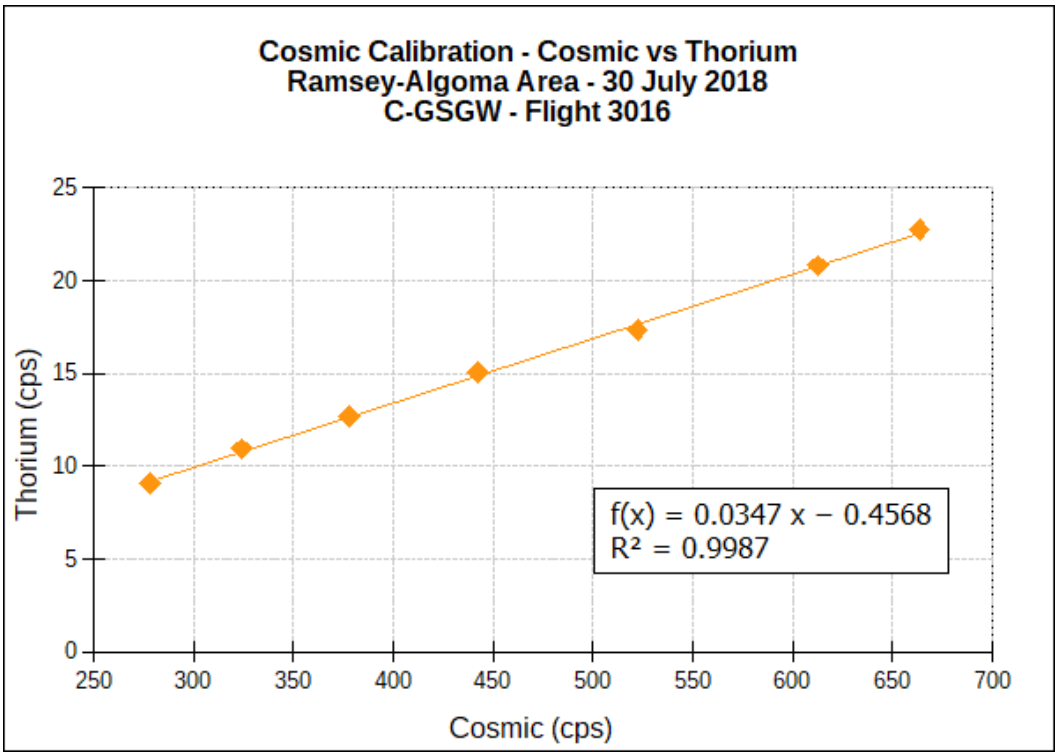

Figure 68. Cosmic calibration, cosmic versus thorium, July 30, 2018, C-GSGW, flight 3016.

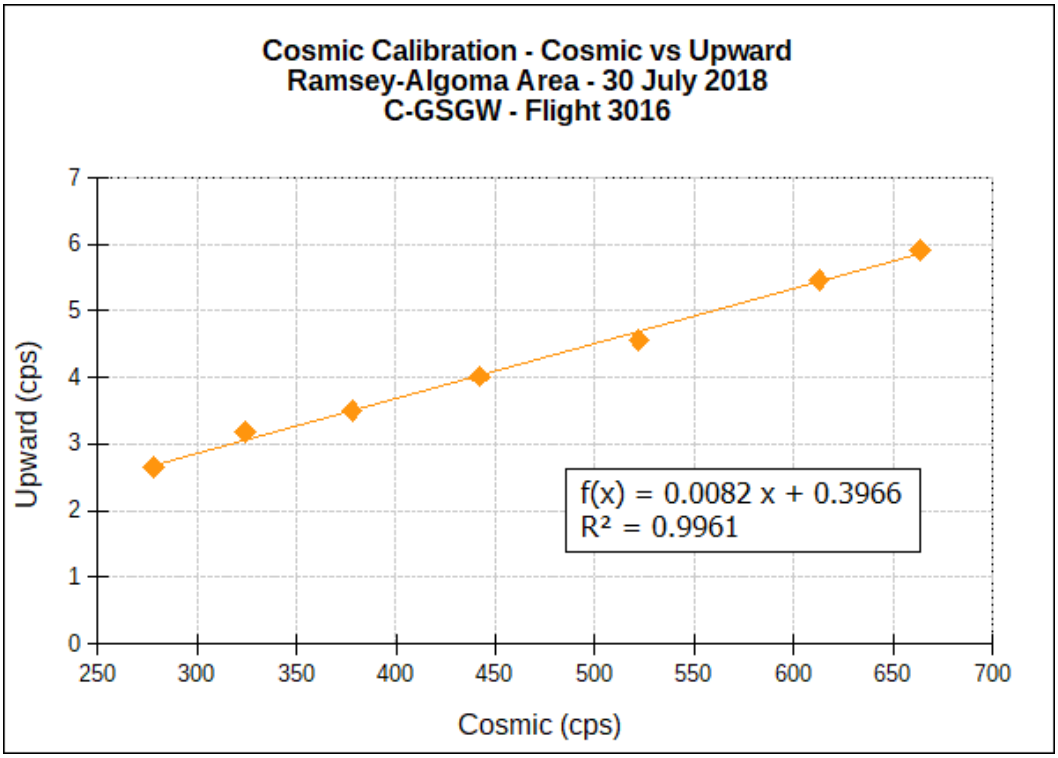

Figure 69. Cosmic calibration, cosmic versus upward, July 30, 2018, C-GSGW, flight 3016.

Table 34. Cosmic and Aircraft Background Coefficients – C-GSGL.

Windows	Background	Linear
Total	34.47	0.6256
Potassium	6.64	0.0376
Uranium	0.02	0.0287
Thorium	−0.61	0.0300
Uranium upward	0.04	0.0077

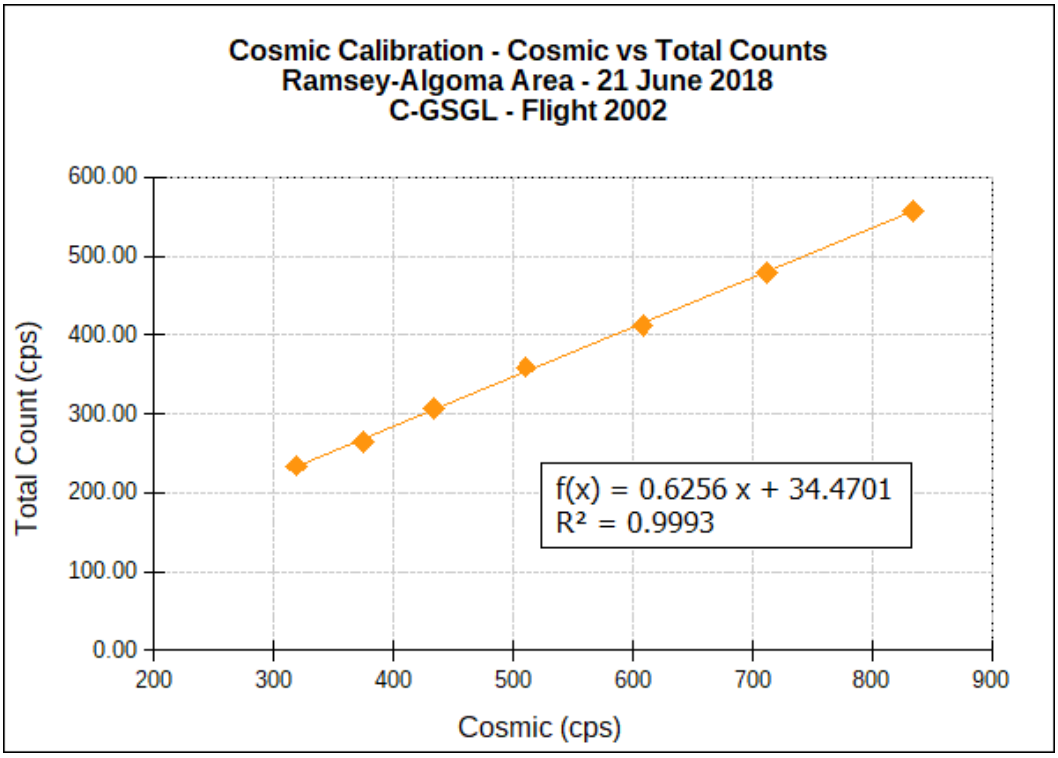

Figure 70. Cosmic calibration, cosmic versus total counts, June 21, 2018, C-GSGL, flight 2002.

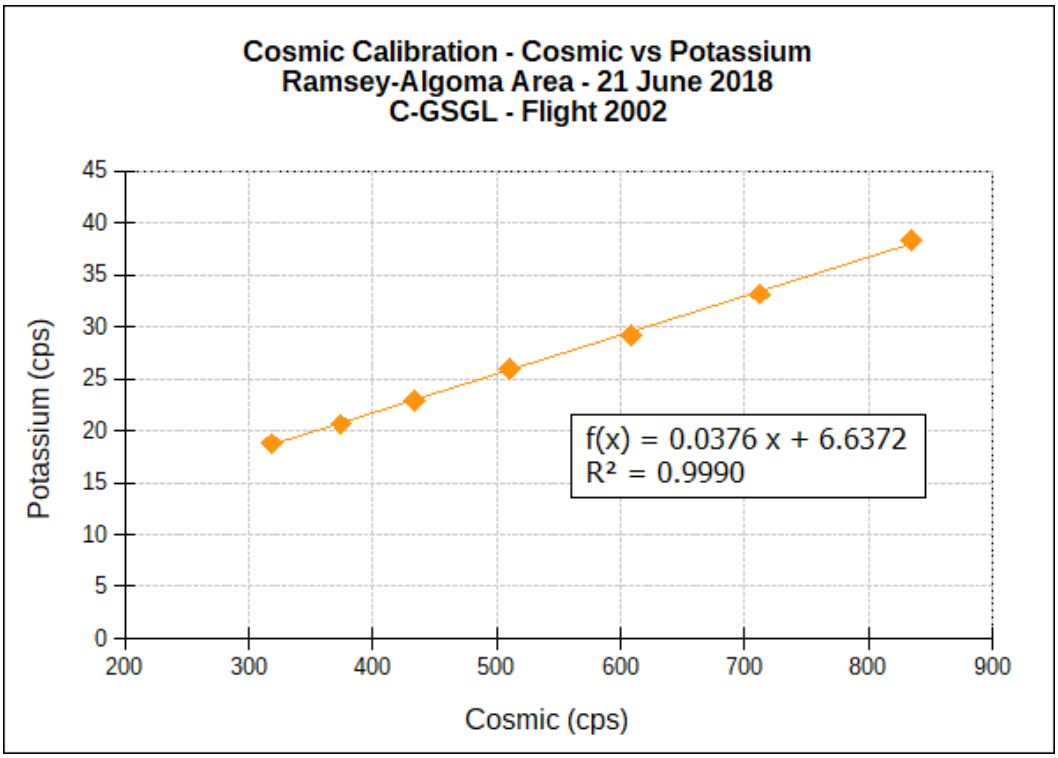

Figure 71. Cosmic calibration, cosmic versus potassium, June 21, 2018, C-GSGL, flight 2002.

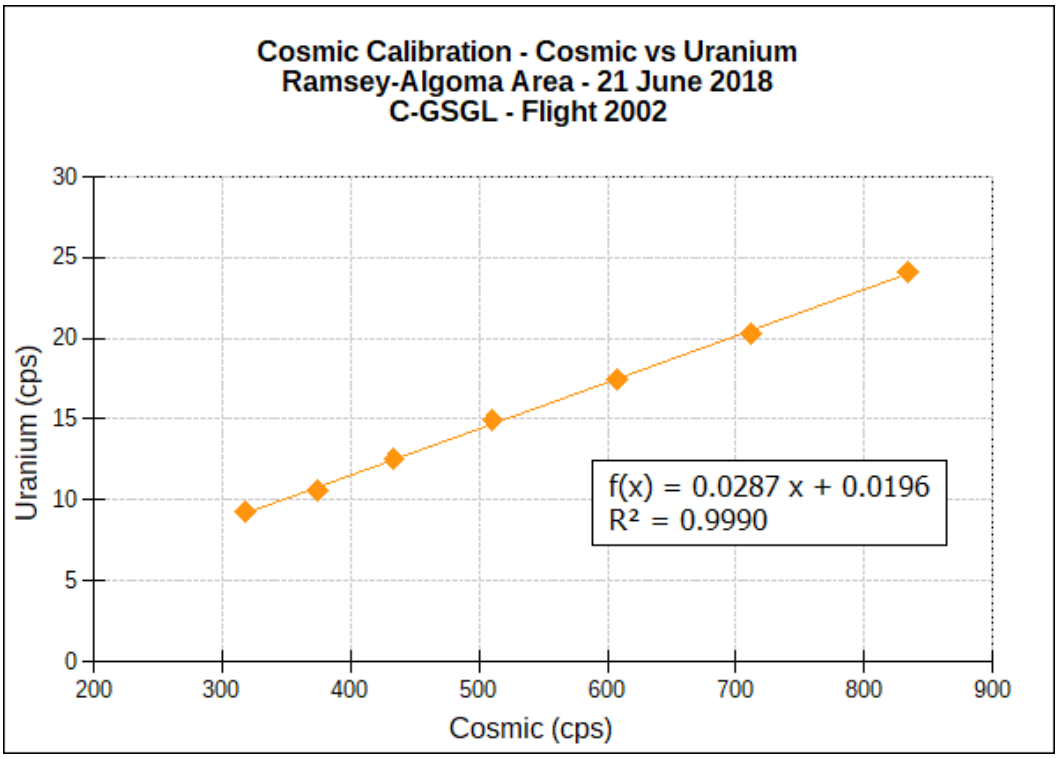

Figure 72. Cosmic calibration, cosmic versus uranium, June 21, 2018, C-GSGL, flight 2002.

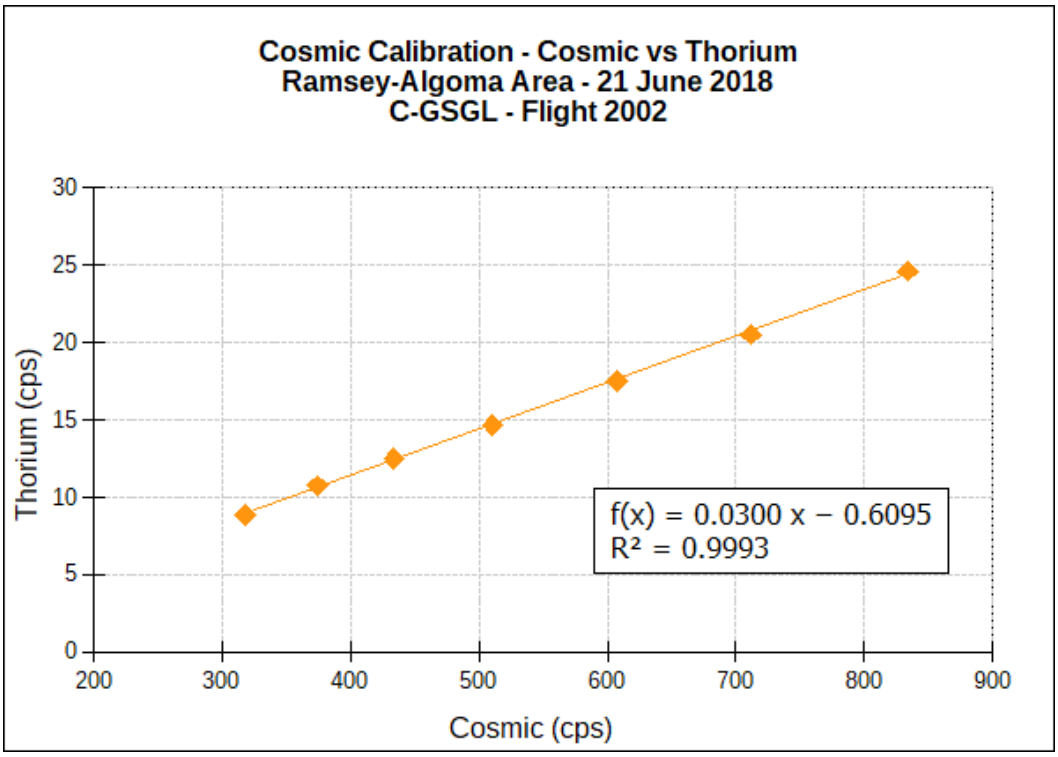

Figure 73. Cosmic calibration, cosmic versus thorium, June 21, 2018, C-GSGL, flight 2002.

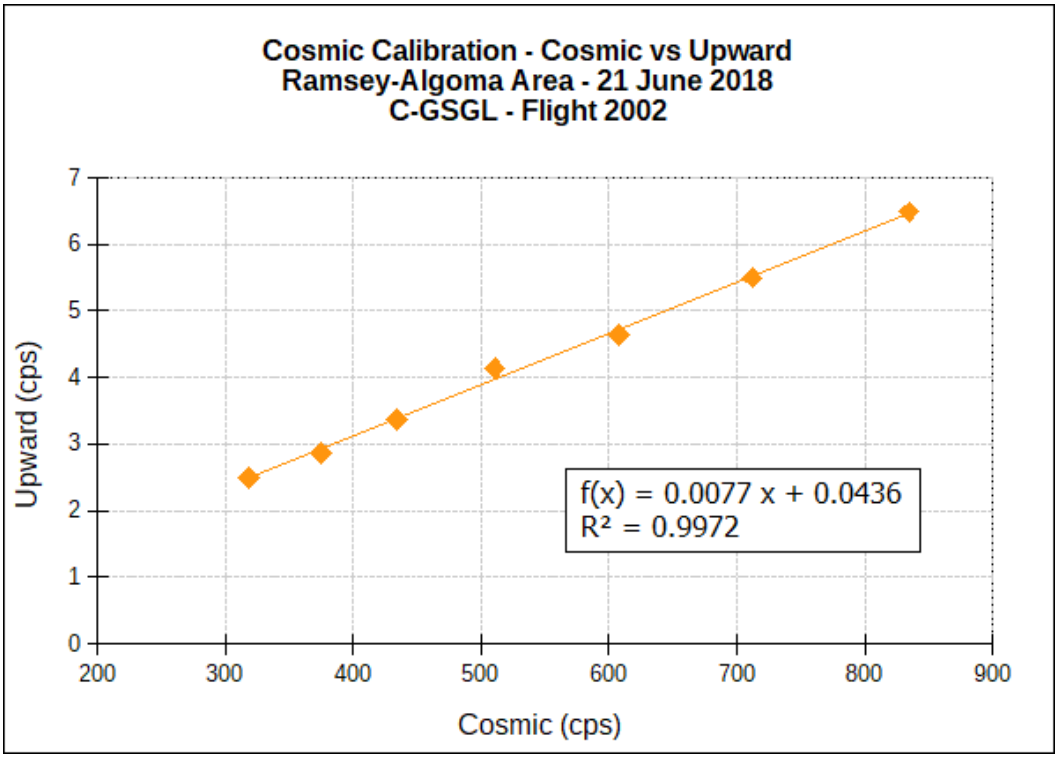

Figure 74. Cosmic calibration, cosmic versus upward, June 21, 2018, C-GSGL, flight 2002.

8. RADON CALIBRATION

Radon background was monitored through the use of 2 upward-looking detectors. Coefficients relating the count rate in the uranium window from the upward detectors to the count rate in the potassium, uranium, thorium and total count windows from the downward-facing detectors were determined using several over-water test lines flown over bodies of water close to the base of operations in the Ramsey–Algoma survey area.

The cosmic and background corrected data from each of the upward ("Up") (u_r), thorium (T_r), potassium (K_r) and total (I_r) windows are plotted against the counts in the uranium (U_r) window for each over-water line flown. The coefficients determined for this survey are provided in Tables 35, 36 and 37. Linear regressions of these plots provide the radon coefficients to be used in the radiometric data processing.

Table 35. Radon correction coefficients for C-GSGV.

	a	b
$I_r = a_I U_r + b_I$	13.64	3.18
$K_r = a_K U_r + b_K$	0.73	0.30
$T_r = a_T U_r + b_T$	0.03	−0.01
$u_r = a_u U_r + b_u$	0.22	0.20

Table 36. Radon correction coefficients for C-GSGW.

	a	b
$I_r = a_I U_r + b_I$	13.74	3.73
$K_r = a_K U_r + b_K$	0.68	0.55
$T_r = a_T U_r + b_T$	0.03	−0.03
$u_r = a_u U_r + b_u$	0.22	0.13

Table 37. Radon correction coefficients for C-GSGL.

	a	b
$I_r = a_I U_r + b_I$	14.06	3.93
$K_r = a_K U_r + b_K$	0.73	1.06
$T_r = a_T U_r + b_T$	0.08	0.16
$u_r = a_u U_r + b_u$	0.22	0.07

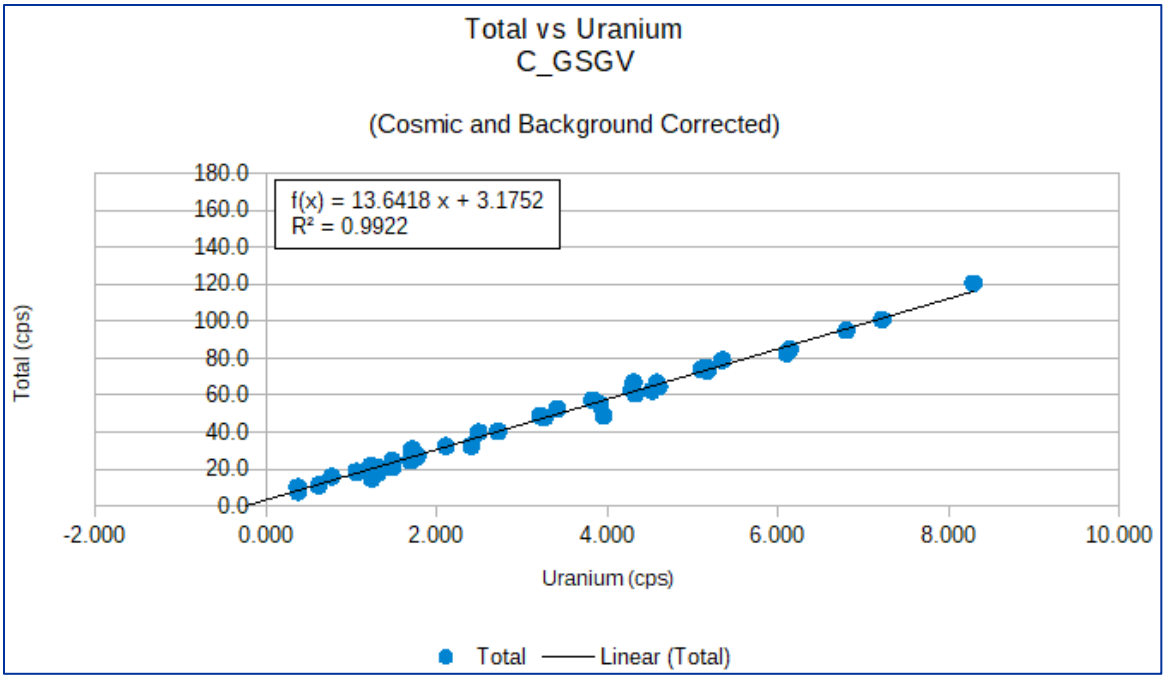

Figure 75. Radon calibration, uranium versus total counts, C-GSGV.

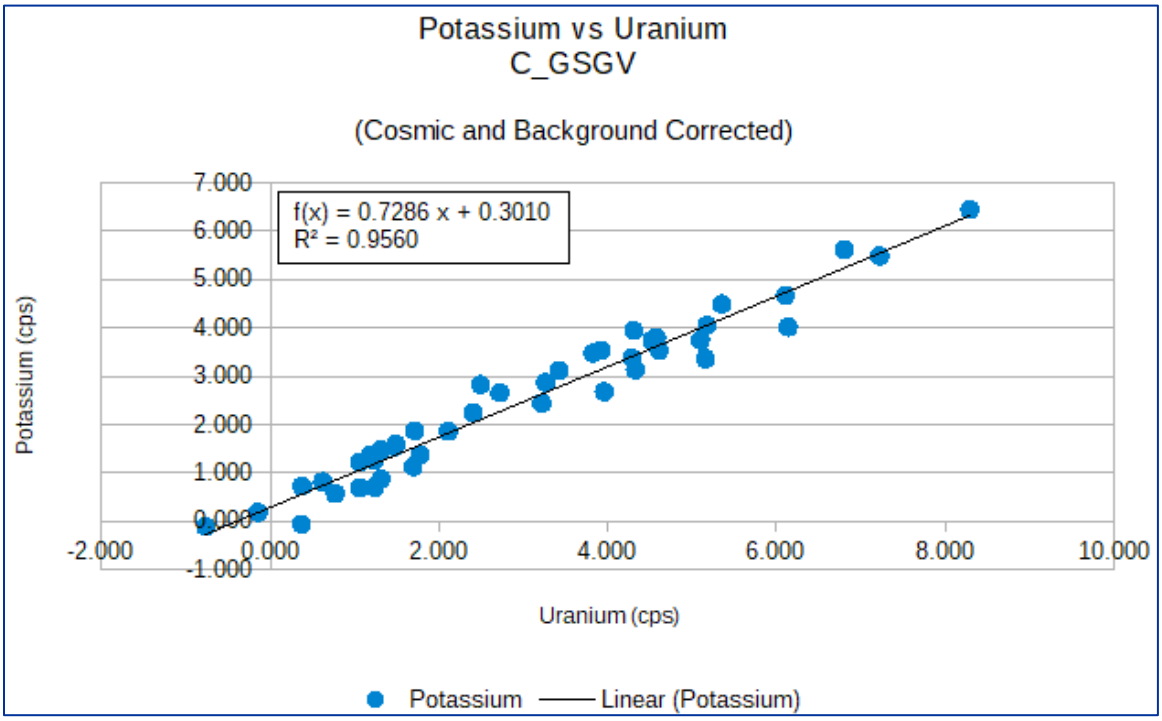

Figure 76. Radon calibration, uranium versus potassium, C-GSGV.

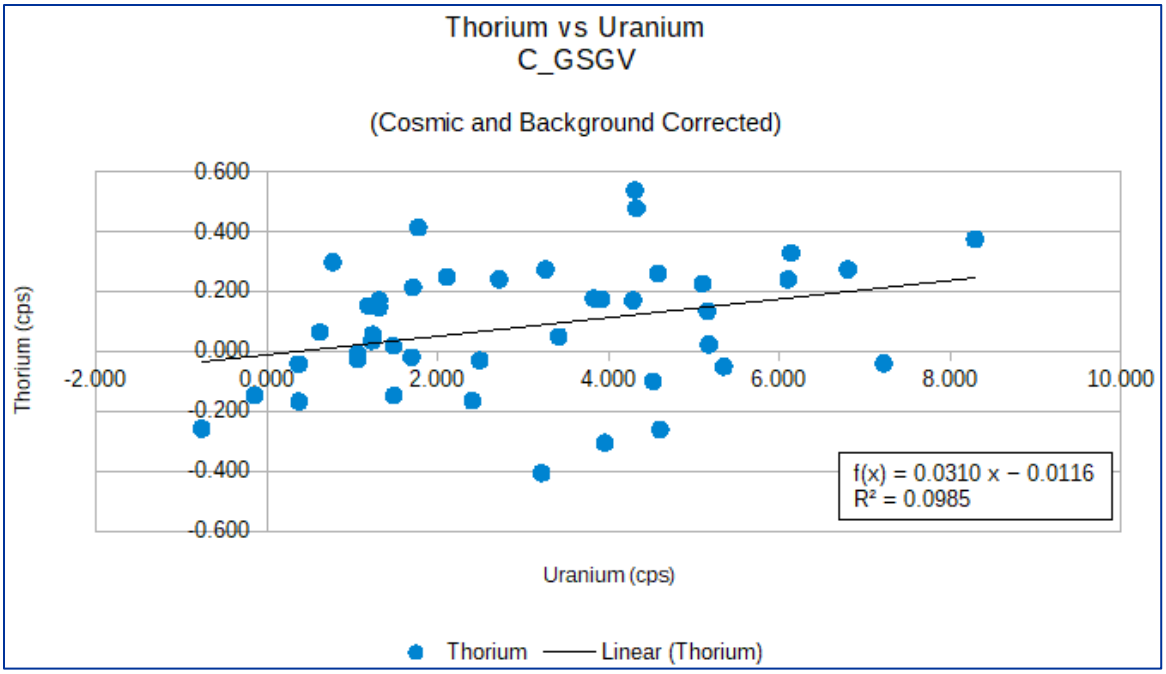

Figure 77. Radon calibration, uranium versus thorium, C-GSGV.

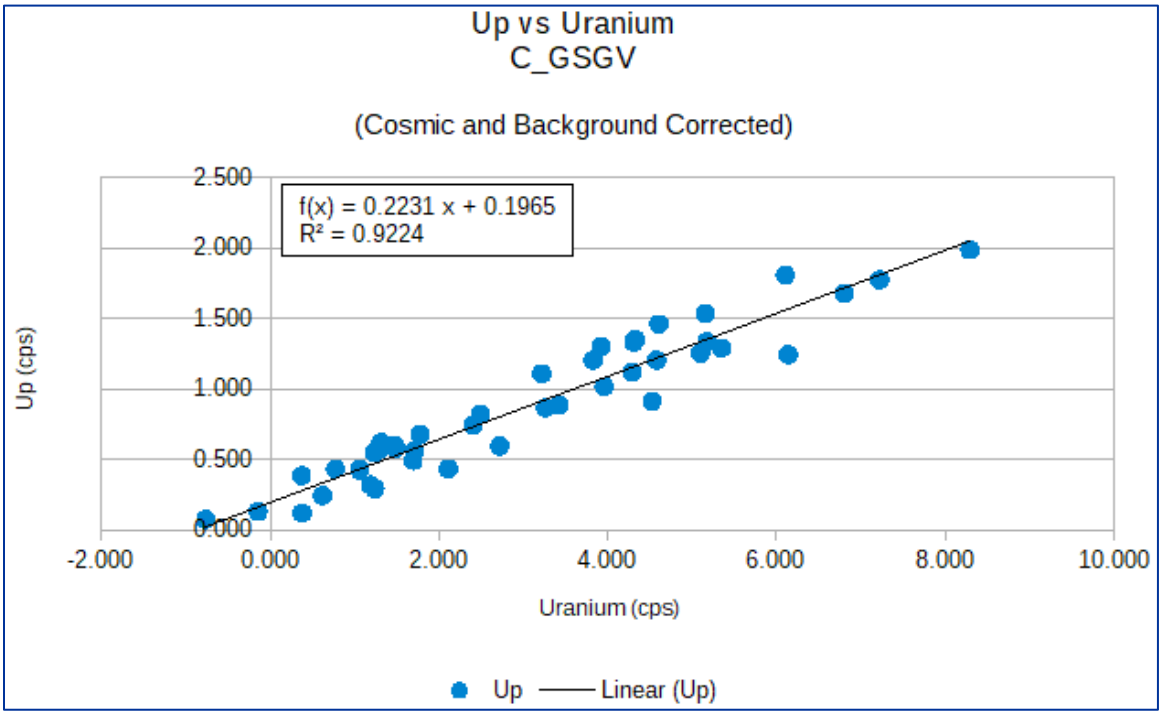

Figure 78. Radon calibration, uranium versus upward ("Up"), C-GSGV.

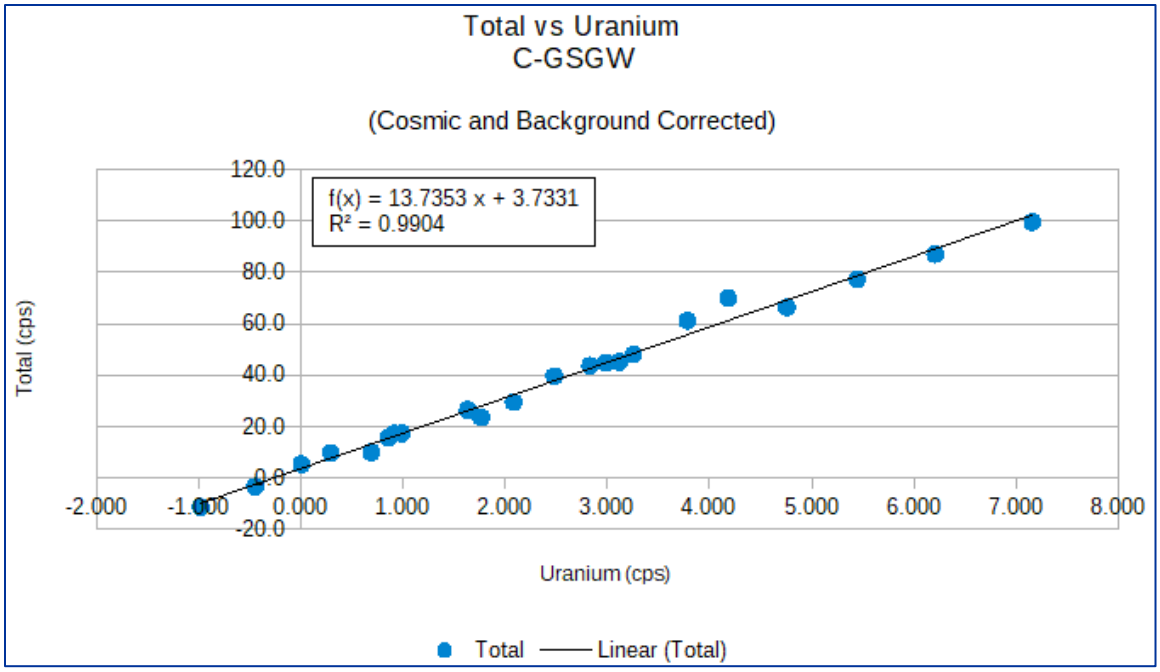

Figure 79. Radon calibration, uranium versus total counts, C-GSGW.

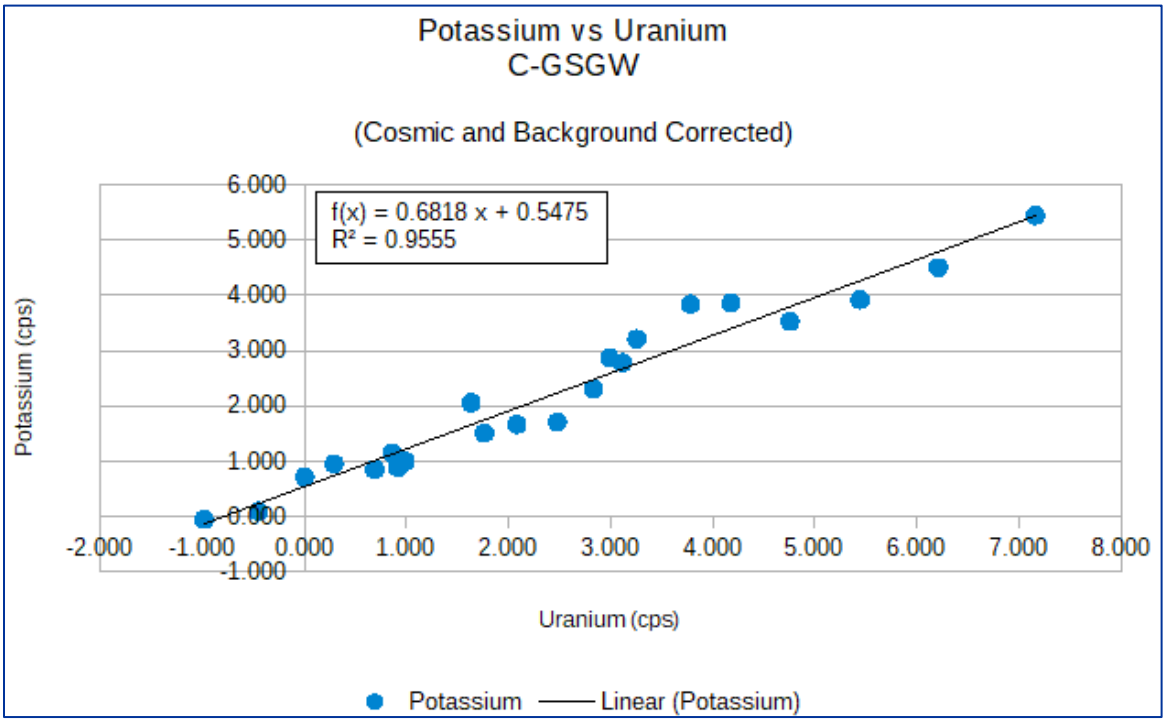

Figure 80. Radon calibration, uranium versus potassium, C-GSGW.

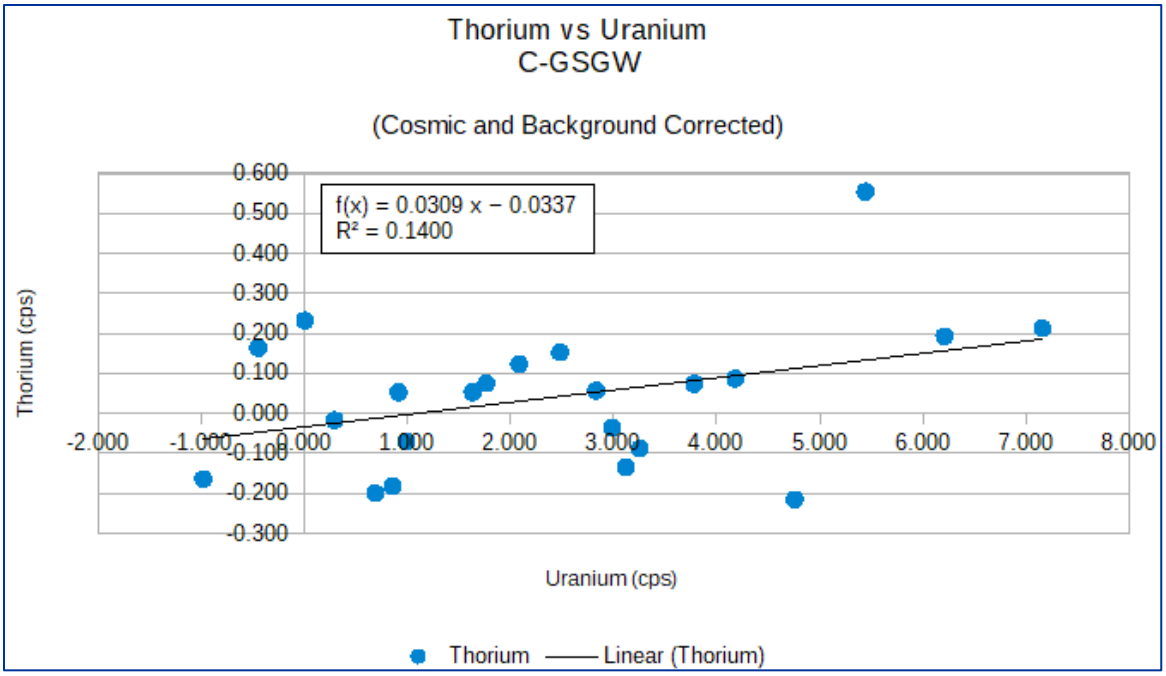

Figure 81. Radon calibration, uranium versus thorium, C-GSGW.

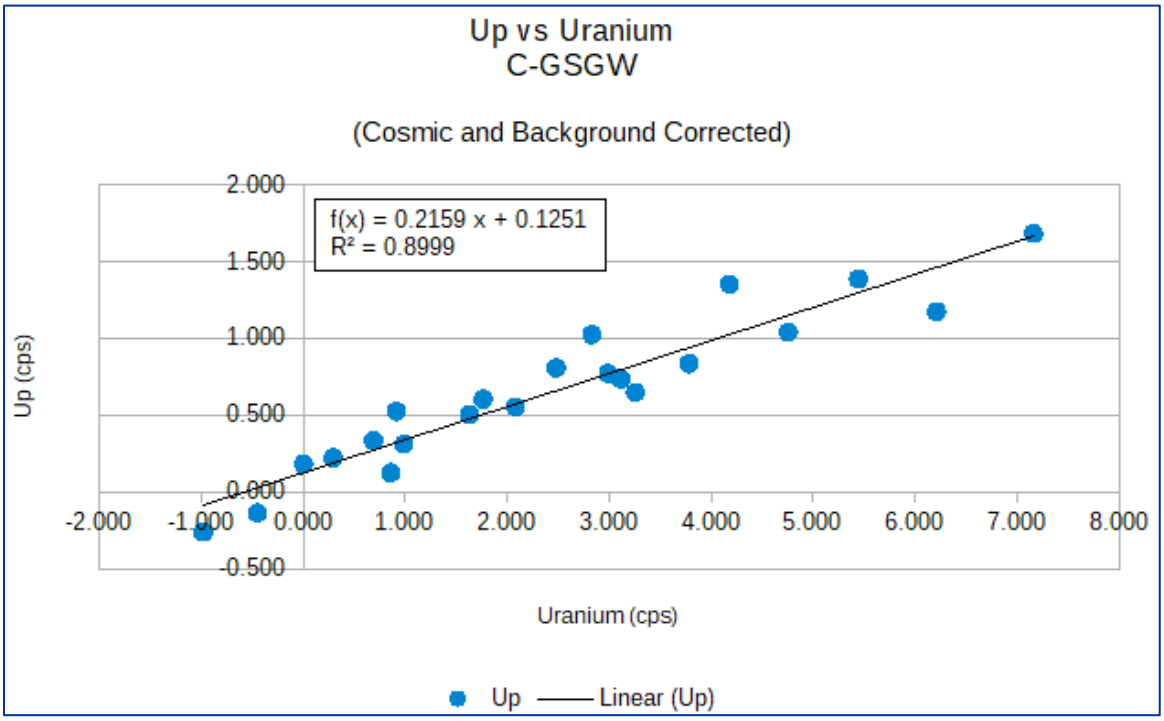

Figure 82. Radon calibration, uranium versus upward ("Up"), C-GSGW.

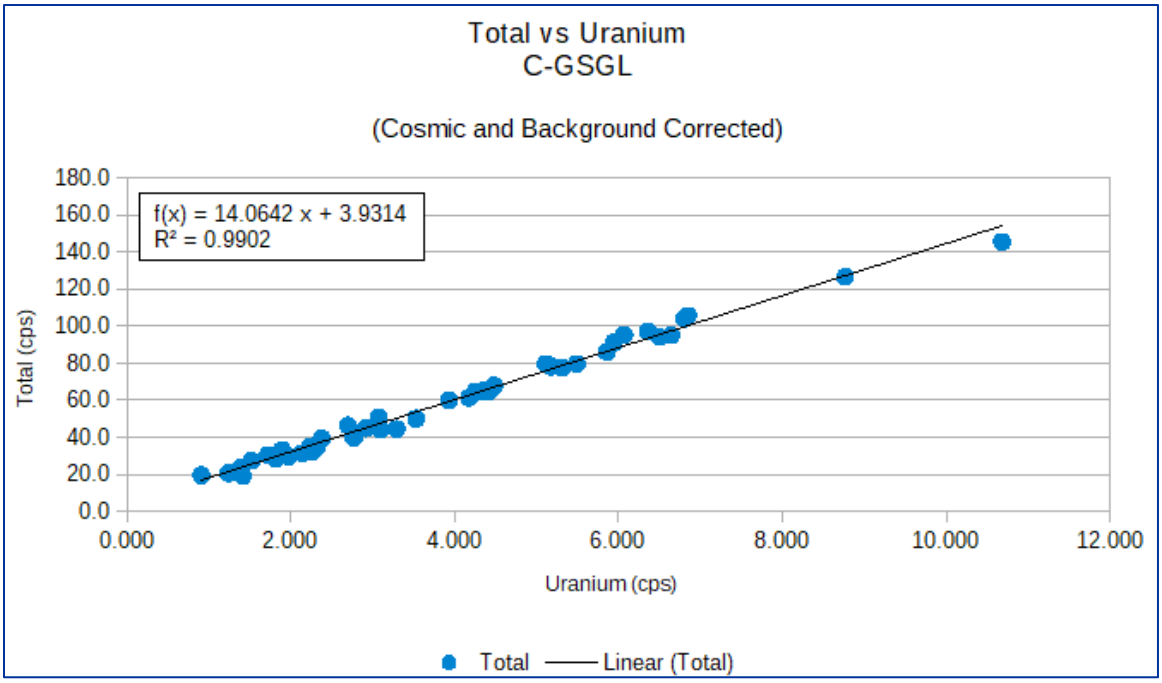

Figure 83. Radon calibration, uranium versus total counts, C-GSGL.

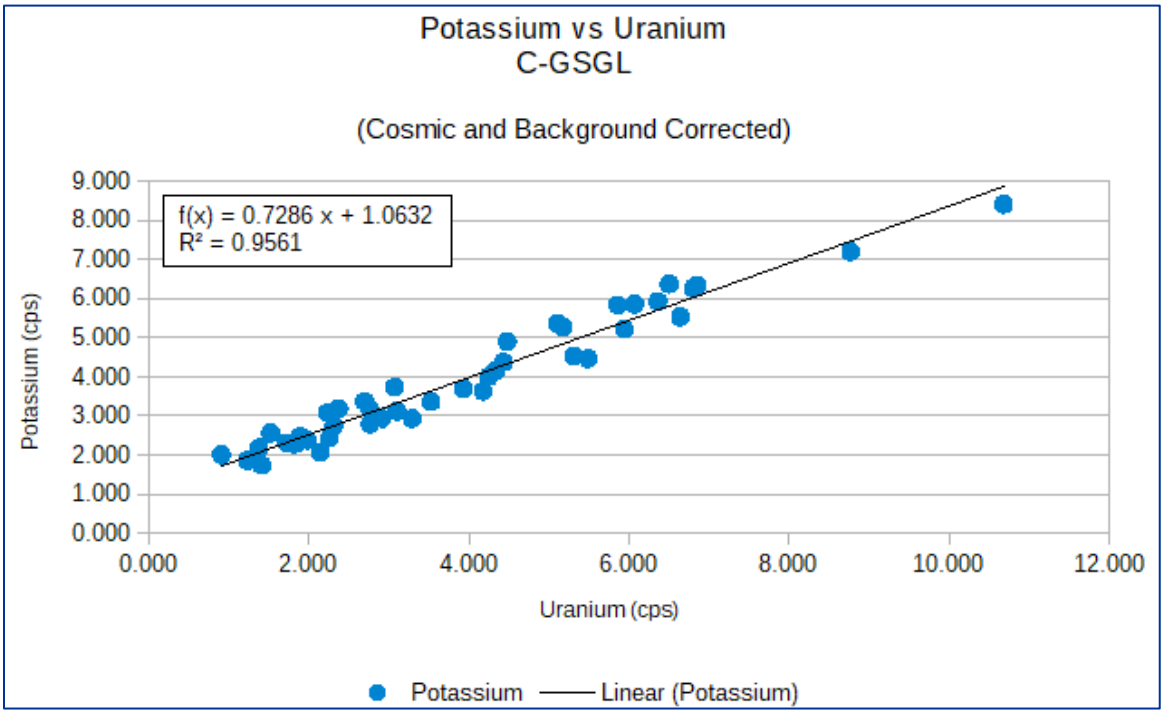

Figure 84. Radon calibration, uranium versus potassium, C-GSGL.

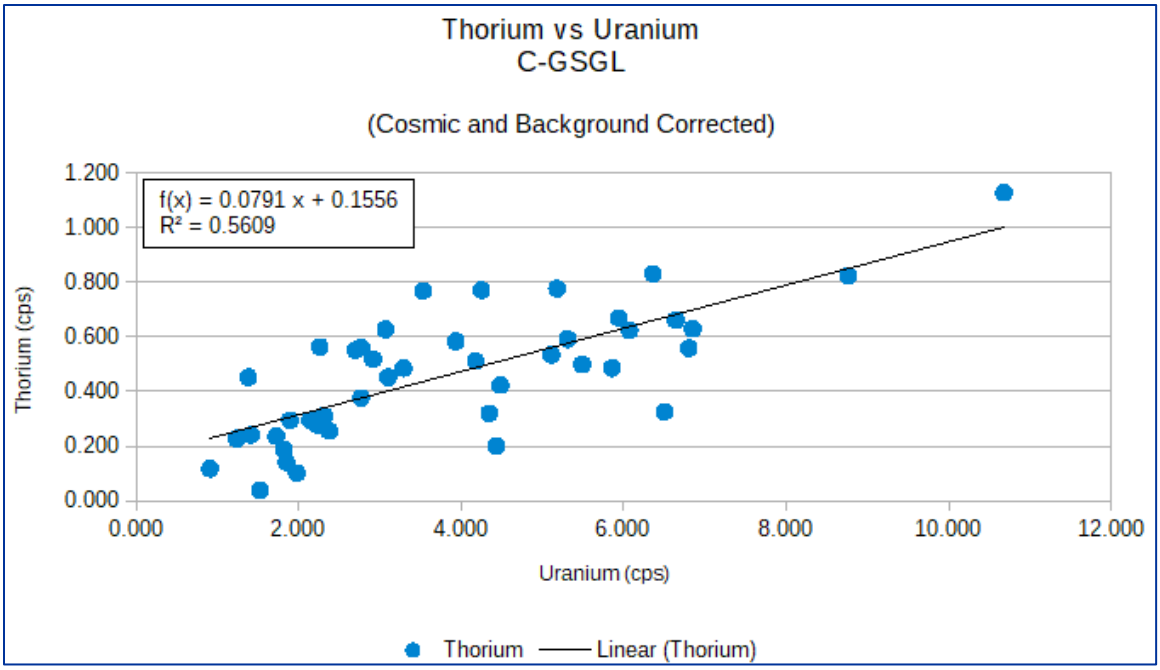

Figure 85. Radon calibration, uranium versus thorium, C-GSGL.

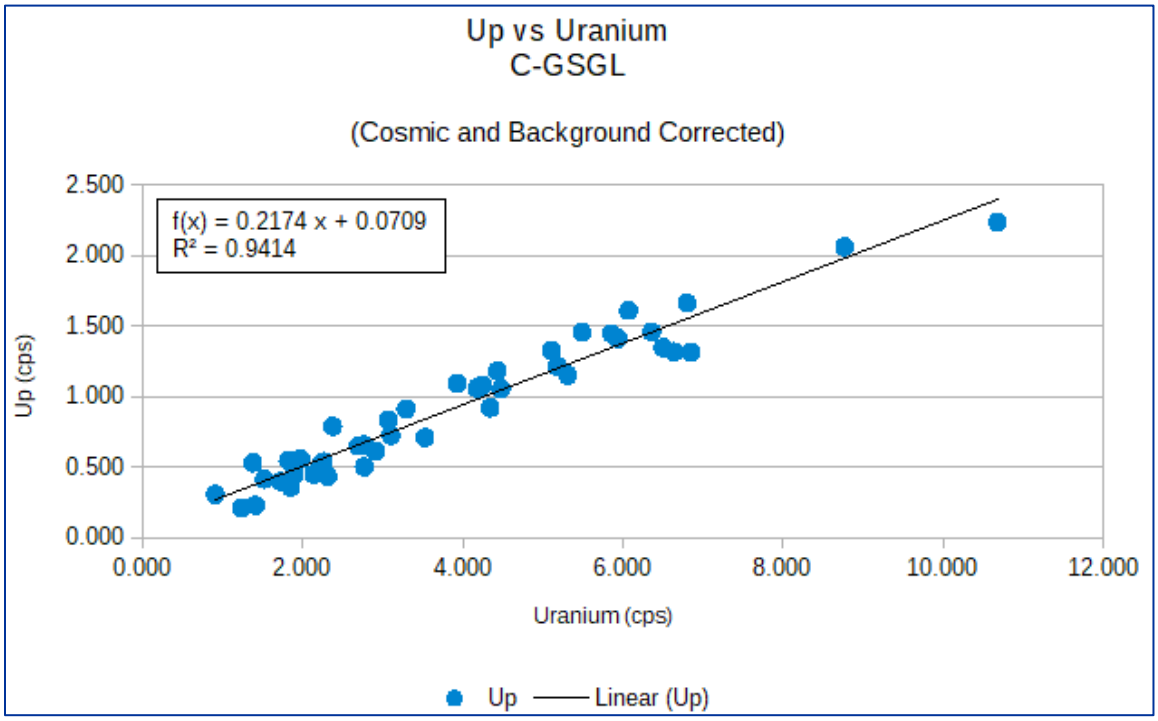

Figure 86. Radon calibration, uranium versus upward ("Up"), C-GSGL.

Appendix B. Archive Definitions

Geophysical Data Sets 1086a and 1086b are derived from surveys using a magnetic gradiometry and gamma-ray spectrometric systems mounted on fixed-wing platforms and carried out by SGL.

1. ARCHIVE LAYOUT

The files for the Ramsey–Algoma Geophysical Survey are archived on 2 DVDs and sold as separate products, as outlined below:

Type of Data	Magnetic Gradiometer and Gamma-Ray Spectrometric
Format	Grid and Profile Data (DVD)
ASCII	Geophysical Data Set (GDS) 1086a
Geosoft® Binary	Geophysical Data Set (GDS) 1086b

The content of the ASCII and Geosoft® binary file types are identical. They are provided in both forms to suit the user's available software. The survey data are divided as follows.

1. Geophysical Data Set 1086a (DVD)

a) ASCII (*.gxf*) grids
- digital elevation model
- total magnetic field
- "GSC-levelled" gradient-enhanced total magnetic field
- second vertical derivative of the "GSC-levelled" gradient-enhanced total magnetic field
- measured lateral (across line) horizontal magnetic gradient
- measured longitudinal (along line) horizontal magnetic gradient
- total air absorbed dose rate
- potassium
- equivalent thorium
- equivalent uranium
- potassium over equivalent thorium ratio

b) Vector (*.dxf*) files
- flight path
- total field magnetic contours
- Keating coefficients

c) GeoTIFF seamless map images
- "GSC-levelled" gradient-enhanced total magnetic field with planimetric base
- shaded second vertical derivative of the "GSC-levelled" gradient-enhanced total magnetic field with planimetric base
- total air absorbed dose rate with planimetric base
- potassium with planimetric base
- equivalent thorium with planimetric base
- equivalent uranium with planimetric base
- potassium, thorium, uranium ternary image with planimetric base

d) ASCII (*.xyz*) data
   - profile database of magnetic data (10 Hz sampling) in ASCII XYZ format
   - profile database of gamma-ray spectrometric data (1 Hz sampling) in ASCII XYZ format
   - profile database of gamma-ray spectrometric data array (1 Hz sampling) in ASCII XYZ format
   - database of Keating coefficients in ASCII CSV (comma-separated values) format

e) Survey report in portable document (*.pdf*) format

2. Geophysical Data Set 1086b (DVD)

a) Geosoft® binary (*.grd*) grids
- digital elevation model
- total magnetic field
- "GSC-levelled" gradient-enhanced total magnetic field
- second vertical derivative of the "GSC-levelled" gradient-enhanced total magnetic field
- measured lateral (across line) horizontal magnetic gradient
- measured longitudinal (along line) horizontal magnetic gradient
- total air absorbed dose rate
- potassium
- equivalent thorium
- equivalent uranium
- potassium over equivalent thorium ratio

b) Vector (*.dxf*) files
- flight path
- total field magnetic contours
- Keating coefficients

c) GeoTIFF seamless map images
- "GSC-levelled" gradient-enhanced total magnetic field with planimetric base
- shaded second vertical derivative of the "GSC-levelled" gradient-enhanced total magnetic field with planimetric base
- total air absorbed dose rate with planimetric base
- potassium with planimetric base
- equivalent thorium with planimetric base
- equivalent uranium with planimetric base
- potassium, thorium, uranium ternary image with planimetric base

d) Geosoft® (*.gdb*) binary data
- profile database of magnetic data (10 Hz sampling) in Geosoft® GDB format
- profile database of gamma-ray spectrometric data (1 Hz sampling) in Geosoft® GDB format
- profile database of gamma-ray spectrometric data array (1 Hz sampling) in Geosoft® GDB format
- Keating coefficients in Geosoft® GDB format

e) Geosoft® (*.map*) map files
- colour-filled contours of gradient-enhanced residual magnetic intensity with flight lines
- shaded colour of the second vertical derivative of the gradient-enhanced total magnetic intensity with Keating coefficients
- histogram-equalized ternary red-green-blue radioelement image with inset images of potassium, equivalent uranium, equivalent thorium and dose rate and flight line

f) Survey report in portable document (*.pdf*) format

2. CO-ORDINATE SYSTEMS

The profile data are provided in 2 co-ordinate systems:

- Universal Transverse Mercator (UTM) projection, Zone 17N, NAD83 CSRS datum, Canada local datum
- latitude/longitude co-ordinates, NAD83 CSRS, Canada local datum

The gridded data are provided in Universal Transverse Mercator (UTM) projection, Zone 17N, NAD83 CSRS datum, Canada local datum.

3. LINE NUMBERING

The line numbering convention for survey data provided in GDS 1086a and GDS 1086b are as follows:

- Traverse-line numbers are 6 digits and control lines are 5 digits with the last 2 digits indicating part or revision number. An example for clarification is presented in the following paragraph:

  Line 1001.00 is the first traverse line of the survey followed by line 1002.00;
  should line 1001.00 be in 2 parts, the first is 1001.00 and the second is 1001.10.
  Should line 1001.00 have been reflown, it will be in the database as line 1001.01.
  The same convention is used for the control lines.
- The control lines flown perpendicular to the traverse lines range from 101.00 to 190.00.
- The control lines flown along the survey block boundary range from 201.00 to 213.00.
- In the Geosoft® Oasis montaj™ binary database, traverse lines are designated with a leading character “L” and control lines are designated with a leading character “T”.

4. DATA FILES

The survey data files are provided as follows:

- RAMAG.gdb — Geosoft® Oasis montaj™ uncompressed binary database file of the magnetic data, sampled at 10 Hz
- RAMAG.xyz — ASCII file of the magnetic data, sampled at 10 Hz
- RASPEC.gdb — Geosoft® Oasis montaj™ uncompressed binary database of the gamma-ray spectrometric data, sampled at 1 Hz
- RASPEC.xyz — ASCII file of the gamma-ray spectrometric data, sampled at 1 Hz
- RASPEC256.gdb — Geosoft® Oasis montaj™ uncompressed binary database file of the gamma-ray spectrometric data array, sampled at 1 Hz
- RASPEC256.xyz — ASCII file of the gamma-ray spectrometric data array, sampled at 1 Hz
- RAKC.gdb — Geosoft® Oasis montaj™ uncompressed binary database file of the Keating coefficients
- RAKC.csv — ASCII file of the Keating coefficients

The contents of RAMAG.xyz/.gdb (both file types contain the same set of data channels) are summarized as follows:

Table 38. Contents of aeromagnetic data files RAMAG.xyz/.gdb.

Channel Name	Description	Units
gps_x_raw	Raw GPS X (NAD83 CSRS datum, UTM zone 17N)	metres
gps_y_raw	Raw GPS Y (NAD83 CSRS datum, UTM zone 17N)	metres
gps_z_raw	Raw GPS Z (CGVD2013)	metres
gps_base_x	GPS base station X (NAD83 CSRS datum, longitude)	degrees
gps_base_y	GPS base station Y (NAD83 CSRS datum, latitude)	degrees
gps_base_z	GPS base station Z (CGVD2013)	metres
gps_x_final	Differentially corrected GPS X (NAD83 CSRS datum, longitude)	degrees
gps_y_final	Differentially corrected GPS Y (NAD83 CSRS datum, latitude)	degrees
gps_z_final	Differentially corrected GPS Z (CGVD2013)	metres
x_nad83	Easting in UTM co-ordinates (NAD83 CSRS datum, UTM zone 17N)	metres
y_nad83	Northing in UTM co-ordinates (NAD83 CSRS datum, UTM zone 17N)	metres
lon_nad83	Raw longitude (NAD83 CSRS datum)	degrees
lat_nad83	Raw latitude (NAD83 CSRS datum)	degrees
radar_raw	Raw radar altimeter (metres above terrain)	metres
radar_final	Corrected radar altimeter (metres above terrain)	metres
radar_dem	Radar based digital elevation model with respect to mean sea level (CGVD2013)	metres
laser_raw	Raw laser altimeter (metres above terrain)	metres
laser_final	Corrected laser altimeter (metres above terrain)	metres
laser_dem	Laser based digital elevation model with respect to mean seal level (CGVD2013)	metres
fiducial	Fiducial	-
flight	Flight number	-
line_number	Full flight-line number (flight-line and part numbers)	-
line	Flight-line number	-
line_part	Flight-line part number	-
time_utc	UTC time	seconds
time_local	Local time	seconds
date	Local date	YYYY/MM/DD
height_mag	Magnetometer height (metres above terrain)	metres
mag_base_raw	Raw magnetic base station data	nanoteslas
mag_base_final	Corrected magnetic base station data	nanoteslas
fluxgate_x	X-component field of the compensation fluxgate magnetometer	nanoteslas
fluxgate_y	Y-component field of the compensation fluxgate magnetometer	nanoteslas
fluxgate_z	Z-component field of the compensation fluxgate magnetometer	nanoteslas
mag_raw_port	Raw magnetic field from port sensor	nanoteslas
mag_comp_port	Compensated magnetic field from port sensor	nanoteslas
mag_lag_port	Compensated, edited and lag corrected magnetic field from port sensor	nanoteslas
mag_raw_stbrd	Raw magnetic field from starboard sensor	nanoteslas
mag_comp_stbrd	Compensated magnetic field from starboard sensor	nanoteslas
mag_lag_stbrd	Compensated, edited and lag corrected magnetic field from starboard sensor	nanoteslas
mag_raw_tail	Raw magnetic field from tail sensor	nanoteslas
mag_comp_tail	Compensated magnetic field from tail sensor	nanoteslas
mag_lag_tail	Compensated, edited and lag corrected magnetic field from tail sensor	nanoteslas
mag_diurn_tail	Diurnally corrected magnetic field from tail sensor	nanoteslas
mag_lev_tail	Levelled magnetic field from tail sensor	nanoteslas
mag_mlev_tail	Microlevelled magnetic field from tail sensor	nanoteslas
igrf	Local IGRF field	nanoteslas
mag_final_tail	Final microlevelled, IGRF-corrected magnetic field from tail sensor	nanoteslas
mag_gsclev_tail	GSC-levelled magnetic field from tail sensor	nanoteslas
grad_lat_raw	Raw lateral horizontal magnetic gradient (from wingtip sensors)	nanoteslas/metre
grad_lat_cor	Levelling correction for lateral horizontal magnetic gradient (from wingtip sensors)	nanoteslas/metre
grad_lat_final	Levelled lateral horizontal magnetic gradient (from wingtip sensors)	nanoteslas/metre

Channel Name	Description	Units
grad_long_raw	Raw longitudinal horizontal magnetic gradient	nanoteslas/metre
grad_long_cor	Levelling correction for longitudinal horizontal magnetic gradient	nanoteslas/metre
grad_long_final	Levelled longitudinal horizontal magnetic gradient	nanoteslas/metre
pitch	Aircraft pitch	degrees
roll	Aircraft roll	degrees
yaw	Aircraft yaw	degrees
azimuth	Aircraft azimuth	degrees

The contents of RASPEC.xyz/.gdb (both file types contain the same set of data channels) are summarized as follows:

Table 39. Contents of gamma-ray data files RASPEC.xyz/.gdb.

Channel Name	Description	Units
gps_x_final	differentially corrected GPS X (NAD83 CSRS datum)	decimal-degrees
gps_y_final	differentially corrected GPS Y (NAD83 CSRS datum)	decimal-degrees
gps_z_final	differentially corrected GPS Z (CGVD2013) metres above sea level	metres above sea level
x_nad83	easting in UTM co-ordinates using NAD83 CSRS datum	metres
y_nad83	northing in UTM co-ordinates using NAD83 CSRS datum	metres
lon_nad83	longitude using NAD83 CSRS datum	decimal-degrees
lat_nad83	latitude using NAD83 CSRS datum	decimal-degrees
radar_raw	raw radar altimeter	metres above terrain
radar_final	corrected radar altimeter	metres above terrain
dem	digital elevation model	metres above sea level
baro_press	barometric pressure	millibars
air_temp	outside air temperature	degrees Celsius
air_temp_f	low-pass filtered outside air temperature	degrees Celsius
fiducial	fiducial	seconds
flight	flight number	
line_number	full flight-line number (flight-line and part numbers)	
line	flight-line number	
line_part	flight-line part number	
time_utc	UTC time	seconds
time_local	local time	seconds after midnight
date	local date	YYYY/MM/DD
height_rad	gamma-ray spectrometer height at STP	metres above terrain
live_time	gamma-ray spectrometer live time	milliseconds
cosmic_raw	raw cosmic window	counts per second
radon_raw	raw upward-looking uranium window	counts per second
radon_final	radon calculated with upward-looking uranium window	counts per second
total_count_win	windowed total count	counts per second
potassium_win	windowed potassium	counts per second
uranium_win	windowed uranium	counts per second
thorium_win	windowed thorium	counts per second
total_count_corr	corrected total air-absorbed dose rate	nanograys per hour
potassium_corr	corrected potassium	percent
euranium_corr	corrected equivalent uranium	parts per million
ethorium_corr	corrected equivalent thorium	parts per million
dose_rate	natural dose rate	nanograys per hour
total_count_final	microlevelled total air absorbed dose rate	nanograys per hour
potassium_final	microlevelled potassium	percent
euranium_final	microlevelled equivalent uranium	parts per million
ethorium_final	microlevelled equivalent thorium	parts per million
k_over_th	ratio of potassium over equivalent thorium	percent over parts per million

The contents of RASPEC256.xyz/.gdb (all file types contain the same set of data channels) are summarized as follows:

Table 40. Contents of gamma-ray spectra data files RASPEC256.xyz/.gdb.

Channel Name	Description	Units
x_nad83	easting in UTM co-ordinates using NAD83 CSRS datum	metres
y_nad83	northing in UTM co-ordinates using NAD83 CSRS datum	metres
lon_nad83	longitude using NAD83 CSRS datum	decimal-degrees
lat_nad83	latitude using NAD83 CSRS datum	decimal-degrees
fiducial	fiducial	seconds
flight	flight number	
line_number	full flight-line number (flight-line and part numbers)	
line	flight-line number	
line_part	flight-line part number	
date	local date	YYYY/MM/DD
DOWN	raw gamma-ray down spectrum (array channel)	counts per second
UP	raw gamma-ray up spectrum (array channel)	counts per second

The contents of RAKC.csv/.gdb (both file types contain the same set of data channels) are summarized as follows:

Table 41. Contents of Keating coefficient files RAKC.csv/.gdb.

Channel Name	Description	Units
x_nad83	easting in UTM co-ordinates using NAD83 CSRS datum	metres
y_nad83	northing in UTM co-ordinates using NAD83 CSRS datum	metres
lon_nad83	longitude using NAD83 CSRS datum	decimal-degrees
lat_nad83	latitude using NAD83 CSRS datum	decimal-degrees
corr_coeff	correlation coefficient	percent
pos_coeff	positive correlation coefficient	percent
neg_coeff	negative correlation coefficient	percent
norm_error	standard error normalized to amplitude	percent
amplitude	peak-to-peak anomaly amplitude within window	nanoteslas

5. GRID FILES

All grids are NAD83 CSRS UTM Zone 17N with a grid cell size of 50 m and are summarized as follows:

- RADEM83.gxf/.grd — digital elevation model
- RAMAG83.gxf/.grd — total magnetic field
- RALAG83.gxf/.grd — measured lateral (across line) horizontal magnetic gradient
- RALOG83.gxf/.grd — measured longitudinal (along line) horizontal magnetic gradient
- RAGMAGGSC83.gxf/.grd — "GSC-levelled" gradient enhanced residual magnetic field
- RAG2VDMAGGSC83.gxf/.grd — second vertical derivative of the "GSC-levelled" gradient-enhanced residual magnetic field
- RATC83.gxf/.grd — natural air absorbed dose rate
- RAK83.gxf/.grd — potassium
- RATH83.gxf/.grd — equivalent thorium
- RAU83.gxf/.grd — equivalent uranium
- RAKTHRATIO83.gxf/.grd — potassium/equivalent thorium ratio

*Notes: *.gxf - Geosoft® uncompressed ASCII grid exchange format*
**.grd - Geosoft® Oasis montaj™ uncompressed binary grid file*

6. GEOREFERENCED IMAGE FILES

Geographically referenced colour images, incorporating a base map, are provided in GeoTIFF format for use in GIS applications.

- RAGMAGGSC83.TIF — "GSC-levelled" gradient-enhanced total magnetic field grid + planimetric base
- RAG2VDMAGGSC83.TIF — shaded second vertical derivative of the "GSC-levelled" gradient-enhanced total magnetic field grid + planimetric base
- RATC83.TIF — total count grid + planimetric base
- RAK83.TIF — potassium grid + planimetric base
- RAU83.TIF — equivalent uranium grid + planimetric base
- RATH83.TIF — equivalent thorium grid + planimetric base
- RATERN83.TIF — potassium, uranium, thorium ternary image + planimetric base

7. VECTOR FILES

Vector line work from the maps is provided in DXF (v.12) ASCII format using the following naming convention:

- RAPATH83.DXF — flight path
- RAKC83.DXF — Keating coefficients
- RAMAG83.DXF — magnetic contours

The layers within the DXF files correspond to the various object types found therein and have intuitive names.

Appendix C. Adjustments Applied to Uranium Data

Table 42. Adjustments applied to uranium data.

Adjustment (cps)	Line	T1	T2	Adjustment (cps)	Line	T1	T2
−15.0	1493.00	48558	48601	−3.0	1483.00	47311	47494
−5.0	1601.00	66280	66469	−3.0	1484.00	50421	50590
−10.0	1229.00	48399	48449	−5.0	1498.01	49428	49650
−10.0	1319.00	46854	46912	−5.0	1499.00	50699	50937

Appendix D. Digital Video Inventory Notes

Table 43. Digital video inventory notes.

Flight Line	Flight	Data Start Time	Data End Time	Note
1241.01	3015	61204.47	62311.19	No Video Data
1242.01	3015	60161.36	61132.81	No Video Data
1243.01	3015	58364.34	60036.69	No Video Data
1244.01	3015	56837.48	58305.18	No Video Data
1245.00	3015	54062.13	56714.21	No Video Data
1246.00	3015	62415.04	64803.47	No Video Data
1247.00	3015	64927.32	66062.67	No Video Data
1248.00	3015	66108.23	67178.00	No Video Data
1283.01	3022	54117.49	55264.43	No Video Data
1284.01	3022	52897.79	54073.44	No Video Data
1302.00	1029	51415.72	53864.39	No Video Data
1333.00	1029	48789.11	51249.60	No Video Data
1335.00	1029	54175.26	56650.09	No Video Data
1336.00	1029	56810.88	59299.88	No Video Data
1337.00	1029	59419.55	61943.50	No Video Data
1338.00	1029	62062.20	64542.39	No Video Data
1339.00	1029	64667.28	66427.90	No Video Data
1340.00	1029	66483.95	68288.66	No Video Data
1469.00	2032	65582.33	66376.21	No Video Data
1538.01	2042	59077.03	59354.02	No Video Data
1577.00	3029	49159.14	51461.86	No Video Data
1578.00	3029	51571.51	53995.22	No Video Data
1579.00	3029	54086.58	56393.60	No Video Data
1580.00	3029	56502.68	58874.55	No Video Data
1581.00	3029	58969.28	61296.39	No Video Data
1582.00	3029	61410.49	63757.45	No Video Data
1583.00	3029	63845.70	66128.47	No Video Data
1584.00	3029	66233.20	68560.39	No Video Data
1649.00	2049	47260.03	47802.14	No Video Data
8315.00	3015	53674.56	53917.10	No Video Data
9129.00	1029	48365.30	48498.03	No Video Data
9315.00	3015	53247.23	53383.52	No Video Data
9321.00	3021	45884.60	46019.98	No Video Data
9329.00	3029	47851.06	47985.45	No Video Data